University of Crete
Department of Physics

Ultrafast Dynamical properties of strongly interacting systems under nonlinear coherent photoexcitation by multiple ultrashort laser pulses

Michalis E.Karadimitriou

Heraklion, Greece, September 2015

Michalis E.Karadimitriou

Ultrafast Dynamical properties of strongly interacting systems under nonlinear coherent photoexcitation by multiple ultrashort laser pulses

Thesis
submitted to the Department of Physics, University of Crete
for the Degree of Doctor of Philosophy in Physics

Heraklion, Greece, September 2015

Ultrafast Dynamical properties of strongly interacting systems under nonlinear coherent photoexcitation by multiple ultrashort laser pulses

Thesis author	Michalis E. Karadimitriou
Thesis supervisor	Ilias Perakis
Thesis committee	Giorgos Tsirwnis Xenofwn Zotos Panagiwtis Tzanetakis Petros Rakitzis Eleftherios Iliopoulos George Froudakis

Department of Physics, University of Crete
Heraklion, Greece

July 2015

Dedicated to my amazing wife Aggeliki
for her support and patience

Abstract

In this thesis we present a non-equilibrium many–body formulation of the coherent ultrafast nonlinear optical response of doped semiconductors and systems with a strongly correlated ground state, such as the quantum Hall system (QHS). Our theory is based on a truncation of the density matrix equations of motion in the absence of a small interaction parameter, obtained by expanding in terms of the optical field and by using Hubbard operator density matrices to describe the exact dynamics within a subspace of many–body states. We identify signatures of non–instantaneous interactions between magnetoexcitons (X) and the incompressible two–dimensional electron gas (2DEG) during femto– and pico–second timescales by describing X coupling to inter–Landau level magnetoroton (MR) and magnetoplasmon (MP) excitations. We show that strong X coupling to X+MR configurations changes the temporal evolution of the nonlinear optical spectra as compared to the Random Phase Approximation (RPA). and leads to an absorption resonance. We calculate the three–pulse four–wave mixing signal, whose dependence on frequency and two time delays reflects the dephasing and relaxation of the strongly coupled X–2DEG system, and demonstrate that the dynamics of the X–2DEG interaction process can be resolved with femtosecond optical pulses. Our results shed light into unexplored sub–picosecond and coherent dynamics of the QHS and may be used to interpret and guide two–dimensional correlation spectroscopy experiments.

Acknowledgements

After several years of studying Physics in Crete, you realize how lucky you were, having chosen this Department and this island. In recent years Crete and the Department contributed greatly to my development. My choice to continue after my undergraduate studies, at a Masters and then a PhD, is owed directly and indirectly to many people. At this point I would like to thank every one of them.

First of all, I would like to thank my thesis supervisor Prof. Ilias Perakis, who brought me close to the area of Theoretical Physics. He gave me the opportunity to explore the beautiful "out of balance" conditions of optical excitations in systems with high correlations, through the possibility of direct comparison of theory with experiment.

I would like to also thank Dr. Eleftheria Kavousanaki for her support. The various discussions with her, helped me considerably, both in the theoretical but also the computational level of this work.

After so many years in the Department of Physics I owe a big thank you to the teachers and staff of the Department. Especially to Stephanos Trachanas, whose educational approach to physics and especially quantum mechanics, was the inspiration for my path.

I would also like to thank all my friends and especially my "roommates" at office 105-b of the Department office for their support over the years.

Finally I owe a big thank you to Angeliki Mantzopoulou for her support on every level over the years, but also to my family which aided my every effort.

Contents

Chapter 1

Introduction

1.1 motivation

The idea of controlling the properties of materials at the quantum level by using femtosecond laser pulses has led to promising developments at the frontier of condensed-matter physics and quantum chemistry. [3, 12, 4, 5, 6, 15] This approach to materials science goes beyond traditional investigations of optical properties and focuses, for example, on the design of fast devices with a functional role in information storage and processing, memories, network components, etc. However, the development of these types of applications poses fundamental non-equilibrium physics questions, especially when sub-picosecond device operation is desired. Advances in this important technological field will be greatly accelerated by a comprehensive description of transient cooperative phenomena and light–induced non-equilibrium phase transitions in condensed matter systems with strongly correlated electronic states. The development of quantum mechanical models able to treat light–induced dynamics of strongly coupled degrees of freedom is a serious challenge. It belongs to an emerging inter-disciplinary field that brings together condensed-matter, optical, and applied physics.

This thesis outlines a systematic approach to the study of many-

body systems with correlated electrons coherently coupled to light. We study non-equilibrium properties dominated by interactions among elementary excitations. While thermodynamic, transport, and linear optical properties do not depend as critically on such quasi-particle interactions, these dominate the nonlinear response to external stimuli. Accepted rules of condensed matter physics, including the cornerstone concept of free energy, fail to describe the time evolution during femtosecond time scales. Our non–equilibrium many-body theory addresses all four of the following fundamental questions: How to describe the coherent photoexcitation of systems with strongly correlated ground state electrons reacting un–adiabatically to light? What is the nonlinear response to such photoexcitation? What detection scheme can best "visualize" this response? What many-body mechanisms are involved in the coherent and non-thermal temporal regimes?

During the last two decades, a good understanding of the ultrafast nonlinear optical response of undoped semiconductors has been achieved. Compared to multi–level atomic systems, the main theoretical challenge here is the description of interactions and correlations among exciton quasiparticles. [3, 16, 17] For this purpose, non–equilibrium theories such as the Semiconductor Bloch Equations, [6, 12] Dynamics Controlled Truncation Scheme (DCTS), [8, 9, 10] Correlation Expansion, [17] Keldysh Green's functions, [12, 6] Correlation functions, [15] and canonical transformation "dressed semiconductor" approach [68] have been developed. In undoped semiconductors, one need not take into account correlations involving ground state electrons. A rigid Hartree–Fock ground state, with full valence bands and empty conduction band, suffices since Auger processes are negligible. However, when the conduction band is partly filled with N_e electrons in the ground state, *low energy* intraband electronic excitations can interact with the photoexcited carriers. If the fundamental reaction time of the ground state system to such interactions

(determined by the period of one oscillation of the lowest excited state and by collective effects among the N_e electrons) is sufficiently long, it responds *un–adiabatically* to the photoexcitation and thus cannot be treated as a "bath". The ultrafast nonlinear response is then strongly influenced by the quantum dynamics of the coupled system of photoexcited and ground state carriers. The theories describing the nonlinear response of undoped semiconductors must be extended to describe such effects. [68, 18, 19, 20, 21] For example, the DCTS truncates the hierarchy of density matrices generated by the interactions based on the assumption that all Coulomb interactions occur between photoexcited e–h pairs. The standard diagrammatic expansions and DCTS factorizations assume a Hartree–Fock reference state and no free ground state carriers. They break down in the case of a strongly correlated electronic ground state.

Photoinduced phase transitions in strongly correlated systems have attracted much attention recently, due to ultrafast switching applications and fundamental physics questions.[22, 23] A prominent example of strong correlations between spin, charge, and orbital/lattice degrees of freedom is the colossal magneto-resistance observed in the $R_{1-x}A_xMnO_3$ manganite materials (R=La,Pr,Nd,Sm,... and A=Ca,Ba,Sr,Pd,...).[23] Of particular interest here are macroscopic changes in the electronic states induced by perturbing strongly coupled degrees of freedom after the coherent excitation of selected modes. The quantum Hall system (QHS) is another example of a well-characterized strongly correlated system. Here, a two–dimensional electron gas (2DEG) is subjected to a perpendicular magnetic field. The quantum well confinement and magnetic field quasi-confinement discretize the energy eigenstates into Landau levels (LL) with degeneracy $N{=}L^2/2\pi\ell^2$, where L is the system size and ℓ is the magnetic length. In the ground state, these LLs are partially filled with the correlated 2DEG. [24, 25, 26] The ratio of occupied states to LL degeneracy defines the filling factor $\nu{=}N_e/N{=}2\pi\ell^2 n_e$, where N_e (n_e)

denotes the number (density) of conduction electrons that populate the ground state. The LL degeneracy N increases with magnetic field and above a threshold value, $\nu \leq 2$, the ground state electrons only occupy the lowest LL (LL0) states; all the higher LLs (LL1, ...) are then empty in the ground state. The coupling of the degenerate LL0 states by the Coulomb interaction results in a strongly correlated incompressible quantum liquid [27], whose collective charge excitations are magnetoplasmons (MP) and magnetorotons (MR),[24, 25, 26, 30, 31, 32, 33] excitons of composite fermions,[72, 73, 74] interband quasiexcitons,[75] etc. The QHS displays different correlated ground states depending on ν. At ν=1, the ground state becomes a ferromagnet with 100% spin polarization when the characteristic Coulomb energy exceeds the LL disorder broadening [76]. For weak disorder, the ground state around ν=1 includes a small population ($\propto |\nu - 1|$) of topologically charged spin texture quasiparticles (skyrmions). [77, 78, 79, 80, 76] For larger disorder, the ground state is maximally spin–polarized, however the empty states with respect to the ν=1 ferromagnetic state are populated by conventional Laughlin quasiparticles. At fractional ν, the e–e interaction removes the degeneracy of the non–interacting system and produces robust ground states, separated from the excited states by an energy gap (incompressibility). This non–perturbative effect can be interpreted by considering the formation of composite fermion quasiparticles, i.e. topological bound states of an electron and an even number of magnetic flux quantized vortices. [73, 74] The strongly interacting electrons are transformed into weakly interacting composite fermions and the partly filled lowest electron LL splits into several composite fermion LLs. Fractional quantum Hall effects occur when an integer number of composie fermion LLs are fully occupied. [73, 74] In terms of applications, the quantum coherence of the QHS may be useful for realizing robust many–body qubits that can be coherently controlled with light for implementing quantum computation schemes. [81] Ultrarafast nonlinear

spectroscopy can shed light into the coherent dynamics of the QHS. [82, 83, 84, 85, 86, 87, 88, 89, 90, 91] The above developments make our theoretical advances, which address transient coherence and relaxation in strongly correlated systems, particularly timely.

1.2 Thesis Structure

The outline of this thesis is as follows. In chapter 2, we discuss about the Quantum Hall System and we provide some basic theoretical background about the GaAs/AlGaAs quantum well. We present the case of the 2D electron in a magnetic field, a quantum well in a magnetic field and 2DEG in a magnetic field. Furthermore, we provide some information about the Ultrafast Nonlinear Optical Spectroscopy and especially about the Four-Wave-Mixing technique that provided us the experimental outcome. In chapter 3, we discuss about the expansion on the theoretical background as far as it concerns the apprehension and tanning of the experimental outcome using Ultrafast Nonlinear Optical Spectroscopy. In chapter 4 we present the Linear and Nonlinear spectrum of the quantum Hall system for $\nu = 1$.In chapter 5 we present the inter LL dynamical couplings, we discuss the results represented by our figures and compare them with the ones showing the experimental outcome.

1.3 Related Publications

- Transient three-pulse four-wave mixing spectra of magnetoexcitons coupled with an incompressible quantum liquid. *M.E. Karadimitriou, E.G. Kavousanaki, I.E. Perakis, and Keshav M. Dani.Phys. Rev. B 82, 165313 (2010)*
- Strong Electronic Correlation Effects in Coherent Multidimensional Nonlinear Optical Spectroscopy.*M. E. Karadimitriou, E.*

G. Kavousanaki, K. M. Dani, N. A. Fromer, and I. E. Perakis, pp 56345647, (2011)

Chapter 2

The quantum Hall system & Ultrafast nonlinear Optical spectroscopy

2.1 Introduction

In this chapter we briefly discuss the background scientific material that is necessary to understand the nonlinear optical response of the quantum Hall system. We begin by reviewing the physics of the quantum Hall System. We first discuss the band structure of GaAs, and explain how a 2DEG is created in a GaAs/AlGaAs hererostructure. We also discuss the 2D exciton eigenstates and calculate the energy spectrum of a 2D electron in a perpendicular magnetic field.We then study the 2DEG in a magnetic field and review its low energy collective excitations.

In the second part of this chapter, we explain the ultrafast nonlinear spectroscopic technique of four-wave-mixing (FWM). We then discuss an ensemble of two-level systems, which will give us a good sense of the physics that is probed by FWM experiments,but also, when compared to our results in the following chapters, will show the effects of many-body interactions. Finally we discuss theories that have been developed to treat the nonlinear response of semicon-

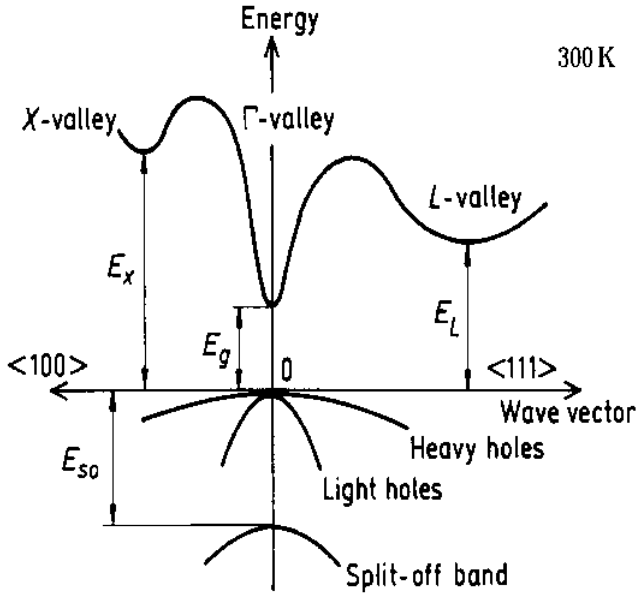

Figure 2.1: Schematic of the band structure of the GaAs around the Γ point. $E_g = 1,519eV$ and $E_{so} = 0,34eV$ at low temperature.[70]

ductors:the semiconductor Bloch equations and the Dynamics Controlled Truncation Sheme. We end by discussing the limits of the DCTS and by explaining why we need to extend it on order to understand the nonlinear optical response of the quantum Hall system.

2.2 The quantum Hall System

2.2.1 GaAs Quantum Wells

Today ,GaAs and GaAs/AlGaAs heterostructures can be grown with remarkable purity using molecular beam epitaxy, leading to sharp resonances and long lifetimes for transitions. Such systems are excellent venues for studying the ultrafast many body correlations in semiconductors.

The band structure of bulk GaAs ner the Γ-point is well described by the effective mass approximation (Fig.2.1).There are 2 degenerate s-like conduction bands, and 6 p-like valence bands. The low

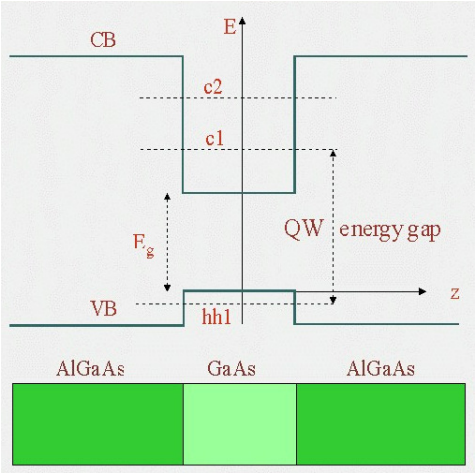

Figure 2.2: Schematic of the GaAs/AlGaAs quantum wells.

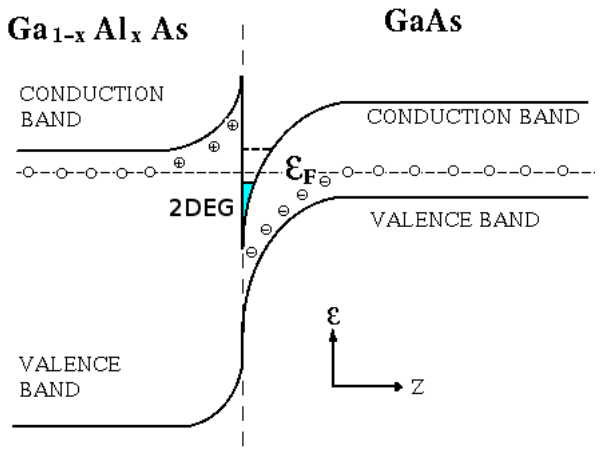

Figure 2.3: Confinement of the 2DEG at the GaAs/AlGaAs interface.

temperature bandgap is $E_g = 1.519$ eV.The total angular momentum is a good quantum number, and thus the bands can be labeled by $\left|J, m_J\right\rangle$. The lowest lying valence bands, $\left|1/2, \pm 1/2\right\rangle$, called the split-off bands, are separated from the other valence bands by the split-orbit coupling. The large splitting between these bands and the other valence bands (≈ 0.4 eV at low temperature) allows us to neglect the split-off bands altogether. The J=3/2 bands are called the heavy hole (hh,$m_J = \pm 3/2$) bands and light hole (lh,$m_J = \pm 1/2$) bands. In bulk GaAs, they are degenarate at $k = 0$, but they have different curvature and therefore different energies away from the zone center. Within the effective mass approximation, the simply means that heavy holes and light holes have different effective masses: $m^*_{hh} = 0.5m_e, m^*_{lh} = 0.082m_e$, where m_e is the bare effective mass, The conduction bands have S = 1/2, $m_S = \pm 1/2$ and $m^*_e = 0.0665m_e$.

An important advantage of GaAs/AlGaAs heterostructures is that while the band gap for AlGaAs is much higher tan that of GaAs, the lattice constants for the two compounds is almost identical.As a result, alternating layers of GaAs and AlGaAs can be grown on top of one another with very little strain induced at the interfaces. By

sandwiching a layer of GaAs between two layers of AlGaAs, a quantum well, i.e. a finite potential well is created in the growth direction (Fig.2.2). Moreover, if donors are added in the AlGaAs layer, known as modulation doping,the electrons get trapped in a small area at the interface of the two compounds, as shown in Fig.2.3.As a result a quasi-two dimensional electron gas is created with the additional advantage of being spacially separated from the charged impurities.

The electronic states of the quantum well are modified from that of bulk GaAs by confinement potential. To first approximation, we can thinh of the confinement potential as an infinite quantum well along the z-direction. Consequently, this discretizes the κ_z momentum states. Since the discrete energy levels of a particle in a box depend on the mass, the degeneracy of the heavy-hole and light-hole bands is lifted and the hh-conduction band transition is at a lower energy than the lh transition.

In addition to the continuum of states of the band structure, there are also excitonic eigenstates just below the band edge. These states comprise of an electron in the conduction band and a hole in the valence band with energy the energy of the band gap minus the bibding energy of the exciton. The latter is due to Coulomb attraction between the electron and the hole. To obtain the energy leves of a 2D excitonic state, we solve the relative Schrödinger equation for a 2D electron-hole pair:

$$\left[\frac{\mathbf{p}^2}{2m} - \frac{e^2}{\epsilon r}\right]\phi_n(r) = E_n\phi_n(r) \tag{2.1}$$

where $r = |\mathbf{r}_e - \mathbf{r}_h|$ is the electron-hole separation, $\mathbf{p} - \mathbf{p}_e - \mathbf{p}_h$ is the relative momentum and m is the reduced mass,$1/m = 1/m_e^* + 1/m_h^*$. The energy levels E_n are given by:

$$E_n = E_g - \frac{R}{(n+1/2)^2}, n = 0, 1, ... \tag{2.2}$$

and the wavefunction for the lowest exciton state (1s) is

$$\phi_{1s}(r) = \left(\frac{2}{\pi}\right)^2 \frac{2}{\alpha} e^{-2r/\alpha} \tag{2.3}$$

where $R = me^4/2\epsilon^2\hbar^2$ is the 3D Rydberg energy and $\alpha = \epsilon\hbar^2/me^2$ is the Bohr radius.

In our study we will consider the quantum well as an ideal 2D system, although this is note the case, as the band gap of AlGaAs is larger than that of GaAs but not infinite. This implies that in the z-direction, the electron and hole wavefunctions are not entirely confined within the quantum well, but rather they penetrate into the barrier regions. Also, the quantum well itself has a finite thickness in the z-direction. In our study we will treat the quantum well as purely 2-dimensional, although there are effects due to deviations from this ideal picture.

2.2.2 2D Electron in a magnetic field

We will begin with the problem of a free electron in a uniform magnetic field $\mathbf{B} = B\mathbf{z}$, which is described by the Hamiltonian

$$H = \frac{1}{2m_e^*}\left(-i\hbar\nabla + \frac{e}{c}\mathbf{A}\right)^2 = \frac{1}{2m_e^*}\left(\Pi_x^2 + \Pi_y^2\right) \tag{2.4}$$

where $\mathbf{A}$ is the vector potential related to the magnetic field as $\mathbf{B} = \nabla \times \mathbf{A}$, and Π_i the kinetic momentum components. It is straightforward to verify tha the x and y componets of Π do not commute:

$$[\Pi_x, \Pi_y] = -i\frac{e\hbar B}{c} \tag{2.5}$$

In analogy with the harmonic oscillator, one may define operators a and $a^\dagger$ as a linear combination of Π_x and Π_y , for wich we can write $:\left[\alpha, \alpha^\dagger\right] = 1$

$$a = \sqrt{\frac{c}{2e\hbar B}}\big(\Pi_x - i\Pi_y\big) \tag{2.6}$$

$$a^\dagger = \sqrt{\frac{c}{2e\hbar B}}\big(\Pi_x + i\Pi_y\big) \tag{2.7}$$

Using these ladder operators, equation (2.4) becomes the same with the harmonic oscillator's problem:

$$H = \hbar\Omega_c\left(a^\dagger a + \frac{1}{2}\right) \tag{2.8}$$

where

$$\Omega_c = \frac{eB}{m_e^* c} \tag{2.9}$$

is the cyclotron energy. Thus, the eigenenergies are discrete states, known as *Landau levels*, given by:

$$E_n = \hbar\Omega_c\left(n + \frac{1}{2}\right), \quad n = 0, 1, 2, ... \tag{2.10}$$

By choosing the Landau gauge, for which $\mathbf{A} = Bx\mathbf{y}$, the Hamiltonian becomes in the form

$$H = \frac{1}{2m_e^*}\left[p_x^2 + \left(p_y + \frac{eB}{c}x\right)^2\right] \tag{2.11}$$

By separate the variables we can write the eigenfunction as

$$\psi = e^{iky}X(x) \tag{2.12}$$

where $\hbar k$ is the eigenvalue of the p_y operator, taking into account the commutator $[p_y, H] = 0$. The function $X(x)$ is the eigenfunction of the time independent Schrödinger equation,

$$-\frac{\hbar^2}{2m_e^*}X'' + \frac{1}{2}m_e^*\Omega_c^2(x - x_k)^2X = EX(x) \tag{2.13}$$

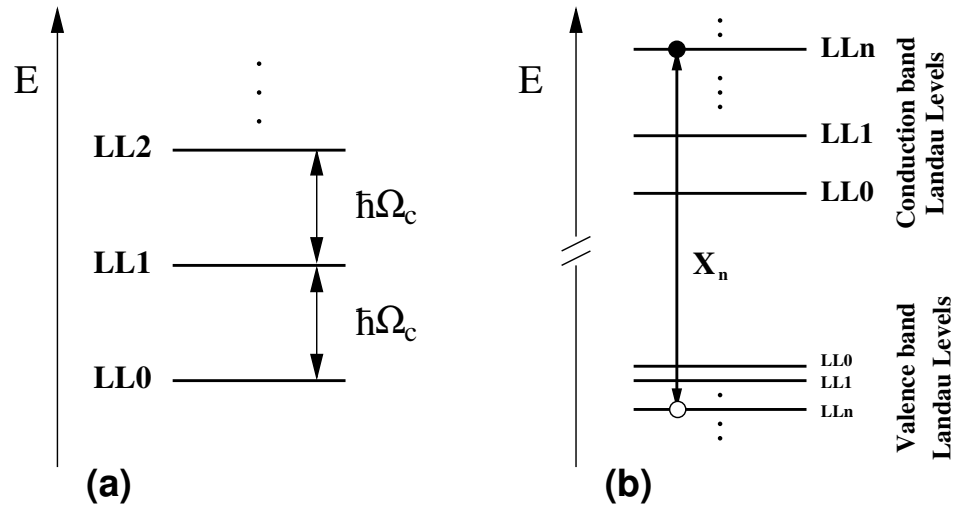

Figure 2.4: (a) The energy spectrum of a 2D electron in a perpendicular magnetic field consists of discrete, equally spaced and highly degenerate Landau levels.(b) The conduction and valence bands in a 2 band quantum well in a magnetic field are split separately into Landau levels for electrons and holes respectively. The inter LL-energy $\hbar\Omega_c$ is different for electrons and holes due to the difference in masses.A magnetoexciton x_n is optically excited by creating a LLn electron and a LLn hole

where $x_k = -kl^2$, and l is the magnetic length (cyclotron radius) given by:

$$l = \sqrt{\frac{\hbar c}{eB}} \tag{2.14}$$

The equation (2.13) is recognised as the harmonic oscillator equation, of spring constant $\hbar\Omega_c = \hbar^2/m_e^* l^2$, with equilibrium point at x_k. Thus the unnormalized eigenfunction is

$$\psi_{nk}(x,y) = e^{iky} H_n\left[(x - x_k)/l\right] e^{-(x-x_k)^2/2l^2} \tag{2.15}$$

where H_n is the Hermite polynomial. The functions are extended in the y direction and localized in x.

When the system is confined in a square cell of side L, the degeneracy of each Landau Level is the number of allowed k values, such tha the center x_k lies between 0 and L. Using periodic boundary conditions we get $k = 2\pi m/L$, with m an integer. The allowed values

of m are then determined by the condition

$$x_k = \frac{2\pi m}{L} l^2, 0 < x_k < L \tag{2.16}$$

The degeneracy N of each Landau Level is

$$N = \frac{L^2}{2\pi l^2} \tag{2.17}$$

The above relation can be expressed in terms of yhe magnetic flux $\Phi = BL^2$ and the flux quantum $\Phi_0 = B2\pi l^2 = hc/e$ as:

$$N = \frac{e}{hc}\Phi = \frac{\Phi}{\Phi_0} \tag{2.18}$$

Thus, the Landau Level degeneracy is the total number of flux quanta in the external magnetic field. An important quantity for our problem is the dimensionless density of the electrons, the *filling factor* of the Landau level,

$$\nu = \frac{N_e}{N} = 2\pi l^2 n_e \tag{2.19}$$

where $N_e(n_e)$ denotes the number (density) of electrons in the system.

2.2.3 Quantum Well in a Magnetic Field

To understand the effect of a magnetic field applied to a quantum well structure, we will first consider a two-band semiconductor quantum well that has just a conduction and valence band with effective masses m_e^* and m_h^* respectively. Ignoring the Coulomb interaction between the carriers in the system, the application of a magnetic field simply splits each band into its own series of Landau levels. The only difference between the conduction band and the valence band LLs is the inter-LL spacing.The cyclotron energy depends on the effective

mass (eq. 2.9) so, due to the large hole mass in GaAs, the valence LLs are much closer to each other than the conduction band LLs.

When an incoming photon is absorbed, a LLn electron ane a LLn hole are created, because of the Coulomb attraction, form a bound electron-hole pair, i.e. an exciton (magnetoexciton, because of the magnetic field existence). The strength of the $e-h$ Coulomb interaction may be characterized by the 3D Rydberg energy R and the Bohr radius α, by the cyclotron energy $\hbar\Omega_c$ and the magnetic length l . The dimensionless parameter used to compare the relative importance of these two energy and length scales is $\lambda = (\alpha/l^2) = \hbar\Omega_c/2R$.For $\lambda \ll 1$ the Coulomb interaction dominates; one may think that the electron and hole being closer to each other than the radius of their cyclotron orbits. For $\lambda \gg 1$ the distance between the electron and hole is large enough to not affect the individual orbits significantly and thus the magnetic field dominates. In GaAs, the cross-over field where $\lambda = 1$ is $B \simeq 3.5T$, and consequently both regimes are easily accessible.

When the $\lambda \ll 1$, the magnetic field is a perturbation to the excitonic state, and the exciton's energy levels depend on the applied field[34],

$$E_n \approx -\frac{R}{(n+1/2)^2} + \frac{\hbar^2 e^2}{8mc^2}\langle r^2\rangle_n B^2 + O(B^4). \tag{2.20}$$

When $\lambda \gg 1$, the Coulomb interaction is a perturbation of the Landau level energy. In this case,

$$E_n \approx \hbar\Omega_c(n+1/2) + A\frac{\pi}{2}\sqrt{R}\sqrt{\hbar\Omega_c} + O(B^0) \tag{2.21}$$

where A a dimensionless constant[34]. The Coulomb correction increases like $\sqrt{B}$, so tha for large magnetic fields, we asymptotically approach the bare energies of the Landau Levels. In our study we will consider the high magnetic field limit, where the carriers can be

thought of as being in their particular Landau Levels.[34, 35, 36, 37, 38, 39, 40, 41, 42, 43, 44].

In the realistic system, multiple bands exist and there is a strong coupling of different valence band spin states in a magnetic field. Moreover, the confinement at the interfaces of the quantum well structures changes the coupling between the bands.

For the s-like conduction band states, the interactions between the electron spin and the magnetic field does not change the picture significantly. The Zeeman Hamiltonian is $H_{Zeeman} = g^* \mu_B \mathbf{S} \cdot \mathbf{B}$ where g^* is the electron g-factor in the material. In the conduction band we can separate the wavefunction $\psi(r, \sigma_z) = \phi(r) X(\sigma_z)$, and the splitting can be super-imposed over the Landau level structure.

However, the valence band structure is more complicated. There is doubly generated pair of p-like bands at the Γ point in the bulk material.A Hamiltonian with the full symmetry of the heavy hole and light hole and exact to second order in k and first order in the magnetic field is the Luttinger Hamiltonian [44]. This Hamiltonian provides an accurate description of the dispersion of the valence band for energies significantly smaller than the split-off energy (0.34 meV). The Luttinger Hamiltonian is

$$H = H_h + H_m \tag{2.22}$$

where

$$\begin{aligned} H_h &= -\frac{\gamma_1}{2m_0} k^2 \\ &+ \frac{\gamma_2}{m_0} \left[\left(J_x^2 - \frac{1}{3} J^2 \right) k_x^2 + \left(J_y^2 - \frac{1}{3} J^2 \right) k_y^2 + \left(J_z^2 - \frac{1}{3} J^2 \right) k_z^2 \right] \\ &- 2\frac{\gamma_3}{m_0} (\{k_y, k_z\}\{J_y, J_z\} + \{k_z, k_x\}\{J_z, J_x\} + \{k_x, k_y\}\{J_x, J_y\}) \end{aligned} \tag{2.23}$$

is the kinetic term, and

$$H_m = \beta_4 (B_x J_x + B_y J_y + B_z J_z) + \beta_5 (B_x J_x^3 + B_y J_y^3 + B_z J_z^3) \tag{2.24}$$

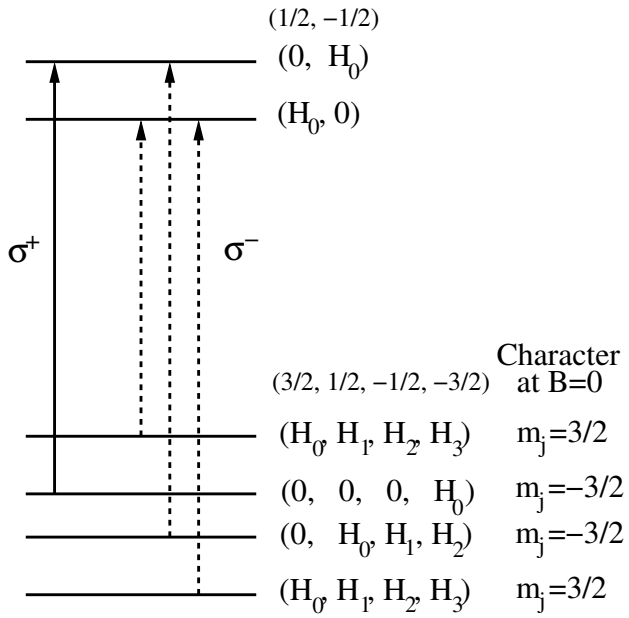

Figure 2.5: Selection rules for optical transitions of GaAs quantum well in a megnetic field. Transitions are only made from h-LLn to e-LLn and must satisfy $\Delta m_j = 1$. For given n, only one possible transition is allowed with σ_+ polarized light

is the magnetic term and $\{J_i, J_j\}$ are symmetrized products of operators. The parameters β, γ describe the effective masses and magnetic field dispersion of the valence band. For bulk material in the absence of a magnetic field, the Hamiltonian can be diagonalized to give the exact eigenvalues and eigenvectors of the valence band For a zinc-blende semiconductor such as GaAs, the energy levels are:

$$E = -\frac{1}{m_0}\left[\frac{1}{2}\gamma_1 K^2 \pm \sqrt{\gamma_2 k^4 + 3(\gamma_3^2 - \gamma_2^2)(k_y^2 k_z^2 + k_z^2 k_x^2 + k_x^2 k_y^2)}\right] \tag{2.25}$$

By setting $\gamma_2 = \gamma_3$ in the above equations we take the axial approximation, assuming tha the band structure is isotropic within the plane. The valence band wavefunctions, will be a combination of the different heavy-hole and light-hole subbands, with a different Landau level associated with each spin subband [43]. The eigenvectors taje the 4-compoment spinor form $(F_{3/2,n-2}, F_{1/2,n-1}, F_{-1/2,n}, F_{-3/2,n+1})$, where the first subscript is the z - component of the angular mo-

mentum m_J , and the second is the harmonic oscillator index which describes the nature of the Landau Level associated with the m_J state.

2.2.4 2DEG in a magnetic field

In the first subsection of this chapter we discussed the formation of a 2DEG in a modulation doped GaAs/AlGaAs heterostructure: because of the larger band gap of AlGaAs as opposed to GaAs, the doped electrons get trapped in a small area of the GaAs quantum well and form the 2DEG. When a large magnetic field is applied perpendicular to the 2DEG plane, the conduction and valence bands split into Landau Levels, which are now populated by the 2DEG. For noninteracting electrons, the ground state of the system is obtained by putting each electron in the lowest available energy state. So first we fill alla LL0 spin $\uparrow$ states, followed by the LL0 spin $\downarrow$ states. As we continue filling in more electrons, they start occupying states in LL1 and so on. The filling factor ν, as defined in Eq.(2.19), shows the percentage of the occupied states. For $\nu = 1$, all LL0 spin $\uparrow$ states are occupied, for $\nu = 2$ all LL0 spin $\uparrow$ and spin $\downarrow$ states are occupied, etc.

As we have shown in Eq. (2.19), the filling factor can be changed if we change the magnetic field for a fixed doping concentration. By increasing the magnetic field, the degeneracy of the Landau Levels is larger and more electrons can fit in the lower LLs (Fig.2.5). In our calculations, we will consider $\nu \sim 1$, i.e. the 2DEG resides in LL0 and mostly in the $\mid 1/2, 1/2\rangle$ states with spin $\uparrow$.

Taking into account the Coulomb interactions, the above discussion is valid in the large magnetic field limit, since cyclotron energy increases linearly to B, while the characteristic Coulomb interaction energy, $e^2/\epsilon l$ increases as $\sqrt{B}$. As a result, for large magnetic fields, Landau level mixing due to Coulomb interactions is negligible. and

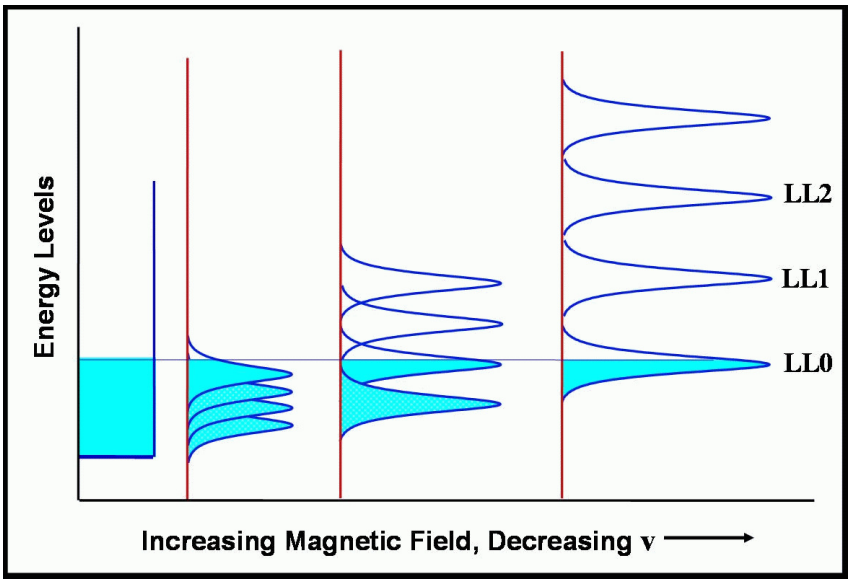

Figure 2.6: Filling factor decreases with increasing magnetic field: As the magnetic field is increased,the degeneracy of each Landau level increases and more electrons fit into the lower Landau levels.

the non-interaction picture we describe is valid.However for law energy collective excitations the presence of Coulomb interactions are important and affect its ultrafast nonlinear optical response.

2.2.5 Collective Excitations

The typical low energy collective excitation of the quantum Hall system are the intra and inter Landau level excitations. The spectrum due to these excitations has been studied theoretically [31, 32, 33]. However, only a few experiments in electron tunnelling or Raman scattering [30, 28] have successfully accessed this information.

The intra-Landau level excitations exist entirely within a single Landau level. The dispersion curve for these excitations exhibits a minimum at a characteristic energy, in parallel with the roton mode made in a superfluid Helium [32]. In the quantum hall community, these objects called *magnetorotons* , and can be thought of as an excitation in which the electron density remains essentially constant, but there is a cilcular modulation built up from the phase of the single

electron orbits.

The more relevant excitations for the experiments of interest here, will be the inter-Landau level excitations. In the case of the well separated Landau levels (high magnetic field), it cost $\sim \Omega_c$ to create an inter-Landau level excitation. These excitations are known as *magnetoplasmons*. Promoting an electron from a full Landau level to the next highest empty level costs energy Ω_c. However, the removal of an electron leaves behind a hole in first level, which can interact with the promoted electron, similar to a magnetoexciton. This interaction must be taken into account to understand the structure of the excitation.

The theory of intra-Landau level excitations has been extended to the calculation of the magnetoplasmon dispersion at partial filling [33]. If we think of the full level case as the creation of an electron-hole pair, similar to a magnetoexciton, than in a partially full level of magnetoplasmon is like an electron-hole pair accompanied by a shake-up of the electron gas.

For all filling factors, the excitation energy at long wavelength approaches the cyclotron energy. This is Kohn's theorem [45], a direct consequence of the translational invariance of the system in the $x - y$ plane.

2.3 Ultrafast nonlinear optical spectroscopy

Optical Spectroscopy is a powerful tool for investigating the electronic and vibrational properties of a variety of systems, like atoms, molecules, and solids. In semiconductors, the techniques of absorption, reflection, luminescence,and light -scattering spectroscopies have provided invaluable information about such diverse aspects as the electronic band structure, phonons, single particle excitation spectra of electrons and holes, and properties of defects, surface and

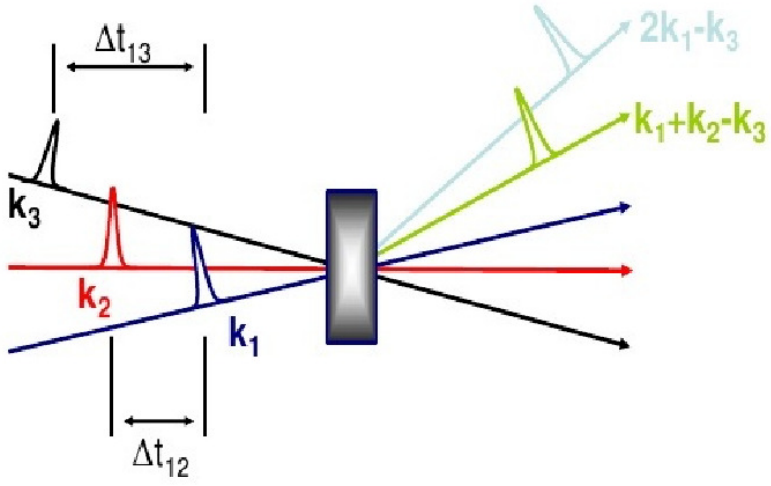

Figure 2.7: Schematic of a 2-pulse and 3-pulse FWM experiment

interfaces.

However, optical spectroscopy has unique stengths since it can provide information about the non-equilibrium and nonlinear properties of semiconductors, on combination with picosecond and femtosecond laser pulses. Ot provides the best means of determining the non equilibrium distribution function of excitations created by the optical field. Moreover, optical techniques provide the ability to investigate the nonlinear properties, including coherent effects, in semiconductors, and thus provide insights into different aspects of semiconductors, such as many-body effects, coherent effects and dephasing phenomena.

Typical linear spectroscopic measurements are absorption, photoluminescense, etc.Standard nonlinear optical experiments are pubprobe, four-wave-mixing,six-wave-mixing, etc. We will focus on the Four-wave-mixing, which is relevant to the experiments of interest[84].

2.3.1 FWM Spectroscopy

In a FWM experiment we study the third order response of the system. We excite the system with three optical pulses. Two of the pulses create a second order excitation and the third pulse is scattered by the excited state in a new direction. Thus this scattered pulse, which is the FWM signal, reflects the third order nonlinear response of the system. The signal can be studied in different ways. For example, one may study the intensity of the signal versus the time delays between the pulses, or can study the spectrum of the signal, etc. A FWM experiment can be dine with two pulses (2-pulse FWM) or three pulses (3-pulse FWM), as shown in Fig.2.7.

In 2-pulse FWM, two pulses impinge on the sample in directions $\mathbf{k}_1$ and $\mathbf{k}_3$. The signal is measured in the background free direction $2\mathbf{k}_1 - \mathbf{k}_3$, and one can study the signal as a function of the time delay between the two pulses. In 3-pulse FWM, the system is excited with three pulses that propagate in the directions $\mathbf{k}_1, \mathbf{k}_2$ and $\mathbf{k}_3$. The signal is measured in the direction $\mathbf{k}_1 + \mathbf{k}_2 - \mathbf{k}_3$ and can now be studied as a function of two time delays in this system: Δt_{12} between the pulses $\mathbf{k}_1$ and $\mathbf{k}_2$, and Δt_{13} between the pulses $\mathbf{k}_1$ and $\mathbf{k}_3$.

In the experiments we will discuss in the following chapters, 3-pulse FWM is performed on the samples under investigation and the FWM signal is measured in the $\mathbf{k}_1 + \mathbf{k}_2 - \mathbf{k}_3$ direction in two different cases: (i) For $\Delta t_{12} = 0$ when $\mathbf{k}_1$ and $\mathbf{k}_2$ arrive together, and we call this *the* Δt_{13} *axis* and (ii) For $\Delta t_{13} = 0$ when $\mathbf{k}_1$ and $\mathbf{k}_3$ arrive together, and we call this *the* Δt_{12} *axis* .

2.3.2 Two level systems

The coherent phenomena in atoms and molecules are generally analysed for an ensemble of independent two-level systems. The independent two level model assumes tha the photon is nearly resonant

with the transition between $\mid a\rangle$ and $\mid b\rangle$ so far off resonance withe respect to all other transitions. It further assumes that there is no interaction between various two-level atoms or molecules making up the ensemble. The transition under consideration can be homogeneously broadened, inhomogeneously broadened or a combination of both.

The electronic states in a semiconductor are considerably more complicated than those in atoms. However, each exciton in a semiconductor can be considered as a two level system in the simplest approximation. The continuum states of a semiconductor can be considered as inhomogeneously broadened in the momentum space in the absence of any interaction between the states. Therefore, in the simplest approximation one may be able to apply the independent two-level model to semiconductors. For this reason, we begin our discussion with the predictions of the independent two-level model in various cases.

The quantum mechanics of transition probabilities in a two-level system by a near-resonant excitation is well known.If the wavefunctions of the two states are known, then one can describe the transition probabilities as bilinear combination of transition amplitudes. Since the expectation value of any observable involves such bilinear combinations, the density matrix method dealing directly with the bilinear combinations has been developed. The density matrix formalism facilitates the treatment of interacting quantum systems. We are interested not in a single two level system but an ensemble of two level systems.In such cases, the wavefunction of the two level systems ensemble is generally not known but certain statistical properties of the ensemble may be known. Such statistical properties are conveniently described in terms of the general matrix operator:

$$\rho = \sum_j P_j |\Psi_j\rangle\langle\Psi_j| \tag{2.26}$$

where P_j is the fraction of the systems which has the state vector $|\Psi_j\rangle$. The density matrix obeys the Liouville variant of the Shrödinger equation:

$$i\hbar\dot{\rho} = [H, \rho] \tag{2.27}$$

where H is the Hamiltonian operator of the system given by:

$$H = H_0 + H_{int} + H_R \tag{2.28}$$

H_0 is the Hamiltonian of the isolated two level system, H_{int} is the Hamiltonian describing the interaction between the radiation field and the two level system and the relaxation Hamiltonian H_R describes all processes that return the ensemble to thermal equilibrium.The expectation value of an operator $\hat{O}$ is given by:

$$\langle\hat{O}\rangle = Tr\hat{O}\rho \tag{2.29}$$

For a two level system with a ground state $|a\rangle$ and energy E_a and an excited state $|b\rangle$ and energy E_b the density operator can be written as:

$$\rho = \begin{bmatrix} \rho_{bb} & \rho_{ba} \\ \rho_{ab} & \rho_{aa} \end{bmatrix} \tag{2.30}$$

The diagonal elements of the density matrix represent the probability of finding the system in the trwo energy eigenstates, i.e the population in the two energy eigenstates The off-diagonal elements represent the coherence intrinsic to a superposistion state.

In a closed two level system, the diagonal components are related by:

$$\rho_{aa} + \rho_{bb} = 1 \tag{2.31}$$

since the sum of the populations in the lower and upper states is constant. Because of the complexity of electronic states in a semiconductor ,the assumption of a closed system may be difficult to satisfy in a semiconductor.

The Unperturbed Hamiltonian

The state vector $|\Psi_j\rangle$ obeys the time independent Schrödinger equation

$$i\hbar|\Psi_j\rangle = H|\Psi_j\rangle \tag{2.32}$$

For an isolated two-level system in the absence of any interactions $H = H_0$ and H_0 has no explicit time-dependence so that for a system at position $\mathbf{R}$

$$\Psi(\mathbf{R}, t) = u_k(\mathbf{R})e^{-E_k t/\hbar} \tag{2.33}$$

and

$$H_0 u_k(\mathbf{R}) = E_k u(\mathbf{R}) \tag{2.34}$$

where $k = a$ or b. Thus, the unperturbed amiltonian H_0 is given by

$$H_0 = \begin{bmatrix} E_b & 0 \\ 0 & E_a \end{bmatrix} \tag{2.35}$$

For an ensemble of two level systems,the state vector for the j-th system is

$$|\Psi_j(t)\rangle = C_{aj}(t)|a\rangle + C_{bj}(t)|b\rangle \tag{2.36}$$

and the density matrix can be put in the more familiar form

$$\rho = \sum_j P_j \begin{bmatrix} |C_{bj}|^2 & C_{bj}C_{aj}^* \\ C_{aj}C_{bj}^* & |C_{aj}|^2 \end{bmatrix} \tag{2.37}$$

where P_j is the probability of being in the state j. If the state vectors for all j's are indentica; (i.e.,amplitudes C_{aj} and C_{bj} are the

same for all j's), but the phases of the coherent superposition are randomly distributed between 0 and 2π, then the off-diagonal elements of the density matrix vanish and there is no coherence in the ensemble. On the other hand,if there is a well defined phase relationship for different j,the ensemble has coherence.

The Interaction Hamiltonian

For an electric-dipole allowed transition, one generally neglects the electric quadrupole and magnetic dipole interactions (these are smaller by the fine structure constant $\approx 1/137$) in the interaction Hamiltonian. This is equivalent to assuming a zero wavevector for the radiation, a good assumption since the photon wavevector q and the characteristic length α_0 generally satisfy $q\alpha_0 \ll 1$. In this dipole approximation,

$$H_{int} = -\mathbf{d} \cdot \mathbf{E}(\mathbf{R}, t), \tag{2.38}$$

$\mathbf{d}$ is the dipole moment operator and $\mathbf{E}(\mathbf{R}, t)$ is the electric field of the light. The components of the dipole moment operator are given by

$$\mathbf{d}_{nk} = \int u_n^* \mathbf{r} u_k d^3\mathbf{r} \equiv -e\mathbf{r}_{nk}, \tag{2.39}$$

where $\mathbf{r}$ is the electron coordinate with respect to the location of the nucleus at $\mathbf{R}$. The components of the operator H_{int} are given by

$$\Delta_{nk} = -\mathbf{d}_{nk} \cdot \mathbf{E}(\mathbf{R}, t) \tag{2.40}$$

The diagonal components of $\mathbf{d}_{nk}$ and Δ_{nk} are zero because $\mathbf{d}$ is an odd-parity operator.

For a monochromatic plane wave at angular frequency ω and linearly polarized in the direction ϵ, the electric field can be written as the sum of two fields

$$\mathbf{E}(\mathbf{R}, t) = \mathbf{E}^+(\mathbf{R}, t) + \mathbf{E}^-(\mathbf{R}, t) \tag{2.41}$$

with

$$\mathbf{E}^+(\mathbf{R}, t) = (1/2)\hat{\epsilon} E_0 e^{i[\mathbf{q}\cdot\mathbf{R} - (\omega t + \eta)]} \tag{2.42}$$

and

$$\mathbf{E}^{-}(\mathbf{R},t) = \mathbf{E}^{+*}(\mathbf{R},t) \tag{2.43}$$

where E_0 is the real electric field amplitude, $\hat{\epsilon}$ is thew polarization vector, and η is a phase factor. In calculating the transition probabilities one generally make the **Rotating Wave Approximation** in which the term with the rapidly varying phase factor $e^{i(\omega+\Omega)t}$ (where $\hbar\Omega = E_b - E_a$) and the large denominator $\omega + \Omega$.corresponding to $\mathbf{d}\cdot\mathbf{E}^{-}$, is neglected. In this approximation,

$$\Delta_{ba} = (\hbar/2)\chi_R e^{i[\mathbf{q}\cdot\mathbf{R}-(\omega t+\eta)]} = \Delta^{*}_{ab}, \tag{2.44}$$

where

$$\hbar\chi_R = e(\mathbf{r}_{ba}\cdot\hat{\epsilon})E_0 \tag{2.45}$$

and the quantity χ_R is known as the *Rabi frequency* at the resonance $\omega = \Omega$.

The matrix form of the interaction Hamiltonian can thus be written as

$$H_{int} = \begin{bmatrix} 0 & \Delta_{ba} \\ \Delta^{*}_{ba} & 0 \end{bmatrix} \tag{2.46}$$

The linear and nonlinear response of the system to electromagnetic field is determined by the macroscopic polarization P, which is related to the macroscopic dielectric polariazation density as

$$P = NTr\{\mathbf{d}\rho\} \tag{2.47}$$

where N is the number density in the ensemble.

The Relaxation Hamiltonian

The process which bring the ensemble back to thermal equilibrium include recombination, collisions with phonons and interaction with other electronic states. The relative time scales of these processes, and their relation to other characteristic times in the system such as laser pulse duration, determine the correct treatment of these relaxation processes.

The most general approach to the description of nonequilibrium properties of semiconductors excited by laser pulses is the quantum-kinetic equations approach based on non-equillibrium Green's functions [56]. These methods have been applied to the description of excitation and relaxation processes in laser-excited semiconductors.Numerical solutions of these equations have shown that non-Markovian behaviour becomes significant on time scales small compared to the dephasing times, a condition that is easily achieved for femptosecond photoexcitation not too far from a resonance. Under these conditions, the interband polarizations do not follow the pulse adiabatically, and the dephasing time is not an instantaneous function of its environment but depends on the "history" of the environment.

A simpler approach to the problem is to make the Markovian approximation under which the relaxation times are determined by the instantaneous distribution and polarization functions, and hence are time dependent. This approximation forms the basis for the classical Boltzmann equation approach to transport in semiconductors.

The simplest approach to the problem is to assume that the dynamical self-energies in the nonequilibrium Green's function approach can be replaced by constant phenomenological transverse and longitudinal relaxation rates for the relevant relaxation processes in the problem and simplify the relaxation Hamiltonian accordingly. Analysis of most coherent experiments and the semiconductor Bloch equations are based in this assumption. In this approach the relaxation Hamiltonian can be approximated as:

$$[H_R, \rho]_{bb} = -\rho_{bb}/T_1 \quad and \quad [H_R, \rho]_{ba} = -\rho_{ba}/T_2 \tag{2.48}$$

where T_1 is the lifetime of the state b and $1/T_2$,the transverse relaxation rate, is the sum of the recombination rate $(1/T_1)$ and the pure dephasing rate.One can think of T_2 sas the lifetime of the

coherent superposition state.

The relaxation-time approximation is valid in the limit that the response of the medium in which the system under study is embedded is either very fast or very slow compared to the system-medium interaction. It can be shown that the linear absorption shape is Lorentzian (corresponding to a homogeneously broadened line) in the limit of very fast response of the medium, and a Gaussian (corresponding to an inhomogeneously broadened line) in the limit of very slow response of the medium.

Optical Bloch Equations

The coupled equations of motion for the polarization and the population if an ensemble of independent two-level systems are known as Optical Bloch Equations, in analogy with the equations first derived by Bloch for the Spin systems. For simplification, we introduce a new notation and substitute $n = \rho_{bb}, 1 - n = \rho_{aa}$ and $p = \rho_{ba}$. Using the Liouville equation and the definitions for $T_1, T_2, \Delta_{ba}, \Delta^*_{ba}$ given above, one gets

$$\rho = \begin{bmatrix} n & p \\ p^* & 1-n \end{bmatrix} \tag{2.49}$$

$$i\dot{n} = -ig_r n + \frac{1}{\hbar}\left(\Delta_{ba}p^* - p\Delta^*_{ba}\right) \tag{2.50}$$

$$i\dot{p} = -igp + \frac{i}{\hbar}\Delta_{ba}(1-2n) \tag{2.51}$$

where $g_r = 1/T_1$ and $g = (i\Omega + 1/T_2)$. Equations (2.50) and (2.51) are known as the optical Bloch equations, and form the basis for analysing coherent transient experiments in independent two-level systems.

Solutions of the Optical Bloch Equations

The coupled optical Bloch equations cannot be solved analytically in the general case. One generally resorts to expanding the density matrix into a Taylor series in the incident fields amplitudes and ob-

tain a solution to the desired order. Numerical techniques have to be employed in the general case. We formally write the density n and polarization p as

$$n = n^{(0)} + n^{(1)} + n^{(2)} + n^{(3)} + ... \tag{2.52}$$

$$p = p^{(0)} + p^{(1)} + p^{(2)} + p^{(3)} + ... \tag{2.53}$$

with $n^{(0)} = 0$ and $p^{(0)} = 0$. For usual initial conditions of $n = 0$ and $p = 0$, it can be shown that the odd powers of n and the even powers of p are zero and low-order components of n and p are given by

$$i\dot{p}^{(1)} = -igp^{(1)} - \frac{1}{\hbar}\Delta_{ba} \tag{2.54}$$

$$i\dot{n}^{(2)} = -ig_r n^{(2)} + \frac{1}{\hbar}\left(\Delta_{ba}p^{(1)*} - p^{(1)}\Delta^*_{ba}\right) \tag{2.55}$$

$$i\dot{p}^{(3)} = -igp^{(3)} - 3\frac{1}{\hbar}\Delta_{ba}n^{(2)} \tag{2.56}$$

The three-pulse FWM experiment

We shown that in a three-pulse FWM experiment the sample is excited by three pulses in the directions $\mathbf{k}_1$, $\mathbf{k}_2$ and $\mathbf{k}_3$. The time delay between pulse 1 , 2 is $\Delta t_{12} = t_1 - t_2$ and between 1,3 is $\Delta t_{13} = t_1 - t_3$. The pulses create a FWM signal in the direction $\mathbf{k}_s = \mathbf{k}_1 + \mathbf{k}_2 - \mathbf{k}_3$. Assuming that the first pulse arrives at time $t = 0$,

$$\begin{aligned} E(\mathbf{R}, t) &= \mathcal{E}(\mathbf{R}, t)e^{i(\mathbf{k}_1\cdot\mathbf{R} - \omega_0 t)} + \mathcal{E}(\mathbf{R}, t + \Delta t_{12})e^{i(\mathbf{k}_2\cdot\mathbf{R} - \omega_0 t)} \\ &+ \mathcal{E}(\mathbf{R}, t + \Delta t_{13})e^{i(\mathbf{k}_3\cdot\mathbf{R} - \omega_0 t)} \end{aligned} \tag{2.57}$$

where $\mathcal{E}(\mathbf{R}, t)$ is the electric field pulse shape at $\mathbf{R}$, and Ω_0 corresponds to thew peak of the mode-locked laser spectrum. For this Electric field,

$$\begin{aligned} \frac{\Delta_{ba}}{\hbar} &= \frac{er_{ba}}{\hbar}e^{-i\omega_0 t}\big[\mathcal{E}(\mathbf{R}, t)e^{i\mathbf{k}_1\cdot\mathbf{R}} + \mathcal{E}(\mathbf{R}, t + \Delta t_{12})e^{i\mathbf{k}_2\cdot\mathbf{R}} \\ &+ \mathcal{E}(\mathbf{R}, t + \Delta t_{13})e^{i\mathbf{k}_3\cdot\mathbf{R}}\big] \equiv ie^{-i\omega_0 t}f(t) \end{aligned} \tag{2.58}$$

If we define $p^{(1)} = p^{(1)}(t)e^{-i\omega_0 t}$, then

$$\dot{p}^{(1)}(t) + Gp^{(1)}(t) = f(t) \tag{2.59}$$

where $G = 1/T_2 + i(\Omega - \omega_0)$, has the solution

$$p^{(1)} = \int_{-\infty}^{t} dt' e^{-G(t-t')} f(t') e^{i\omega_0 t} \tag{2.60}$$

The signal along $\mathbf{k}_s$ results from the diffraction of the pulse 1 from a grating created by pulses 2 and 3, or from a diffraction of pulse 2 from grating created by pulses 1 and 3 i.e., it is related to either $p^{(3)}_{123}$ or $p^{(3)}_{213}$. We therefore need to calculate only the $\mathbf{k}_2 - \mathbf{k}_3$ and $\mathbf{k}_1 - \mathbf{k}_3$ components in the density $n^{(2)}$, i.e., $n^{(2)}_{23}$ and $n^{(2)}_{13}$ which, using Eq.(2.50), can be shown to be given by

$$n^{(2)}_{i3} = \int_{-\infty}^{t} dt'' e^{-(t-t'')/T_1} f_{i3}(t'') \quad (i = 1, 2) \tag{2.61}$$

where

$$\begin{aligned} f_{13}(t) &= \frac{e^2|r_{ba}|^2}{\hbar^2} e^{i(\mathbf{k}_1 - \mathbf{k}_3)\cdot\mathbf{R}} \left[\mathcal{E}(\mathbf{R}, t) \int_{-\infty}^{t} dt' \mathcal{E}(\mathbf{R}, t' + \Delta t_{13}) e^{-G^*(t-t')} \right. \\ &+ \left. \mathcal{E}(\mathbf{R}, t + \Delta t_{13}) \int_{-\infty}^{t} dt' \mathcal{E}(\mathbf{R}, t') e^{-G(t-t')} \right] \end{aligned} \tag{2.62}$$

$$\begin{aligned} f_{23}(t) &= \frac{e^2|r_{ba}|^2}{\hbar^2} e^{i(\mathbf{k}_2 - \mathbf{k}_3)\cdot\mathbf{R}} \left[\mathcal{E}(\mathbf{R}, t + \Delta t_{12}) \int_{-\infty}^{t} dt' \mathcal{E}(\mathbf{R}, t' + \Delta t_{13}) e^{-G^*(t-t')} \right. \\ &+ \left. \mathcal{E}(\mathbf{R}, t + \Delta t_{13}) \int_{-\infty}^{t} dt' \mathcal{E}(\mathbf{R}, t' + \Delta t_{12}) e^{-G(t-t')} \right] \end{aligned} \tag{2.63}$$

The third order polarizations p^3_{123} and p^3_{213} can be obtained from Eq.(2.51)

$$p^{(3)}_{123} = - 2i(e|r_{ba}|/\hbar)^3 e^{-i\Omega t} e^{-t/T_2} \int_{-\infty}^{t} dt''' \int_{-\infty}^{t''} dt'' \int_{-\infty}^{t''} dt' e^{Gt'''} e^{-(t'''-t'')/T_1}$$
$$\times \mathcal{E}(\mathbf{R}, t''') \Big[\mathcal{E}(\mathbf{R}, t'' + \Delta t_{12}) \mathcal{E}(\mathbf{R}, t' + \Delta t_{13}) e^{-G^*(t''-t')}$$
$$+ \mathcal{E}(\mathbf{R}, t'' + \Delta t_{13}) \mathcal{E}(\mathbf{R}, t' + \Delta t_{12}) e^{-G(t''-t')} \Big] \tag{2.64}$$

$$p^{(3)}_{213} = - 2i(e|r_{ba}|/\hbar)^3 e^{-i\Omega t} e^{-t/T_2} \int_{-\infty}^{t} dt''' \int_{-\infty}^{t''} dt'' \int_{-\infty}^{t''} dt' e^{Gt'''} e^{-(t'''-t'')/T_1}$$
$$\times \mathcal{E}(\mathbf{R}, t''' + \Delta t_{12}) \Big[\mathcal{E}(\mathbf{R}, t'') \mathcal{E}(\mathbf{R}, t' + \Delta t_{13}) e^{-G^*(t''-t')}$$
$$+ \mathcal{E}(\mathbf{R}, t'' + \Delta t_{13}) \mathcal{E}(\mathbf{R}, t') e^{-G(t''-t')} \Big] \tag{2.65}$$

In order to determine the signal at a given point in space and time, the Maxwell's propagation equations have to be solved in general. However for an optical thin sample with thickness small compared to the wavelength of light, the signal diffracted signal along $\mathbf{k}_s$ can be approximated by the macroscopic polarization given by

$$P^{(3)}_{ij3} = NTr\{d\rho\} \tag{2.66}$$

with appropriate order and component of ρ

These equations can be numerically integrated to obtain the temporal evolution of the FWM signal (SR-FWM) in the $\mathbf{k}_s$ direction.

$$S^{(3)}_{ij3}(\Delta t_{12}, \Delta t_{13}, \omega) = | \int_{-\infty}^{\infty} P^{(3)}_{ij3}(t) e^{i\omega t} dt \, |^2 \tag{2.67}$$

and the time integrated (TI-FWM) signal

$$I^{(3)}_{ij3}(\Delta t_{12}, \Delta t_{13}) = \int_{-\infty}^{\infty} |P^{(3)}_{ij3}(t) \, |^2 \, dt \tag{2.68}$$

as a function of the time delays Δt_{12} and Δt_{13} .

Analytical Solutions for Delta Pulses

The iterative equations can be solved numerically for a given pulse shape. However, we consider in this section a simpler case of pulses that can be described by the Dirac δ-functions in time. We further assume tha the sample is thin and the propagation effects can be neglected, as discussed above, and the first pulse arrives at the sample at time $t = 0$, and the other pulses after Δt_{12} and Δt_{13}. In this case , Eq.(2.59) gives

$$p^{(1)} = \frac{er_{ba}}{i\hbar} E_0 \left[e^{-Gt}\theta(t) + e^{-G(t+\Delta t_{12})}\theta(t+\Delta t_{12}) + e^{-G(t+\Delta t_{13})}\theta(t+\Delta t_{13}) \right] e^{i\omega t} \tag{2.69}$$

where $\theta(t)$ is the Heaviside step function, and we recall that $G = 1/T_2 + i(\Omega - \omega_0)$. Thus at resonance ($\Omega = \omega_0$), the first order polarization is a sum of three damped oscillations at ω_0 displaced by a time delays Δt_{12} and Δt_{13}.

Similarly we can integrate Eq.(2.61) and take

$$\begin{aligned} n_{13}^{(2)} &= \frac{e^2|r_{ba}|^2}{\hbar^2} E_0^2 \\ &\times \left[\theta(t)\theta(\Delta t_{13}) e^{-t/T_1} e^{-G^*\Delta t_{13}} + \theta(t+\Delta t_{13})\theta(-\Delta t_{13}) e^{(t+\Delta t_{13})/T_1} e^{G\Delta t_{13}} \right] \end{aligned} \tag{2.70}$$

There are two terms of which only one is non-zero for a given Δt_{13}: the first term in non-zero only when $\Delta t_{13} > 0$, i.e., for positive time delays, whereas the second term in non-zero only for negative time delays ($\Delta t_{13} < 0$). This equation simply states that, after the arrival of the second pulse (pulse 1 for $\Delta t_{13} > 0$, and pulse 3 for $\Delta t_{13} < 0$), $n_{13}^{(2)}$ decreases exponentially with Δt_{13}. For a given Δt_{13}, n_{13}^2 decreases with the population decay constant T_1 as a function of time. Similar results are obtained for negative Δt_{13}, as well for $n_{23}^{(2)}$.

This process can be repeated to obtain an expression for the third order polarization on the $\mathbf{k}_s$ direction from Eq.(2.65). For the $p_{213}^{(3)}$ we obtain

$$\begin{aligned} p^{(3)}_{213} &= -\frac{e^3|r_{ba}|^3}{\hbar^3}E_0^3 e^{-i\omega t}e^{-t/T_2}e^{i\mathbf{k}_s\cdot\mathbf{R}}\theta(t+\Delta t_{12})e^{-G\Delta t_{12}} \\ &\quad\times[\theta(\Delta t_{13})\theta(-\Delta t_{12})e^{-\Delta t_{12}/T_1}e^{-G^*\Delta t_{13}} \\ &+ \theta(\Delta t_{13}-\Delta t_{12})\theta(-\Delta t_{13})e^{(\Delta t_{12}-\Delta t_{13})/T_1}e^{-G\Delta t_{13}}] \quad (2.71) \end{aligned}$$

from which we obtain the decay of the third order polarization for given time delays between the pulses.

2.4 Coulomb correlations in semiconductors

Semiconductors are a highly complex, interacting many-body system. Incoming photons excite electrons and holes. If we neglet the Coulomb interactions between them, we can treat each state in k-space as a separate two-level system. Optical experiments in semiconductors have been explained using multi-level models (see e.g. Refs [111, 112]). However, the Coulomb interaction has drastic effects even on the linear optical properties of the semiconductor. Ignoring these interactions, or including them in *ad hoc* manner, is a poor way to explain the nonlinear results.

To account for the interactions between photo-excited electrons and holes, we need to start from the Hamiltonian for the electron-hole subsystem of the semiconductor [6]

$$\begin{aligned} H_{tot} &= \sum_k \left[\epsilon_{c\mathbf{k}}\hat{e}^\dagger_{\mathbf{k}}\hat{e}_{\mathbf{k}} + \epsilon_{v\mathbf{k}}\hat{h}^\dagger_{\mathbf{k}}\hat{h}_{\mathbf{k}}\right] \\ &+ \frac{1}{2}\sum_{\mathbf{k}\neq\mathbf{k'}} V_{\mathbf{q}}\left[\hat{e}^\dagger_{\mathbf{k}+\mathbf{q}}\hat{e}^\dagger_{\mathbf{k'},-\mathbf{q}}\hat{e}_{\mathbf{k'}},\hat{e}_{\mathbf{k}} + \hat{h}^\dagger_{\mathbf{k}+\mathbf{q}}\hat{h}^\dagger_{\mathbf{k'},-\mathbf{q}}\hat{h}_{\mathbf{k'}},\hat{h}_{\mathbf{k}} - 2\hat{e}^\dagger_{\mathbf{k}+\mathbf{q}}\hat{h}^\dagger_{\mathbf{k'},-\mathbf{q}}\hat{h}_{\mathbf{k'}},\hat{e}_{\mathbf{k}}\right] \\ &- \sum_{\mathbf{k}}\left[\mu_{cv}E(t)\hat{e}^\dagger_{\mathbf{k}}\hat{h}^\dagger_{-\mathbf{k}} + \mu^*_{cv}E^*(t)\hat{h}_{-\mathbf{k}}\hat{e}_{\mathbf{k}}\right] \quad (2.72) \end{aligned}$$

The first line of this equation gives the single particle energies of the electrons an holes. The operator $\hat{e}^\dagger_{\mathbf{k}}$ creates an electron with

wavevector k and the $\hat{h}^{\dagger}_{\mathbf{k}}$ creates a hole. The $\epsilon_{c\mathbf{k}}$ and $\epsilon_{v\mathbf{k}}$ give the dispersion of the conduction and valence bands respectively. The second line of the Eq.(2.73) describes the Coulomb interaction between electrons in the first term, between holes in the second terms, and between electrons and holes in the third term. $V_{\mathbf{q}}$ is the unscreened Coulomb potential in $\mathbf{k}$-space. The last line describes the interaction between the semiconductor and the applied electric field. The dipole momentum $\vec{\mu}_{cv}$ can be taken to be independent of the wavevector $\mathbf{k}$. We consider the band dispersions to be parabolic, and given by the effective mass approximation ($\hbar = 1$):

$$\epsilon_{c\mathbf{k}} = E_{c,0} + \frac{k^2}{2m_e^*} \quad and \quad \epsilon_{v\mathbf{k}} = E_{v,0} + \frac{k^2}{2m_h^*} \tag{2.73}$$

The bandgap ($E_{c,0} - E_{v,0}$) contains the Coulomb interaction of the full valence band.

The polarization is given by

$$\vec{P} = \sum_{\mathbf{k}} \mu^* \langle \hat{P}_{\mathbf{k}} \rangle = \sum_{\mathbf{k}} \mu^* \langle \hat{h}_{\mathbf{k}} \hat{e}_{\mathbf{k}} \rangle \tag{2.74}$$

If we write the Heisenderg equation of motion for the operator $\hat{P}_{\mathbf{k}}$, we fond that in addition to being driven by other two particle correlations (polarization and electron or hole population), the Coulomb interaction couples the two particle correlations to four particle correlations (products of four operators). To solve our equation, we must solve equations of motion for these four particle correlations. These are in turn drives be six particle correlations, and so on in an infinite hierarchy. In order to solve the system, we must make some approximations which truncate the hierarchy an give a closed set of equations.

2.4.1 Bloch equations for Semiconductors

The most common method for dealing with this problem has been to factorize thw four particle correlations into products of two particle correlations, and then make the random phase approximation (RPA), wich neglects the terms which oscillate rapidly due to large momentum differences. The RPA is also called the time dependent Hartree-Fock approximation. This leads to a closed set of equations for the two-particle density matrix elements ($n_{e,\mathbf{k}}, n_{h,\mathbf{k}}$ and $P_{\mathbf{k}}$),well known as semiconductor Bloch equations (SBE)[29], given here within the relaxation time approximation:

$$\begin{aligned} i\frac{\partial}{\partial t}P_{\mathbf{k}} &= (\epsilon_{c,\mathbf{k}} + \epsilon_{h,\mathbf{k}} - i\gamma) - \sum_{\mathbf{q}\neq\mathbf{k}} V_{\mathbf{k}-\mathbf{q}}P_{\mathbf{q}} - \mu_{cv}E(t)\left[1 - n_{e,\mathbf{k}} - n_{h,\mathbf{k}}\right] \\ &+ \sum_{\mathbf{q}\neq\mathbf{k}} V_{\mathbf{k}-\mathbf{q}}\left[P_{\mathbf{q}}(n_{e,\mathbf{k}} + n_{h,\mathbf{k}}) - P_{\mathbf{k}}(n_{e,\mathbf{q}} + n_{h,\mathbf{q}})\right] \end{aligned} \tag{2.75}$$

$$i\frac{\partial}{\partial t}n_{j,\mathbf{k}} = -2Im\left\{P^*_{\mathbf{k}}\left[\mu_{cv}E(t) + \sum_{\mathbf{k}\neq\mathbf{q}} V_{\mathbf{k}-\mathbf{q}}P_{\mathbf{q}}\right]\right\} - \frac{1}{T_1}(n_{j,\mathbf{k}}) \quad (j = e, h) \tag{2.76}$$

The density matrix elements in the Equations (2.76) , (2.77) are driven by both the electric field of the laser and a term due to the polarization from all other k-states.The SBE have been quite successfull in explaining many experiments in semiconductors, such as the AC stark effect [46, 47],TR-FWM effects[48], and photon echoes from continuum states [49, 50].

One very important effect of the Coulomb interaction is the existence of a FWM signal for $\Delta t < 0$, seen in experiments on GaAs quantum wells [51, 52]. The prediction of rise time of $T_2/4$ is a general result of the SBE, independent for the excitation or the material, assuming the system is homogeneously broadened. For a inhomogeneous system there is a weaker signal for $\Delta t < 0$ [53].

It is possible to transform the SBE from k-space into the exciton basis [3]. A useful model can be extracted by averaging over the lowest lying exciton states, and generating an equation of motion for a single average polarization, P. The average polarization model (APM) was introduced to clarify the RPA theory for FWM, since it captured the essential physics while simplifying the equations to keep the interpratation transparent [52]. In addition to the averaging, we will make the assumption that we are in the coherent regime, and that the length of the Bloch vector is constant, or $n \approx |P|^2$. We then hav only a single equation to solve perturbatively:

$$i\frac{\partial}{\partial t}P(t) = (\Omega - i\gamma)P(t) - \mu E(t)\left[1 - \frac{|P(t)|^2}{P_s^2}\right] + VP(t)|P(t)|^2 \quad (2.77)$$

Here, P_s is a saturation parameter an V is an effective Coulomb coupling parameter.It is straightforward to generalize the Eq.[2.78]to include several levels [3] for example the different hole states. The Average Polarization Model (AVM) has been useful in explaining a number of experiments at the RPA level[52]. However, for a quantitaly accurate simulation of experiments, it is necessary to use the full numerical solutions of the SBE, including all band structure and selection rules.

We can also apply the RPA factorization technique when we have a magnetic field applied to the sample. We start by expanding the magnetoexciton states in terms of the Landau levels, and generate a set of equations for the polarization P_n and the excited population n_n, of the n Landau level respectively [54]:

$$i\frac{\partial}{\partial t}P_n = \left(E_n - 2\sum_{n'} V_{n,n'}n_{n'}\right)P_n - (1-2n_n)\left(\mu_{cv}E(t) + \sum_{n'} V_{nn'}P_{n'}\right) \quad (2.78)$$

$$\frac{\partial}{\partial t} n_n = 2Im \left\{ P_n \left(\mu^*_{cv} E^*(t) + \sum_{n'} V_{nn'} P^*_{n'} \right) \right\} \tag{2.79}$$

The Coulomb interaction $V_{nn'}$ couples different Landau levels together. Eqs.(2.79) and (2.80) have been solved numericall for up to 1000 Landau levels [54, 55]. An APM can be generated from this system as well, by keeping only the few Landau levels which are directly excited.

2.5 The Dynamics controlled truncation scheme

Over the past several years, numerous experimental effects have been measured which require a theoretical description beyond the RPA, such the contribution of biexcitons to the nonlinear optical response[57, 58, 100].The correct interpretation of these experiments requires a formalism which naturally extends the SBE in the dynamics controlled truncation scheme (DCTS) [8, 9, 10]

Calculating the optical responce starts, as before, with many-body Hamiltonian Eq.(2.73), and the Polarization's equation of motion. However, unlike in the RPA treatment, the four-particle correlations are not factorized. The results of the DCTS theory are several mathematical theorems which show that certain higher correlations contribute to higher order in the electric field, an can thus be neglected for a calculation of the optical response to a given order [8, 60]. This can be accomplished because of the correspondence between the number of the electron-hole pairs in the system and the sequence of photon absorption and emission. The theory systematically includes all correlations which contribute to a specified order. In the limit of third order processes ($\chi^{(3)}$- truncation), and within the coherent limit,there is only one four-particle correlation function which must be taken into account, the biexciton operator B [60, 71].The effects of additional four-particle correlations, such as

the exciton density, and correlations which contribute to fifth order in the electric field, have been investigated as well [62, 63].

The necessary four-particle correlation, $B^{ehe'h'} = \langle \hat{e}\hat{h}\hat{e'}\hat{h'}\rangle - \langle \hat{e}\hat{h}\rangle\langle \hat{e'}\hat{h'}\rangle + \langle \hat{e}\hat{h'}\rangle\langle \hat{e'}\hat{h}\rangle$ gives the biexcitonic structure, both the bound and unbound states. By subtracting the factorized components, we let B characterize the deviation from the RPA theory [71].The DCTS equations will then contain several driving terms: (1) the Pauli Blocking (PB) nonlinearity present even in atomic systems,(2) the Coupomb interaction of the RPA theory, and (3) a new source term which describes the coupling between excitons and the full spectrum of two-exciton states. This final driving term is beyond the RPA, and has a dramatic effect on the FWM signal.

To understand the effect of this correlation, we can update the APM to include higher order correlations, based on the DCTS microscopic theory [71, 100]. For the case of co-circularly polarized laser pulses (which cannot excite a bound biexciton), the new APM equation of motion for the polarization is [100]:

$$\begin{aligned} i\frac{\partial}{\partial t}P(t) &= (\Omega - i\gamma)P(t) - \mu E(t)\left[1 - \frac{|P(t)|^2}{P_s^2}\right] \\ &+ VP(t)|P(t)|^2 + V_B\mathcal{B}(t)P(t)^* \end{aligned} \tag{2.80}$$

where $\mathcal{B}(t)$ is an effective four-particle correlation function describing the continuum of unbound biexciton states, and satisfying the equation

$$i\frac{\partial}{\partial t}\mathcal{B}(t) = (2\Omega - i\Gamma)\mathcal{B}(t) + P(t)^2 \tag{2.81}$$

Unlike the Pauli blocking nonlinearity which exists only for $\Delta t > 0$, or even the mean field X-X nonlinearity for which the rise time is half the decay time, a new source term due exciton-exciton correlations grows in a non-exponential fashion, and for $\Delta t < 0$ can dominate the signal.

These equations can easily be generalized to include the four Zee-

man split heavy hole and light hole transitions in a magnetic field [65] . The updated average polarization model has also been used to explain the effects of the bound biexciton on the pumb-probe spectrum of ZnSe Quantum Wells [66, 67]. The functional form of the model is directly related to the full microscopic theory, which makes it qualitatively different from a simple multi-level scheme.

Several different formalisms have been developed which are able to account for higher order correlations, and many are in fact equivalent to the DCTS [4, 69, 70]. Recently a theory has been presented which bridges the gap between the DCTS ant theories based on Green functions which explain the build up of screening effects[71]. Within this theory it is possible to simulate remarkable accuracy the results of FWM in bulk GaAs in a high magnetic field.

Limits of the DCTS

The DCTS theory is successful because in many semiconductor systems, there is a correspondence between the number of electron-hole pairs and the absorption of the photons. In semiconductor systems where this scheme is applicable, we have been to explain the experimental results with incredible accuracy. However, if the correspondence break down, the DCTS fails. This is the case, for instance, in modulation doped quantum wells where a high mobility 2DEG exists in the sample before excitation, and can react to photons and photopexcited carriers.

2.6 Conclusions

In this chapter we reviewed FWM in atomic systems, and also how the Coulpmb interaction change the picture. We first discussed the properties of GaAs quantum wells, and the physics of the 2DEG in a magnetic field. We then discussed the ultrafast nonlinear optical experiments in semiconductors, introducing the FWM method. To

illustrated the physics of all this experiments we also discussed the two level system. We then reviewed the theoretical methods that have been used to explain such experiments and more specifically the Semiconductor Bloch equations and Dynamics Controlled Truncation Scheme.

Chapter 3

Theoretical framework

3.1 Hamiltonian & Collective excitations

The general second-quantization Hamiltonian describing the system in the absence of optical fields reads

$$H = \sum_{\alpha}(E_g + \varepsilon_{\alpha}^{c})\hat{e}_{\alpha}^{\dagger}\hat{e}_{\alpha} + \sum_{\alpha}\varepsilon_{\alpha}^{v}\hat{h}_{\alpha}^{\dagger}\hat{h}_{\alpha} + H_{int}, \tag{3.1}$$

where we assume two bands well–separated in energy by E_g: a "conduction band" and a "valence band". The operators $\hat{e}_{\alpha}^{\dagger}$ ($\hat{h}_{\alpha}^{\dagger}$) create a conduction (valence) electron (hole) state labeled by a composite index α that contains all relevant single -particle quantum numbers $\alpha = (k, n, \sigma)$ of a σ LLn conduction (valence) state, $\varepsilon_{\alpha}^{e,h}$ are the corresponding energies, determined by the bandstructure (e.g. Kohn–Sham orbitals).[101]. H_{int} describes e–e, e–h, h–h, Coulomb interactions:

$$H_{int} = \frac{1}{2}\sum_{\alpha_1\alpha_2\alpha_3\alpha_4}\Big[v^{ee}_{\alpha_1\alpha_2\alpha_3\alpha_4}\hat{e}^{\dagger}_{\alpha_3}\hat{e}^{\dagger}_{\alpha_1}\hat{e}_{\alpha_2}\hat{e}_{\alpha_4} + v^{hh}_{\alpha_1\alpha_2,\alpha_3\alpha_4}\hat{h}^{\dagger}_{\alpha_3}\hat{h}^{\dagger}_{\alpha_1}\hat{h}_{\alpha_2}\hat{h}_{\alpha_4} - v^{eh}_{\alpha_1\alpha_2,\alpha_3\alpha_4}\hat{h}^{\dagger}_{\alpha_3}\hat{e}^{\dagger}_{\alpha_1}\hat{e}_{\alpha_2}\hat{h}_{\alpha_4} - v^{he}_{\alpha_1\alpha_2,\alpha_3\alpha_4}\hat{e}^{\dagger}_{\alpha_3}\hat{h}^{\dagger}_{\alpha_1}\hat{h}_{\alpha_2}\hat{e}_{\alpha_4}\Big]. \tag{3.2}$$

In the two-dimensional system the Coulomb interaction matrix elements $v^{ij}_{\alpha_1\alpha_2,\alpha_3\alpha_4}$ (with $i, j = e, h$) in the Landau gauge are given by

$$v^{ij}_{\alpha_1\alpha_2,\alpha_3\alpha_4} = \int \frac{d\mathbf{q}}{(2\pi)^2}\, v_q\, F^i_{\alpha_1\alpha_2}(\mathbf{q}) F^j_{\alpha_3\alpha_4}(-\mathbf{q}), \tag{3.3}$$

where v_q is the Fourier transformed Coulomb potential [9]

$$v_q = \frac{2\pi e^2}{\epsilon q} \tag{3.4}$$

ϵ is the material dielectric constant, $q = \sqrt{q_x^2 + q_y^2}$ and

$$F^e_{\alpha_1\alpha_2}(\mathbf{q}) = \phi_{n_1 n_2}(\mathbf{q}) e^{iq_x(k_1+k_2)\ell^2/2} \delta_{k_1,k_2+q_y} \delta_{\sigma_1,\sigma_2}, \tag{3.5}$$

and

$$F^h_{\alpha_1\alpha_2}(\mathbf{q}) = F^e_{-\alpha_2,-\alpha_1}(\mathbf{q})\ ,\ -\alpha = (-k, n, \sigma). \tag{3.6}$$

In the above equations,

$$\phi_{mn}(\mathbf{q}) = \frac{n!}{m!}\left[\frac{(-q_y + iq_x)l}{\sqrt{2}}\right]^{m-n} L_n^{m-n}\left(\frac{q^2\ell^2}{2}\right) e^{-q^2\ell^2/4} \tag{3.7}$$

for $m \geq n$ and $\phi_{mn}(\mathbf{q}) = \phi^*_{nm}(-\mathbf{q})$ for $m < n$, where L_n^{m-n} is the generalized Laguerre polynomial.

$$L_n^{m-n}(x) = \sum_{r=0}^{n} \frac{(-1)^r m! x^r}{(n-r)!(m-n+r)!r!} \tag{3.8}$$

The Coulomb's potential symmetry lead us to use the polar coordinates, obtained by substitung $q_x = q\cos(\theta)$ and $q_y = q\sin(\theta)$,for a more useful expression of $\Phi(\mathbf{x})$:

$$\Phi(\mathbf{q}) = \frac{n!}{m!}\left(\frac{iql}{\sqrt{2}}\right)^{m-n} e^{i(m-n)\theta} L_n^{m-n}\left(\frac{q^2l^2}{2}\right) e^{-q^2l^2/4} \tag{3.9}$$

By treating the coupling of the optical field $E(t)$ within the dipole approximation, [6] the total Hamiltonian reads

$$H(t) = H - \left[d(t)\hat{X}^\dagger + h.c.\right] \tag{3.10}$$

where $d(t)$=$\mu E(t)$ is the Rabi energy, μ is the interband transition matrix element,determined by the bandstructure, and $\hat{X}^\dagger$ is the interband transition operator, expressed as a linear combination of e–h pair creation operators $\hat{e}^\dagger_\alpha \hat{h}^\dagger_\beta$.

To demonstrate the generic qualitative features due to the non–equilibrium correlations, one can adopt a simple two–band Hamiltonian H describing two–dimensional electrons and holes subject to a perpendicular magnetic field.[6, 12] We also consider for simplicity right–circularly (σ_+) polarized light, which gives a single LL0 absorption peak via a single interband transition that creates spin–$\downarrow$ electrons, and simplifies he interpretation of the experiments. [85] In the Landau gauge,α =(k, n, σ), where k is proportional to the cyclotron orbit center x–coordinate, n is the LL index, and s denotes the spin. The electron and hole cyclotron energies($\hbar$=1) are

$$\varepsilon^{e,h}_\alpha = \omega^{e,h}_c(n + 1/2), \qquad \omega^{e,h}_c = \frac{eB}{m_{e,h}} \tag{3.11}$$

The optical dynamics of the Quantum Hall system is determined by interband and intraband excitations of the ground state $|G\rangle$. In the case of photoexcitation with right-circularly polarized light,wich excites spin-$\downarrow$ e-h pairs, the transition operator $X^\dagger$ can be expanded in terms of the exciton creation operators $X^\dagger_i$ that create {1-LLn-e + 1-LLm-h} excitons with total momentum $\mathbf{q}$ is

$$\hat{X}^\dagger_{\mathbf{q}nm} = \frac{1}{\sqrt{N}} \sum_k e^{ikq_x\ell^2} \hat{e}^\dagger_{k+q_y/2n\downarrow} \hat{h}^\dagger_{-k+q_y/2m\downarrow}. \tag{3.12}$$

In the absence of disorder, the selection rules allow the direct photoexcitation of $\mathbf{q}$=0. Furthermore, in a ideal system, the only allowed optical transitions correspond to $m = n$. We then have that e–h pairs, created by

$$\hat{X}^\dagger_n = \hat{X}^\dagger_{q=0nn} = \sum_k \hat{e}^\dagger_{kn\downarrow} \hat{h}^\dagger_{-kn\downarrow} \tag{3.13}$$

In the realistic system the disorder can relax the momentum conservation condition [20,37,70,106], thus mixing exciton states with different momenta.

The Pauli exchange effects between such Xs are described by the deviation of their commutator from bosonic behaviour:

$$[\hat{X}_n, \hat{X}_m^\dagger] = \delta_{nm}(1 - \hat{\nu}_{nm}), \tag{3.14}$$

where $\hat{\nu}_{nm} = \hat{\nu}^e_{nm} + \hat{\nu}^h_{nm}$. The operators

$$\hat{\nu}^h_{nm} = \frac{1}{N}\sum_k \hat{h}^\dagger_{-kn\downarrow}\hat{h}_{-km\downarrow}\ ,\ \hat{\nu}^e_{nm} = \frac{1}{N}\sum_k \hat{e}^\dagger_{kn\downarrow}\hat{e}_{km\downarrow} \tag{3.15}$$

describe the LLn filling factors(n=m), due to ground state or photoexcited carriers, and create inter–LL excitations ($n \neq m$).For the intraband excitations, we introduce the collective electron and hole excitation operators analogous to the magnetoexciton operato Eq.(5.3):

$$\hat{\rho}^e_{\mathbf{q}nm\sigma} = \frac{1}{\sqrt{N}}\sum_k e^{iq_xk\ell^2}\hat{e}^\dagger_{k+q_y/2n\sigma}\hat{e}^\dagger_{k-q_y/2m\sigma} \tag{3.16}$$

and

$$\hat{\rho}^h_{\mathbf{q}nm\sigma} = \frac{1}{\sqrt{N}}\sum_k e^{iq_xk\ell^2}\hat{h}^\dagger_{-k+q_y/2n\sigma}\hat{h}^\dagger_{-k-q_y/2m\sigma}, \tag{3.17}$$

Similar to the collective excitations of quantum liquids, [**?**] the states $\hat{\rho}_{\mathbf{q}n'n\sigma}|G\rangle$ have been used as a basis to describe the neutral excitations of the Laughlin state at certain ν (single mode approximation).[24, 25, 33, 72] Within this approximation, the neutral collective charge excitations of the 2DEG correspond to Magnetoplasmon modes created by $\hat{\rho}_{\mathbf{q}nm\sigma}$.[24, 25, 33, 72]

In contrast to phonons,[10] the Pauli exchange effects between excitons and 2DEG collective excitations, as well as between photoexcited carriers, are described by the commutators:

$$\left[\hat{\rho}^{e}_{\mathbf{q}nm\sigma}, \hat{X}^{\dagger}_{\mathbf{q'}n'm'}\right] = \frac{1}{\sqrt{N}}\delta_{\sigma\downarrow}\delta_{mn'}e^{i(\mathbf{q}\times\mathbf{q'})_z\ell^2/2}\hat{X}^{\dagger}_{\mathbf{q}+\mathbf{q'}nm'} \tag{3.18}$$

and

$$\left[\hat{\rho}^{h}_{\mathbf{q}nm\sigma}, \hat{X}^{\dagger}_{\mathbf{q'}n'm'}\right] = \frac{1}{\sqrt{N}}\delta_{\sigma\downarrow}\delta_{mm'}e^{-i(\mathbf{q}\times\mathbf{q'})_z\ell^2/2}\hat{X}^{\dagger}_{\mathbf{q}+\mathbf{q'}n'n} \tag{3.19}$$

A LLm $\rightarrow$ LLn MP can be considered as an "exciton" formed by a LLn electron and a hole in the LLm 2DEG.However, such "excitons"couple to the 2DEG electrons. Comparisons to small system exact diagonalizations showed that the single mode approximation describes well the excitation energy dispersion for ν=$1/(2m+1)$, where m is an integer, at small and intermediate wavevectors q close to the roton minimum. However, it does not work well for other ν or for large q. In this case, one can consider composite fermion quasielectron–quasihole excitations.[72, 75]

The collective 2DEG excitations at ν=$n/(2mn+1)$, where n is an integer,are then described by acting with the collective electron and hole excitation operators Eq.(3.17 - 3.18) on the Slater determinant of n filled LLs,multiplying by the Jastrow factor, and then projecting to the lowest LL.[72] For ν=$1/(2m+1)$, the two above approaches produce the same results for small q, while for other ν they differ for all q.

Analogous to the above 2DEG "excitons", we introduce the zero momentum interband exciton states

$$|X_n\rangle = \hat{X}^{\dagger}_{\mathbf{q}=0nn}|G\rangle \tag{3.20}$$

The difference from undoped semiconductors is that $\hat{X}^{\dagger}_{n}$ act on the strongly correlated ground state $|G\rangle$ of the Hamiltonian H with N_e electrons. Using Eq.(3.13), we obtain the orthogonality relation

$$\langle X_n|X_m\rangle = (1-\nu_n)\delta_{nm}, \tag{3.21}$$

where

$$\nu_n = \langle G|\hat{\nu}^e_{nn}|G\rangle \tag{3.22}$$

is the ground state filling factor of the LLn electron states. At ν=1, excitons and quasiexcitons coincide. At fractional ν, exact diagonalization calculations at ν=1/3 [75] showed that the zero momentum exciton and quasiexciton states give equivalent results when used to approximate the q=0 eigenstates.

3.2 Interaction Effects

In this section we obtain equations of motion for the nonlinear polarization, in a form that establishes the connection with undoped semiconductor and atomic systems. We also use the ideal 2D system Hamiltonian to discuss the interaction effects in a system with hidden symmetry, which simplifies the optical response [106]

We start by expanding the interband transition operator $\hat{X}$, which describes the coupling of the optical field in the Hamiltonian $H(t)$, in terms of e–h pair creation operators:

$$\hat{X}^\dagger = \sqrt{N}\sum_n \hat{X}^\dagger_n \tag{3.23}$$

In the ideal 2D system, where

$$\hat{X}^\dagger = \sum_{nk} \hat{e}^\dagger_{kn}\hat{h}^\dagger_{-kn} \tag{3.24}$$

a natural choice are the zero–momentum LL exciton operators $\hat{X}^\dagger_{\mathbf{q}=0nn}$ due to the hidden symmetry.[106] However, in our discussion

below $\hat{X}_n^\dagger$ can be any combination of e–h creation operators $\hat{e}_\alpha^\dagger \hat{h}_\beta^\dagger$.

Within the dipole approximation, the optical response is described by the polarization (e–h coherence) [12, 5]

$$P(t) = \mu \sum_n P_n(t), \qquad P_n(t) = \frac{\langle \hat{X}_n \rangle}{\sqrt{N}}, \tag{3.25}$$

whose equation of motion is obtained from the general equation for an $\hat{O}$ operator

$$i\partial_t \langle \hat{O} \rangle = \langle [\hat{O}, H] \rangle - d(t)\sqrt{N} \sum_m \langle [\hat{O}, \hat{X}_m^\dagger] \rangle - d^*(t)\sqrt{N} \sum_m \langle [\hat{O}, \hat{X}_m^\dagger] \rangle \tag{3.26}$$

In the doped system, this equation of motion depends on the interactions between the e–h pair X_n and the 2DEG thermal carriers,which can lead to a strong perturbation of the 2DEG.[18, 75] Such X_n–2DEG interactions couple X_n with the X+2DEG* states $|Y_n\rangle$ (2DEG* denotes from now on an excited 2DEG configuration) defined by [20]

$$H|X_n\rangle = \Omega_n |X_n\rangle - (1 - \nu_n) \sum_{m \neq n} V_{mn} |X_m\rangle + |Y_n\rangle \tag{3.27}$$

with the orthogonality requirement $\langle X_m | Y_n \rangle = 0$. The latter condition, together with Eq.(3.20), gives

$$\Omega_n = \frac{\langle X_n | H | X_n \rangle}{\langle X_n | X_n \rangle} \ , \ V_{nn'} = -\frac{\langle X_n | H | X_{n'} \rangle}{(1 - \nu_n)(1 - \nu_{n'})} \tag{3.28}$$

for any strongly correlated ground state.It is then useful to introduce the operator

$$\hat{Y}_n = [\hat{X}_n, H] - \Omega_n \hat{X}_n + (1-\nu_n)\sum_{n' \neq n} V_{nn'} \hat{X}_{n'}. \tag{3.29}$$

and obtain the equation of motion

$$i\partial_t P_n(t) - \Omega_n P_n(t) + (1-\nu_n)\sum_{n' \neq n} V_{nn'} P_{n'}(t) = -d(t)[1-n_n(t)] + \frac{\langle \hat{Y}_n \rangle}{\sqrt{N}} \tag{3.30}$$

Eq(3.26) subtracts the static and non–interacting contributions on the right-hand side of Eq.(3.29) and also defines the first step in a Lanczos computational approach to the time–dependent problem of the nonlinear optical response, [20] whose advantages have been discussed in the context of quantum chemistry.[104] The first term on the right hand side (rhs) of Eq.(3.29) describes the Phase Space Filling (PSF) effects, determined by the time–dependent LLn filling factor

$$n_n(t) = \langle \hat{\nu}_{nn} \rangle, \ \hat{\nu}_{nn} = \hat{\nu}^e_{nn} + \hat{\nu}^h_{nn}, \tag{3.31}$$

which describes the LLn ground state and photoexcited electron and hole populations Eq.(3.14)

In the absence of interactions, $\hat{Y}_n$ =0 and Eq.(3.29) reduces to optical Bloch equations of an atomic–like system of discrete LLs. In the undoped system, $\langle \hat{Y}_n \rangle$ describes the interactions between X_n and the photoexcited carriers.[**?**] The understanding the effect of the 2DEG and incompressible quantum liquid on $\langle \hat{Y}_n \rangle$ is the main goal of our work.

To elucidate this interaction–induced contribution, we consider the ideal 2D system and obtain after straightforward algebra by using Eqs (C1) and (3.27),

$$\begin{aligned}\hat{Y}_n &= \frac{1}{2\pi\ell^2\sqrt{N}}\sum_{\mathbf{q}m} v_q\hat{\rho}_{\mathbf{q}}\left[\phi_{nm}(-\mathbf{q})\hat{X}_{\mathbf{q}mn} - (n\leftrightarrow m)\right] \\ &- \sum_m\left[\frac{\hat{X}_m}{1-\nu_m}\int\frac{d\mathbf{q}}{(2\pi)^2}v_q\phi_{mn}(\mathbf{q})\langle G\mid\hat{\rho}_{-\mathbf{q}}\hat{\rho}^e_{\mathbf{q}mn\downarrow}\mid G\rangle\right. \\ &- \left.\frac{\hat{X}_n}{1-\nu_n}\int\frac{d\mathbf{q}}{(2\pi)^2}v_q\phi_{nm}(\mathbf{q})\langle G\mid\hat{\rho}_{-\mathbf{q}}\hat{\rho}^e_{\mathbf{q}nm\downarrow}\mid G\rangle\right], \qquad (3.32)\end{aligned}$$

where we introduced for simplicity the operator

$$\hat{\rho}_{\mathbf{q}} = \sum_{n'm'\sigma}\left[\phi_{m'n'}(\mathbf{q})\hat{\rho}^e_{\mathbf{q}m'n'\sigma} - \phi_{n'm'}(\mathbf{q})\hat{\rho}^h_{\mathbf{q}m'n'\sigma}\right]. \qquad (3.33)$$

The second term on the right hand side (rhs) of Eq.(3.31) subtracts the noninteracting/static 2DEG contribution to the X energies and couplings,Eq.(3.28), determined by the ground state static structure factor.[24, 25] We note from Eq.(3.31) that, due to the hidden symmetry,[106, 107] $\hat{Y}_n$ vanishes if we project to states in a given LL, n=m. Therefore, in the absence of LL mixing, the optical response of the ideal 2D system resembles that of an atomic–like system and X_n is approximately decoupled from the 2DEG.

In the general system, $\langle\hat{Y}_n\rangle$ can be expanded in terms of density matrices of the form $\langle\hat{e}^\dagger\hat{e}\hat{e}\hat{h}\rangle$ and $\langle\hat{h}^\dagger\hat{h}\hat{e}\hat{h}\rangle$, which describe the interaction of an e–h pair with an additional carrier. The factorization of such density matrices gives the Semiconductor Bloch equations. [6, 12, 54] However, this Hartree–Fock approximation misses biexciton, trion, and X–2DEG inelastic scattering effects by assuming a static 2DEG.

In the undoped system, where the conduction band is empty and the valence band is full, $\hat{Y}^\dagger_n|G\rangle = 0$ and Eq.(3.31) describes interactions among photoexcited carriers only. These can be treated similar to the DCTS by projecting to a subspace of X and X+X states.[103]

In the QHS, Eq.(3.31) describes, in addition, X–2DEG interactions and the resulting dynamical 2DEG response. Such effects are described by considering the action of $\hat{Y}_n^\dagger$, or more generally operators of the form $\hat{e}^\dagger\hat{e}^\dagger\hat{h}^\dagger\hat{e}$, on the subspace of 0–$h$+$N_e$–$e$ states. For example, in the general system the state $\hat{Y}_n^\dagger|G\rangle$ is a linear combination of e–h pair + 2DEG excitation states.Recalling that the operators $\hat{\rho}^e_{\mathbf{q}nm\sigma}$ create/annihilate the MPs,one can interpret $|\ Y_n\rangle$, as a linear combination of the continuum of X+MP configurations that couple to X_n via the X–2DEG interaction.

In the limit N_e=1,relevant for $\nu \ll 1$, $|Y_n\rangle$ describes one hole and two electrons in excited states unoccupied in the ground state, i.e. trion configurations,while in $|X_n\rangle$ one of the two electrons remains in its ground state configuration. In the doped system, the strong interaction between a finite momentum exciton and the 2DEG can bind a 2DEG electron and form a trion state analogous to the N_e=1 case,which is correlated with a 2DEG hole. This is the case when the symmetry of the ideal 2D system is broken.[99] At fractional ν, the above trion effects occur between composite fermions, leading to quasi–excitons.[75] It is clear that, when calculating the optical response, given by $\langle\hat{X}_n\rangle$, in the doped system, the coupling to the density matrices $\langle\hat{Y}_n\rangle$ in Eq.(3.29) must be treated nonperturbatively.

We now turn to the populations n_n, Eq.(3.30),which are obtained from the equation of motion for $\langle[\hat{X}_n,\hat{X}_n^\dagger]\rangle$ and Eq.(3.13).Calculating the commutator $[H,[\hat{X}_n,\hat{X}_n^\dagger]]$ from Eq. (3.28) by using the property

$$[A,[B,C]]+[C,[A,B]]+[B,[C,A]]=0 \tag{3.34}$$

which holds for any operators A,B,C we obtain

$$\frac{\partial n_n}{\partial t}(t)=2\,\mathrm{Im}\left[2\,\mathrm{d}^*(\mathrm{t})\,\mathrm{P_n(t)}+\langle[\hat{\mathrm{Y}}_\mathrm{n},\hat{\mathrm{X}}_\mathrm{n}^\dagger]\rangle^*\right], \tag{3.35}$$

with initial condition given by the ground state filling factor ν_n. The first term on the rhs describes the photoexcitation process, while

the density matrix $\langle[\hat{Y}_n, \hat{X}_n^\dagger]\rangle$ describes the interaction effectson the population quantum kinetics, i.e. the redistribution of the photoexcited carriers among the LLs and the intraband coherences among the photoexcited many–body states. The corresponding physical processes become more clear by calculating the above commutator in the ideal 2D system using Eq.(3.32):

$$\begin{aligned}
\langle[\hat{Y}_n, \hat{X}_n^\dagger]\rangle &= \frac{1}{2\pi l^2 N}\sum_{\mathbf{q}m'n'} v_q \langle\Big[\phi_{n'n}(\mathbf{q})\hat{X}^\dagger_{\mathbf{q}n'n} - \phi_{nn'}(\mathbf{q})\hat{X}^\dagger_{\mathbf{q}nn'}\Big] \\
&\times \Big[\phi^*_{m'n}(\mathbf{q})\hat{X}_{\mathbf{q}m'n} - \phi^*_{nm'}(\mathbf{q})\,\hat{X}_{\mathbf{q}nm'}\Big]\rangle \\
&- \frac{1}{2\pi l^2 N}\sum_{\mathbf{q},m'\neq n} v_q\left[\phi_{nm'}(\mathbf{q})\Delta\langle\hat{\rho}_{-\mathbf{q}}\hat{\rho}^e_{\mathbf{q}nm'\downarrow}\rangle - \phi_{m'n}(\mathbf{q})\langle\hat{\rho}_{-\mathbf{q}}\hat{\rho}^h_{\mathbf{q}nm'\downarrow}\rangle\right] \\
&- \frac{\Delta\langle\hat{\nu}_{nn}\rangle}{2\pi l^2 N(1-\nu_n)}\sum_{\mathbf{q},n''m''\sigma}\sum_{m'\neq n} v_q\phi_{nm'}(\mathbf{q})\phi^*_{n''m''}(\mathbf{q}) \\
&\quad \langle G|\hat{\rho}^e_{-\mathbf{q}m''n''\sigma}\hat{\rho}^e_{\mathbf{q}nm'\downarrow}|G\rangle
\end{aligned} \tag{3.36}$$

where $\Delta\langle\hat{O}\rangle = \langle\hat{O}\rangle - \langle G|\hat{O}|G\rangle$. The first term on the rhs of Eq.(3.36) is determined by the interactions of the X populations and X↔X coherences $\langle\hat{X}^\dagger_{\mathbf{q}nm}\hat{X}_{\mathbf{q}n'm'}\rangle$, similar to the undoped system.[10] Analogous effects determine the second term, with additional contributions in the QHS due to the scattering of the photoexcited carriers with the thermal 2DEG.The last term is due to the ground state correlations,described by the static 2DEG structure factor.

Eq.(3.36) reduces the X–2DEG quantum kinetics to the calculation of the density matrices $\langle\hat{X}^\dagger\hat{X}\rangle$, $\langle\hat{\rho}^e_\uparrow\hat{\rho}^e_\downarrow\rangle$, $\langle\hat{\rho}^e_\uparrow\hat{\rho}^h_\downarrow\rangle$, and $\langle\hat{\rho}^h_\downarrow\hat{\rho}^h_\downarrow\rangle$. To second order in the optical field,only many–body states with a single valence hole contribute to such intraband density matrices (discussed in the next section).Thus, $\langle\hat{h}^\dagger\hat{h}^\dagger\hat{h}\hat{h}\rangle$=$O(E^4)$ and

$$\langle\hat{\rho}^h_{-\mathbf{q}m'n'\sigma}\hat{\rho}^h_{\mathbf{q}nm\sigma}\rangle = \delta_{\sigma\downarrow}\nu^h_{m'm}\delta_{nn'} + O(E^4). \tag{3.37}$$

This factorization of the density matrix $\langle\hat{\rho}^h\hat{\rho}^h\rangle$ is *exact* to O(E^2).In

the undoped system, the same holds true for the density matrices $\langle\hat{\rho}^e\hat{\rho}^e\rangle$ sinceonly states with a single electron contribute to $O(E^2)$.In the QHS this is not true due to the ground state electron populations. By subtracting the factorizable contribution and noting that $\mathbf{q}\neq 0$ in Eq.(3.36), we obtain

$$\langle\hat{\rho}^e_{-\mathbf{q}m'n'\downarrow}\hat{\rho}^e_{\mathbf{q}nm\downarrow}\rangle = (\delta_{n,n'}-\nu^e_{nn'})\,\nu^e_{m'm}+C^{m'n'}_{mn}(\mathbf{q}), \tag{3.38}$$

where we introduced the four–electron density matrix

$$C^{m'n'}_{mn}(\mathbf{q}) = \nu^e_{nn'}\nu^e_{m'm}+\frac{1}{N}\sum_{kk'}e^{iq_x(k-k')\ell^2}\times\langle\hat{e}^\dagger_{k+q_y/2n\downarrow}\hat{e}^\dagger_{k'-q_y/2m'\downarrow}\hat{e}_{k'+q_y/2n'\downarrow}\hat{e}_{k-q_y/2m\downarrow}\rangle.$$

In the undoped system, C=0 to $O(E^2)$ since it involves operators that annihilate two electrons. In the QHS, a finite $O(E^2)$ contribution can arise due to the scattering of spin–$\downarrow$ photoexcited and ground state electrons.Similarly, the density matrices $\langle\hat{\rho}^e_\uparrow\hat{\rho}^e_\downarrow\rangle$ and $\langle\hat{\rho}^e_\uparrow\hat{\rho}^h_\downarrow\rangle$, which vanish to $O(E^2)$ in the undoped system, contribute in the QHS due to photoexcited carrier scattering with spin–$\uparrow$ ground state electrons.

To establish the connection with the DCTS, we note when calculating $\nu^{e,h}_{nn'}$ that, to $O(E^2)$, in the undoped system the operators $\hat{\nu}^{e,h}_{nn'}$ act on states with a single e–h pair. One can thus multiply $\hat{\nu}^{e,h}_{nn'}$ by the h or e number operator and express the above density matrices in terms of $\langle\hat{X}^\dagger\hat{X}\rangle$. In the QHS, this is also possible in the case of spin–$\downarrow$ photoexcited electrons when the ground state 2DEG is spin–$\uparrow$ polarized and C=$O(E^4)$. [108] The density matrices $\langle\hat{\rho}^e_\uparrow\hat{\rho}^e_\downarrow\rangle$ and $\langle\hat{\rho}^e_\uparrow\hat{\rho}^h_\downarrow\rangle$ can then be expressed in the form $\langle\hat{\rho}^e_\uparrow\hat{X}^\dagger\hat{X}\rangle$[89] and describe the coherent coupling of an X initial state to a final state consisting of an X plus an excitation of the spin–$\uparrow$ 2DEG. The equations of motion of the above independent density matrices require however

the consideration of multiple 2DEG excitations,[75, 18] discussed in the next section.

3.3 Linear Interband Polarization

In this section we obtain P_n to $O(E)$, which determines the linear absorption spectrum. We note that the Hamiltonian H conserves the number of valence holes, while in the ground state the valence band is full. As a result, the $O(E)$contribution to P_n comes from 1–h+(N_e+1)–e states. We denote $|\psi_{1L}(t)\rangle$ the $O(E)$ 1–h contribution to the many–body state that evolves in time from the correlated ground state $|G\rangle$ according to the Hamiltonian $H(t)$, Eq.(3.10).[89, 20] The $O(E)$ contribution to the interband density matrix $\langle\hat{Z}\rangle$, where $\hat{Z}$ is any operator that reduces the number of holes by one, is then given by

$$\langle\hat{Z}\rangle^L = \langle G|\hat{Z}|\psi_{1L}(t)\rangle = \langle|G\rangle\langle G|\hat{Z}|\rangle^L, \tag{3.39}$$

which coincides with the linearized density matrix of the Hubbard operator $|G\rangle\langle G|\hat{Z}|$.[70] We can thus reduce the calculation of $\langle\hat{Z}\rangle^L$ to a closed system of equations of motion of Hubbard operator density matrices $\langle|G\rangle\langle\alpha|\rangle$, where the states $|\alpha\rangle$ span the 1–h subspace of interest. $|\psi_{1L}(t)\rangle$evolves in time as follows: [20]

$$i\partial_t|\psi_{1L}\rangle = H|\psi_{1L}\rangle - d(t)\sum_n\langle X_n|\hat{X}^\dagger|G\rangle|X_n\rangle. \tag{3.40}$$

The Fermi's golden rule calculation of the linear absorption spectrum is recovered by expanding $|X_n\rangle$ in terms of the many–body eigenstates of H, while the solution is trivial if $|X_n\rangle$ is an eigenstate of H. However, $|X_n\rangle$ is not an eigenstate of H, so the time evolution leads to the static couplings $V_{nn'}$, Eq.(3.28), in both doped and undoped systems [54] and to the coupling to "trion" configurations,

Eq.(3.27). In the doped system, the nontrivial problem is to describe the dynamical 2DEG response due to the interactions of the ground state electrons with X_n. In the case of the Fermi Edge Singularity, this was accomplished by considering a time–dependent coupled cluster expansion expression for $|\psi_{1L}\rangle$, which describes an exciton dressed by an infinite number of e–h pairs. [18] In the QHS, previous Fermi's golden rule calculations of quasiexciton [75] and trion [99] contributions to the photoluminescence at fractional ν used a basis of 1–h+(N_e+1)–e Slater determinants to diagonalize H for small N_e.We note that small system exact diagonalizations have been successful in describing both ground state and excitation properties of the QHS.[99, 75, 24]

Given a set of orthonormal states $|X_i\rangle$ and $|Y_\alpha\rangle$, where

$$\langle Y_\alpha|\hat{X}^\dagger|G\rangle = 0 \tag{3.41}$$

that describe the main 1–h+(N_e+1)–e configurations of interest, we can express any density matrix $\langle\hat{Z}\rangle^L$ in terms of the linearized density matrices

$$P_i^L = \frac{\langle|G\rangle\langle X_i|\rangle^L}{\sqrt{N}} \ , \ \bar{P}_\alpha^L = \frac{\langle|G\rangle\langle Y_\alpha|\rangle^L}{\sqrt{N}}. \tag{3.42}$$

For example, for N_e=1, the X_i states can be chosen as an e–h pair plus a second electron in its ground state configuration (i.e. the states $|X_n\rangle$), while the Y_α states describe two electrons in states unoccupied in the ground state plus one hole. Using the relations

$$H|X_i\rangle = \Omega_i|X_i\rangle - \sum_{j\neq i} V_{ji}|X_j\rangle + \frac{1}{\sqrt{N}}\sum_\alpha W_{\alpha i}|Y_\alpha\rangle, \tag{3.43}$$

and

$$H|Y_\alpha\rangle = \bar{\Omega}_\alpha|Y_\alpha\rangle + \frac{1}{\sqrt{N}}\sum_i W^*_{\alpha i}|X_i\rangle + \frac{1}{N}\sum_{\alpha'\neq\alpha} W^*_{\alpha\alpha'}|Y_{\alpha'}\rangle, \tag{3.44}$$

where

$$\Omega_i = \langle X_i|H|X_i\rangle \ , \ \bar{\Omega}_\alpha = \langle Y_\alpha|H|Y_\alpha\rangle \ ,$$
$$V_{ij} = -\langle X_i|H|X_j\rangle, W_{\alpha\alpha'} = N\langle Y_\alpha|H|Y_{\alpha'}\rangle,$$
$$W_{\alpha i} = \sqrt{N}\langle Y_\alpha|H|X_i\rangle, \tag{3.45}$$

which are exact within the subspace of interest, we obtain the following closed system of equations of motion:

$$i\partial_t P_i^L = (\Omega_i - i\Gamma_i)P_i^L - \sum_{j\neq i} V_{ij}P_j^L - \frac{d(t)}{\sqrt{N}}\langle X_i|\hat{X}^\dagger|G\rangle/ + \frac{1}{\sqrt{N}}\sum_\alpha W_{i\alpha}\bar{P}_\alpha^L \tag{3.46}$$

where we introduced the dephasing rates Γ_i, and

$$i\partial_t \bar{P}_\alpha^L = (\bar{\Omega}_\alpha - i\gamma_\alpha)\bar{P}_\alpha^L + \frac{1}{\sqrt{N}}\sum_i W_{\alpha i}P_n^L + \frac{1}{N}\sum_{\alpha'\neq\alpha} W_{\alpha\alpha'}\bar{P}_{\alpha'}^L \tag{3.47}$$

where we introduced the dephasing rates γ_α. By choosing a basis of many–body eigenstates of H, $W_{\alpha i}$=V_{ij}=0 and the above equations of motion decouple.This however requires a precise calculation of all excited many–body eigenstates.Given any convenient set of 1–h+(N_e+1)–e states, Eq.(3.46,3.47) can be used to calculate, in the time domain, any interband density matrix (to $O(E)$), including dephasing,without solving the eigenvalue problem. Such a nonperturbative solution, exact within a given subspace, is analogous to the Green's function calculations of relaxation in the manganites and the Hubbard Hamiltionian[93, 94] and applies for any correlated ground state.

3.4 Intraband density matrices

In this section we obtain the O(E^2) contributions to any intra–band density matrix $\langle\hat{M}\rangle$, where $\hat{M}$ conserves the number of holes. With-

out loss of generality we assume that the ground state contribution has already been subtracted out and $\langle G|\hat{M}|G\rangle$=0. Examples of such density matrices are the carrier populations and intraband coherences between many–body states with the same number of electrons and holes.We first note that the 2–h contribution to $\langle\hat{M}\rangle$ is of $O(E^4)$. Within the 1–h subspace,$\langle\hat{M}\rangle$ can be expressed in terms of the Hubbard operator density matrices $\langle|X_i\rangle\langle X_j|\rangle$, $\langle|X_i\rangle\langle Y_\alpha|\rangle$, and $\langle|Y_\alpha\rangle\langle Y_{\alpha'}|\rangle$ for the chosen 1–h+(N_e+1)–e states. Within a wavefunction approach, these density mstrices can be expressed as products of the interband amplitudes P_i^L and $\bar{P}_\alpha^L$.However, relaxation introduces additional intraband dynamics,described by non–factorizable contributions to the above density matrices:

$$N_{ij} = \frac{1}{N}\langle|X_i\rangle\langle X_j|\rangle - P_j^L P_i^{L*} \tag{3.48}$$

describes the coherent $X_i \leftrightarrow X_j$ coupling,

$$M_{j\alpha} = \frac{1}{N}\langle|X_j\rangle\langle Y_\alpha|\rangle - P_j^{L*}\bar{P}_\alpha^L \tag{3.49}$$

describe coherences between the X_i and Y_α states,and

$$N_{\alpha\alpha'} = \frac{1}{N}\langle|Y_\alpha\rangle\langle Y_{\alpha'}|\rangle - \bar{P}_\alpha^{L*}\bar{P}_{\alpha'}^L \tag{3.50}$$

describe the coupling of the Y_α states. A non–perturbative scheme for describing the full intraband dynamics within the subspace of interest is obtained similar to the previous section by noting that Eq.(3.43,3.44) allow for a closed system of equations of motion for the above Hubbard operator density matrices.From Eq.(B.5) we obtain to $O(E^2)$

$$
\begin{aligned}
i\partial_t N_{ij} &= (\Omega_j - \Omega_i - i\Gamma_{ij})\, N_{ij} + i(\Gamma_i + \Gamma_j - \Gamma_{ij}) P_j^L P_i^{L*} \\
&+ \sum_{i' \neq i} V_{i'i} N_{i'j} - \sum_{j' \neq j} V_{jj'} N_{ij'} + \frac{1}{\sqrt{N}} \sum_{\alpha} \left(W_{\alpha j}^* M_{i\alpha} - W_{\alpha i} M_{j\alpha}^* \right),
\end{aligned} \tag{3.51}
$$

$$
\begin{aligned}
i\partial_t M_{i\alpha} &= \left(\bar{\Omega}_\alpha - \Omega_i - i\Gamma_{i\alpha}\right) M_{i\alpha} + i(\Gamma_i + \gamma_\alpha - \Gamma_{i\alpha}) P_n^{L*} \bar{P}_\alpha^L \\
&+ \frac{1}{\sqrt{N}} \sum_{i'} W_{\alpha i'} N_{ii'} - \frac{1}{\sqrt{N}} \sum_{\alpha'} W_{\alpha' i} N_{\alpha' \alpha} + \sum_{i' \neq n} V_{i'i} M_{i'\alpha} \\
&+ \frac{1}{N} \sum_{\alpha' \neq \alpha} W_{\alpha\alpha'} M_{i\alpha'},
\end{aligned} \tag{3.52}
$$

and

$$
\begin{aligned}
i\partial_t N_{\alpha\alpha'} &= \left(\bar{\Omega}_{\alpha'} - \bar{\Omega}_\alpha - i\Gamma_{\alpha\alpha'}\right) N_{\alpha\alpha'} + i\left(\gamma_\alpha + \gamma_{\alpha'} - \Gamma_{\alpha\alpha'}\right) \bar{P}_\alpha^{L*} \bar{P}_{\alpha'}^L \\
&+ \frac{1}{\sqrt{N}} \sum_{i} \left(W_{\alpha' i} M_{i\alpha}^* - W_{\alpha i}^* M_{i\alpha'} \right) + \frac{1}{N} \sum_{\alpha'' \neq \alpha'} W_{\alpha'' \alpha'}^* N_{\alpha\alpha''} \\
&- \frac{1}{N} \sum_{\alpha'' \neq \alpha} W_{\alpha'' \alpha} N_{\alpha'\alpha''}^*,
\end{aligned} \tag{3.53}
$$

The interaction matrix elements and excitation energies entering in the above equations are the same as in the linear absorption calculation. We note that the above non–factorizable density matrices vanish in the coherent limit, defined as $\Gamma_{ij}{=}\Gamma_i + \Gamma_j$,$\Gamma_{i\alpha}{=}\Gamma_i + \gamma_\alpha$, and $\Gamma_{\alpha\alpha'}{=}\gamma_\alpha + \gamma_{\alpha'}$. However, as already known from the undoped system [110], the deviations from this limit are strong and result, e.g, in long–lived incoherent carrier populations and intraband coherence. The closed system Eq.(3.51,3.52,3.53)can be used to describe the light–induced population and intraband coherence dynamics for any ν.

3.5 Third–Order Nonlinear Polarization

In this section we obtain, to O(E^3), an expression for the interband density matrix $\langle \hat{Z} \rangle$, where $\hat{Z}$ is any operator that reduces the number of holes by one. Our result separates the contributions that can be expressed as products of the linear polarizations P_n^L, whose dependence on the dynamical 2DEG response, was described in Section 3.3,from fully correlated contributions with different dynamics. Our main goal is to use this expression to calculate the $O(E^3)$ contribution to the interaction–induced density matrix $\langle \hat{Y}_n \rangle$ in the nonlinear polarization equation of motion, Eq.(3.30). We separate out the contribution from the states $\hat{Y}_n^\dagger |G\rangle$, which describe X_n–2DEG interactions that can be treated by using equations of motion and expansions similar to Section 3.3, from the contributions due to interactions of X_n with photoexcited carriers.

Similar to the DCTS,[8, 70] we first expand in terms of the optical field and note the one to one correspondence between the photon absorption/emission and the e–h pair creation/destruction processes.The nonlinear response arises from multiple e–h pair creation/destruction processes. During each transition, the photoexcited e–h pair interacts with the 2DEG, as described by P_n^L. In the nonlinear optical response, we must also consider the correlations among the different photoexcited e–h pairs, such as e.g. four–particle correlations between two photoexcited e's and two photoexcited h's.[100, 3, 103] In the undoped system, the DCTS cumulant expansions separate the contributions to the density matrices due to correlated and uncorrelated e-h pair transitions.[8, 9, 10] Here we accomplish this for a strongly correlated populated ground state, where Wick's theorem does not apply as in the DCTS. For this we introduce a decomposition of the many–body state $|\psi(t)\rangle$, which evolves from the exact ground state $|G\rangle$ according to $H(t)$,into correlated and uncorrelated parts.In this way we separate out the parts of $|\psi(t)\rangle$ whose ampli-

tudes can be expressed in terms of products of the linear coherent amplitudes. Such factorizable contributions assume that, although the photoexcited excitons or quasiexcitons are strongly correlated with the 2DEG, their interactions with each other can be treated within a mean field approximation.Our scheme recovers the DCTS in the undoped system.

Since here electrons are present prior to the photoexcitation, when following the effects of the applied fields we count the number of valence band holes in a given state. Therefore, we use the shorthand notation 0–h, 1–h, 2–h ... to label the many–body states. We then express the many–body state state as

$$|\psi\rangle = |\psi_0\rangle + |\psi_1\rangle + |\psi_2\rangle, \tag{3.54}$$

where $|\psi_n\rangle$ is the projection to the n–h subspace. [20, 89]

It is clear that states with three or more holes do not contribute to the third–order nonlinear polarization when the Hamiltonian H conserves the number of holes:

$$\langle \hat{Z} \rangle = \langle \psi_0 | \hat{Z} | \psi_1 \rangle + \langle \psi_{1L} | \hat{Z} | \psi_2 \rangle + O(E^5). \tag{3.55}$$

Next we consider the linearized time–evolved state $|\psi_{1L}\rangle$, calculated in the previous section, and separate the linear polarization contribution by projecting the $|X_n\rangle$ states:

$$|\psi_{1L}\rangle = \sum_n \frac{\langle \hat{X}_n \rangle^L}{1 - \nu_n} |X_n\rangle + |\bar{\psi}_{1L}\rangle, \tag{3.56}$$

where $\langle X_n | bar \psi_{1L} \rangle = 0. | \bar{\psi}_{1L} \rangle$ satisfies the equation of motion Eq.(B.37) and describes X+2DEG* configurations, including trion configurations, which contribute to the optical spectra via their coupling to the X configurations in the many–body 1–h eigenstates of H. The two–photon processes excite two e–h pairs on top of the 2DEG, whose time evolution is given by

$$i\partial_t|\psi_2\rangle = H|\psi_2\rangle - d(t)\hat{X}^\dagger|\psi_{1L}\rangle + O(E^4). \tag{3.57}$$

Similar to the time evolution of $|\psi_{1L}\rangle$ discussed in the previous section, $|\psi_2\rangle$ can be obtained by introducing a basis of 2–h+(N_e+2)–e states.[**?**, 103] Given the complexity of treating such states, we decompose $|\psi_2\rangle$ into an uncorrelated part, which assumes that each photoexcited e–h pair evolves independently by interacting with the 2DEG, and a correlated part, which describes correlations among the photoexcited e–h pairs:

$$\begin{aligned} |\psi_2\rangle &= \frac{1}{2}\sum_{nm}\frac{\langle\hat{X}_n\rangle^L\langle\hat{X}_m\rangle^L}{(1-\nu_n)(1-\nu_m)}\hat{X}_n^\dagger\hat{X}_m^\dagger|G\rangle \\ &+ \sum_n\frac{\langle\hat{X}_n\rangle^L}{1-\nu_n}\hat{X}_n^\dagger|\bar{\psi}_{1L}\rangle + |\bar{\psi}_2\rangle + O(E^4). \end{aligned} \tag{3.58}$$

The first term on the rhs of the above equation comes from two independent optical transitions X_n and X_m, which create two e–h pairs that interact independently with the 2DEG but not with each other. The second term describes {1-h/2DEG*} configurations, which contribute to the optical response via their coupling to X_m in the many–body eigenstates, that interact with the 2DEG independently of X_n. For example, for N_e=1, the first term on the rhs of Eq.(3.58)describes two zero momentum e–h pairs plus an electron in its ground state configuration.During the time evolution, each pair interacts separately with the 2DEG and thus the amplitude of this configuration in the 2–h many–body wavefunction is the product of the linear polarizations, as in $|\psi_{1L}\rangle$ Eq.(3.56). The second term describes two electrons in excited configurations correlated with a hole plus a second e–h pair with zero momentum. This term describes the time evolution of a non–interacting trion and exciton configuration. $|\bar{\psi}_2\rangle$ then describes a biexciton state interacting with the 2DEG or a correlated five–particle complex.

$$i\partial_t|\bar{\psi}_2\rangle - H|\bar{\psi}_2\rangle = \frac{1}{2}\sum_{nm}\langle\hat{X}_n\rangle^L\langle\hat{X}_m\rangle^L[\hat{Y}_n^\dagger,\hat{X}_m^\dagger]|G\rangle + \sum_n\left[\langle\hat{X}_n\rangle^L\ \hat{Y}_n^\dagger - \langle\hat{Y}_n\rangle^L\ \hat{X}_n^\dagger\right]|\bar{\psi}_{1L}\rangle. \quad (3.59)$$

The first term on the rhs of the above equation describes the time evolution of the correlated four–particle excitation analogous to the undoped system. [100, 3] $[\hat{Y}_n^\dagger,\hat{X}_m^\dagger]|G\rangle$, as can be seen by using the ideal 2D system Hamiltonian H to obtain the commutator

$$[\hat{X}_m,\hat{Y}_n] = \frac{1}{2\pi\ell^2 N}\sum_{\mathbf{q}m'm''} v_q \times \left[\phi_{nm'}(-\mathbf{q})\hat{X}_{\mathbf{q}m'n} - \phi_{m'n}(-\mathbf{q})\hat{X}_{\mathbf{q}nm'}\right] \times \left[\phi_{mm''}(\mathbf{q})\hat{X}_{-\mathbf{q}m''m} - \phi_{m''m}(\mathbf{q})\hat{X}_{-\mathbf{q}mm''}\right]. \quad (3.60)$$

This contribution vanishes if we project to a single LL in the ideal 2D system, due to the hidden symmetry, [106]and also describes biexciton effects as in the undoped system.[100, 3, 103] The last term in Eq.(3.59) describes correlations between X and 1-h/2DEG* configurations or two 1-h/2DEG* configurations. In an analogous way, we decompose the $O(E^2)$ contribution to the 0–h - state $|\psi_0\rangle$, created by two–photon Raman processes of excitation and then de-excitation of an e–h pair, as

$$|\psi_0\rangle = \langle G|\psi\rangle|G\rangle - \sum_n \frac{\langle\hat{X}_n\rangle^{L*}}{1-\nu_n}\hat{X}_n|\bar{\psi}_{1L}\rangle + |\bar{\psi}_0\rangle + O(E^4) \quad (3.61)$$

where

$\langle G|\bar{\psi}_0\rangle$=0. The 0-$h$/2DEG* state $|\bar{\psi}_0\rangle$ is determined by the equation of motion Eq.(B.36). Eq.(3.59,B.36)can be solved similar to the

undoped system [103] by projecting to a subspace of 2–h and 0–h states.

By substituting the wavefunction decompositions Eq.(3.56,3.58,3.61) to Eq.(3.55) we obtain the following exact expression for $\langle\hat{Z}\rangle$, which separates out all nonlinear contributions that are proportional to the linear polarizations P_n^L: [20, 89]

$$\begin{aligned}
\langle\hat{Z}\rangle &= \sum_n \frac{\langle\hat{X}_n\rangle^{L*}}{1-\nu_n}\langle G|[\hat{X}_n,\hat{Z}]|\psi_2\rangle \\
&+ \frac{1}{2}\sum_{nn'}\frac{\langle\hat{X}_n\rangle^L\langle\hat{X}_{n'}\rangle^L}{(1-\nu_n)(1-\nu_{n'})}\langle\bar{\psi}_{1L}|[[\hat{Z},\hat{X}_n^\dagger],\hat{X}_{n'}^\dagger]|G\rangle \\
&+ \sum_n \frac{\langle\hat{X}_n\rangle^L}{1-\nu_n}\langle[\hat{Z},\hat{X}_n^\dagger]\rangle_c \\
&+ \langle\ |G\rangle\langle G|\hat{Z}\ \rangle + \sum_n \frac{\langle\hat{X}_n\rangle^{L*}}{1-\nu_n}\langle G|\hat{Z}\hat{X}_n|\psi_2\rangle \\
&- \frac{\langle\hat{X}_n\rangle^L}{1-\nu_n}\langle G|\hat{Z}\hat{X}_n^\dagger|\bar{\psi}_0\rangle \\
&+ \langle\bar{\psi}_{1L}|\hat{Z}|\bar{\psi}_2\rangle + \langle\bar{\psi}_0|\hat{Z}|\bar{\psi}_{1L}\rangle. \qquad (3.62)
\end{aligned}$$

By using Eq.(3.62) to obtain the interaction–induced density matrix $\langle\hat{Y}_n\rangle$ in Eq.(3.30), we establish the connection to the known results for the ultrafast nonlinear optical response of undoped semiconductors.[9, 10] The first term on the rhs of Eq(3.62) describes the X–X interband coherence and recovers the well–known treatment of X–X interactions in undoped semiconductors. [103, 70] The 2–h stste amplitude $\langle G|[\hat{X}_m,\hat{Y}_n]|\psi_2\rangle$ coincides to $O(E^2)$ with the density matrices $\langle[\hat{X}_m,\hat{Y}_n]\rangle$ and $\langle|G\rangle\langle G|[\hat{X}_m,\hat{Y}_n]\rangle$, which in turn can be expressed in terms of X–X density matrices $\langle\hat{X}\hat{X}\rangle$ (see Eq.(3.60). The dynamics and dephasing of this X–X coherence can be described by using Eq,(3.58,3.59). The familiar decomposition of the X–X coherence

into Hartree–Fock and correlated parts[103, 70, 100] is obtained by using Eq,(3.58)for $|\psi_2\rangle$.Similar to the undoped system, [70] Eq.(3.59) can be used to express the effects of the X–X correlations in terms of a memory kernel determined by the dynamics within the 2–h subspace.

The second and third lines on the rhs of Eq.(3.62) come from the interaction of the interband polarization with intraband coherences and populations and describe light–induced time–dependent corrections to the X energies and inter–LL couplings.The third term is determined by the non–factorizable intraband density matrix

$$\begin{aligned}
\langle[\hat{Z},\hat{X}_n^\dagger]\rangle_c &= \langle[\hat{Z},\hat{X}_n^\dagger]\rangle \\
&- \sum_{n'm'} \frac{\langle\hat{X}_n^{'}\rangle^{L*}\langle\hat{X}_{m'}\rangle^{L}}{(1-\nu_{n'})(1-\nu_{m'})}\langle X_{n'}|[\hat{Z},\hat{X}_n^\dagger]|X_{m'}\rangle \\
&- \sum_{n'} \frac{\langle\hat{X}_{n'}\rangle^{L*}}{1-\nu_{n'}}\langle G|[\hat{X}_{n'},[\hat{Z},\hat{X}_n^\dagger]]|\bar{\psi}_{1L}\rangle \\
&- \sum_{n'} \frac{\langle\hat{X}_{n'}\rangle^{L}}{1-\nu_{n'}}\langle\bar{\psi}_{1L}|[[\hat{Z},\hat{X}_n^\dagger],\hat{X}_{n'}^\dagger]|G\rangle, \qquad (3.63)
\end{aligned}$$

which in terms of many–body states is given by

$$\langle[\hat{Z},\hat{X}_n^\dagger]\rangle_c = \langle\bar{\psi}_{1L}|[\hat{Z},\hat{X}_n^\dagger]|\bar{\psi}_{1L}\rangle + \langle G|[\hat{Z},\hat{X}_n^\dagger]|\bar{\psi}_0\rangle + \langle\bar{\psi}_0|[\hat{Z},\hat{X}_n^\dagger]|G\rangle \qquad (3.64)$$

In the undoped system, this term describes X scattering from incoherent X populations and X $\leftrightarrow$ X coherences due to X–X interactions and relaxation. [10]

The fourth and fifth lines on the rhs of Eq.(3.62) describe a contribution determined by the state $\hat{Z}^\dagger|G\rangle$. Since here $\hat{Z}^\dagger$ acts on the ground state, as in the calculation of the linearized density matrix

in Section3.3,this contribution for $\hat{Z} = \hat{Y}_n$ describes a X–2DEG coupling similar to Eq.(3.27) and the calculation of the linear polarization. This contribution describes the trion formation and can be described by its equation of motion after expanding $\hat{Z}^\dagger|G\rangle$ in terms of the basis states $|X_i\rangle$ and $|Y_\alpha\rangle$.We can thus obtain a closed system of equations of motion similar to Section 3.3.The last two terms in Eq.(3.62) can also be obtained from the equations of motion Eq.(3.59, B.37)after projecting the 1–h and 0–h basis states. Noting thst here $\hat{Z}^\dagger$ acts on 1-h/2DEG* configurations and not the ground state, $\langle\bar{\psi}_{1L}|\hat{Y}_n|\bar{\psi}_2\rangle$ describes both trion–trion and exciton–trion interactions.In the undoped system, it describes the incoherent exciton–biexciton transition contribution determined by the fully correlated part of the density matrices $\langle X^\dagger X X\rangle$. [9] In the next section we use the above results to study the role of the LL0→LL1 excitations of an incompressible quantum liquidin the ideal 2D system.

Chapter 4

Dynamics of coherences in a dopped Quantum Well

4.1 outline

In this chapter we describe the optical dynamics of the ideal 2D system at ν=1.This ground state simplifies the calculation of the interaction matrix elements and excitation energies and allows us to highlight in a simple way the qualitative dynamical features that can arise from X interactions with an incompressible quantum liquid. For this we develop a model that describes the dynamical inter–LL coupling revealed by the FWM experiments of Chemla and coworkers.[83, 84, 85]

4.2 Description of the model

At ν=1, the 2DEG in the ground state Laughlin wavefunction [27] populates all N of the spin–$\uparrow$ LL0 states, while all spin–$\downarrow$ LL0 states and all higher LLs are empty.Signatures of spin polarization were observed in linear absorption experiments[25, 108] at temperatures as high as a few Kelvin. [109]

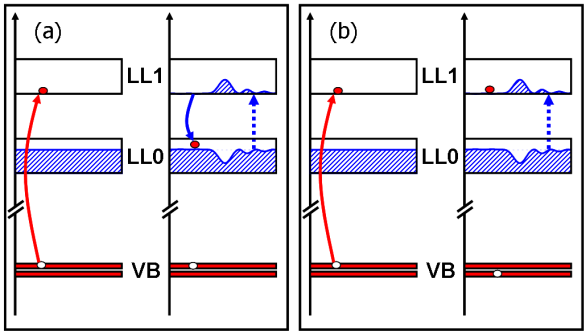

Figure 4.1: (Color online) Interaction–induced coupling of X_1 and (a) the {1-LL0-e + 1-LL1-h + LL0→LL1} four–particle excitations $|Y_{\mathbf{q}}\rangle$ (resonant process), (b) {1-LL1-e + 1-LL0-h + LL0→LL1} excitations (non–resonant process).

$$\hat{\rho}^{e}_{\mathbf{q}00\uparrow}|G\rangle = \delta_{q,0}\sqrt{N}|G\rangle \tag{4.1}$$

for the ν=1 ground state, in which case the lowest 2DEG neutral excitations are LL0→LL1 excitations.Also, the screening of the interaction is suppressed due to the LL0–LL1 energy gap.[31] Eq.(3.32) then reduces to

$$\hat{Y}_1 = -\hat{Y}_0 = \hat{Y} \tag{4.2}$$

where

$$\hat{Y} = \frac{1}{2\pi\ell^2\sqrt{N}} \sum_{\mathbf{q}\neq 0} v_q \hat{\rho}_{\mathbf{q}} \left[\phi_{10}(-\mathbf{q})\hat{X}_{\mathbf{q}01} - \phi_{01}(-\mathbf{q})\hat{X}_{\mathbf{q}10}\right]. \tag{4.3}$$

Due to the hidden symmetry, [106]$\hat{Y}$ vanishes if we project within a single LL. We thus retain both LL0 and LL1 carrier states. For optical pulses tuned to excite LL0 and LL1 transitions, we neglect states with energy comparable to LL2 or higher, whose contribution is suppressed due to their small energetic overlap with the optical pulses in the FWM experiments.The FWM experiments in the

QHS[83, 84, 85] did not show any significant FWM signal at LL2 or higher energies.However, their results indicate a strong dynamical coupling of the LL0 and LL1 resonances, which differ by an energy ∼18meV of the order of the electron cyclotron energy. We thus break the hidden symmetry by considering the LL0–LL1 mixing due to an inter–LL 2DEG excitations.Since states with two or more inter–LL excitations have energy comparable to LL2 or higher, we solve a polaronic problem where the magnetoexciton states $|X_0\rangle$ and $|X_1\rangle$ couple to a continuum of X_0+(LL0→LL1) MP or MR configurations. Neglecting configurations with energy comparable to LL2 or higher in the many–body eigenstates is justified for sufficiently large magnetic fields, when the Coulomb-to-cyclotron energy ratio $e^2/(\epsilon l\omega_c^e)$ becomes smaller than 1. We note however that, in GaAs,the Coulomb-to-cyclotron energy ratio is comparable to 1 for the magnetic fields up to ∼10T in FWM experiments For example, at 10T, ω_c ∼18meV for electrons, while the characteristic Coulomb energy is $e^2/\epsilon l$ ∼14meV. Therefore, quantitative comparisons with experiments must include higher LLs. Nevertheless, we expect that the higher energy states will not change the qualitative features, as is often the case for the 2DEG excitation spectrum.[33, 72]

In the case of X_1 in the QHS,the e–2DEG interaction scatters the LL1 electron to LL0 by emitting a LL0→LL1 2DEG excitation at small total energy cost see Fig.5.1(a)). This resonant interaction process couples X_1 to the $\{1\text{-}h/2\text{DEG}^*\}$ orthonormal states

$$|Y_{\mathbf{q}}\rangle = \hat{Y}^{\dagger}_{\mathbf{q}}|G\rangle = \hat{X}^{\dagger}_{\mathbf{q}01}\hat{\rho}^{e}_{-\mathbf{q}10\uparrow}|G\rangle \tag{4.4}$$

that enter in Eq.(4.3). We include this *continuum* of basis states to our subspace, which allows us to treat the quantum kinetics of the X_1→X_{01}+MP scattering process non–perturbativelyin the Coulomb interaction, rather than use the semiclassical Fermi's Golden Rule. Due to the resonance between the X_1 and $Y_{\mathbf{q}}$ states, their coupling

is strong. In the ideal 2D system, $|Y_0\rangle$, Eq.(3.27), is a linear combination of the same states as $|Y_1\rangle$ due to the hidden symmetry (Eq. (4.2)). However, their energies are higher than that of $|X_0\rangle$. Therefore, the X_0–2DEG interactions, treated here on the same basis as the X_1–2DEG scattering, are suppressed in the ideal 2D system for sufficiently large mgnetic fields. We show below that this asymmetry between the two QHS magnetoexcitons is important for understanding the optical dynamics.

Turning to the h–2DEG scattering,we note that the X_1 hole can scatter to LL0 by emitting a LL0→LLn 2DEG excitation, which leads to the {1-LL1-e + 1-LL0-h + LL0 → LLn} final states in Eq.(4.3) (see Fig.5.1(b)). However,noting that the hole cyclotron energy is ∼4meV at 10T, the energy of these states is close to that of LL2 or higher and therefore their contribution to the optical response at the LL1 and LL0 energies is suppressed.The only other{1-h/2DEG*} excitations with energies comparable to LL0 or LL1 {1-LL0-e + 1-LLn-h + LL0 → LL1} configurations, where n=0,2,$\cdots$, which in the ideal 2D system couple to $Y_{\mathbf{q}}$ via inter–LL hole scattering,However, such configurations are not expected to change significntly the LL0–LL1 resonance coupling observed in the experiments and we neglect them for simplicity, after noting that the complicated valence bandstructure must be treated for quantitative comparisons to experiment and that the characteristic disorder energy is often comparable to the hole cyclotron energy.Below we calculate the full optical dynamics within the subspace spanned by $|X_n\rangle$, n=0,1, and the continuum of $|Y_{\mathbf{q}}\rangle$ states Eq.(5.1).

4.3 Linear absorption at ν=1

In this section we present our results for the linear absorption spectrum. From Eq.(3.45) we obtain by using Eq.(4.2,4.3,5.1)that the X_n–$Y_{\mathbf{q}}$ interaction,

$$W_{\mathbf{q}n} = W_{n\mathbf{q}} = (\delta_{n,1} - \delta_{n,0})v_{01}^{01}(\mathbf{q}), \tag{4.5}$$

is proportional to the interaction potential

$$v_{nn'}^{mm'}(q) = \frac{1}{2\pi l^2} v_q \phi_{mm'}^*(\mathbf{q})\phi_{nn'}(\mathbf{q}). \tag{4.6}$$

Eq.(3.46) and Eq.(3.47) then reduce to

$$i\partial_t P_0^L = (\Omega_0 - i\Gamma_0)P_0^L - V_{01}P_1^L - d(t) - \frac{1}{\sqrt{N}}\sum_{\mathbf{q}} v_{01}^{01}(\mathbf{q})\bar{P}_{\mathbf{q}}^L \tag{4.7}$$

for the LL0 polarization and to

$$i\partial_t P_1^L = (\Omega_1 - i\Gamma_1)P_1^L - V_{10}P_0^L - d(t) + \frac{1}{\sqrt{N}}\sum_{\mathbf{q}} v_{01}^{01}(\mathbf{q})\bar{P}_{\mathbf{q}}^L \tag{4.8}$$

for the LL1 polarization. The exciton dephasing rates, Γ_0=Γ_1=0.5meV,are chosen similar to the undoped system.The energies of the X states are given by

$$\Omega_n = E_g + \left(n + \frac{1}{2}\right)\left(\omega_c^e + \omega_c^h\right) - V_{nn}, \tag{4.9}$$

where, as obtained from Eq.(3.45),

$$V_{nm} = \int \frac{d\mathbf{q}}{(2\pi)^2} v_q |\phi_{nm}(\mathbf{q})|^2 \tag{4.10}$$

are the X binding energies (n=m) and static inter–LL coupling energies (n≠m). The equations of motion for the $Y_{\mathbf{q}}$ coherences are obtained from Eqs.(3.47,4.5):

$$i\partial_t \bar{P}^L_{\mathbf{q}} = (\bar{\Omega}_{\mathbf{q}} - i\gamma)\bar{P}^L_{\mathbf{q}} + \frac{\upsilon^{01}_{01}(\mathbf{q})}{\sqrt{N}}\left(P^L_1 - P^L_0\right) + \frac{1}{N}\sum_{\mathbf{q}'\neq\mathbf{q}} W_{\mathbf{q}\mathbf{q}'}\bar{P}^L_{\mathbf{q}'}, \quad (4.11)$$

where we introduced a Y–excitation dephasing rate γ=0.35meV. The coupling between P^L_n and $\bar{P}^L_{\mathbf{q}}$ in the above equations of motion gives eigenstates that are a linear combination of X and $Y_{\mathbf{q}}$ configurations. From Eq.(3.45), we obtain after using

Eqs.(B.10,B.9)

$$\begin{aligned} W_{\mathbf{q}\mathbf{q}'} = W_{\mathbf{q}'\mathbf{q}} &= 2\upsilon^{00}_{11}(\mathbf{q}'-\mathbf{q})\cos\left[(\mathbf{q}\times\mathbf{q}')_z\ell^2\right] \\ &- \upsilon^{11}_{11}(\mathbf{q}'-\mathbf{q}) - \upsilon^{00}_{00}(\mathbf{q}'-\mathbf{q}). \end{aligned} \quad (4.12)$$

The interaction $W_{\mathbf{q}\mathbf{q}'}$ leads to rescattering among the continuum of $Y_{\mathbf{q}}$ states with different momenta, which corresponds to non–perturbative vertex corrections beyond the Born approximation. The Y–state dispersion

$$\bar{\Omega}_{\mathbf{q}} = \Omega_{\mathbf{q}01} + \omega_{-\mathbf{q}} \quad (4.13)$$

is obtained in Appendix Eq.(B.3).$\Omega_{\mathbf{q}01}$, Eq.(B.13), is the X_{01} excitation energy and $\omega_{\mathbf{q}}$, Eq.(B.14), is the energy of the LL0→LL1 2DEG excitations, given by [31]

$$\begin{aligned} \omega_{\mathbf{q}} - \omega^e_c &= \frac{e^2}{\epsilon\ell}\frac{q\ell}{2}e^{-q^2\ell^2/2} + \frac{e^2}{\epsilon\ell}\frac{1}{2}\sqrt{\frac{\pi}{2}}\Bigg\{1 - e^{-q^2\ell^2/4} \\ &\left[\left(1+\frac{q^2\ell^2}{2}\right)I_0\left(\frac{q^2\ell^2}{4}\right) - \frac{q^2\ell^2}{2}I_1\left(\frac{q^2\ell^2}{4}\right)\right]\Bigg\} \end{aligned} \quad (4.14)$$

where I_n is a modified Bessel function of the first kind and ϵ is the dielectric constant. The first term on the rhs of the above equation corresponds to the RPA treatment of the 2DEG interactions.The second term results from the many–body corrections to

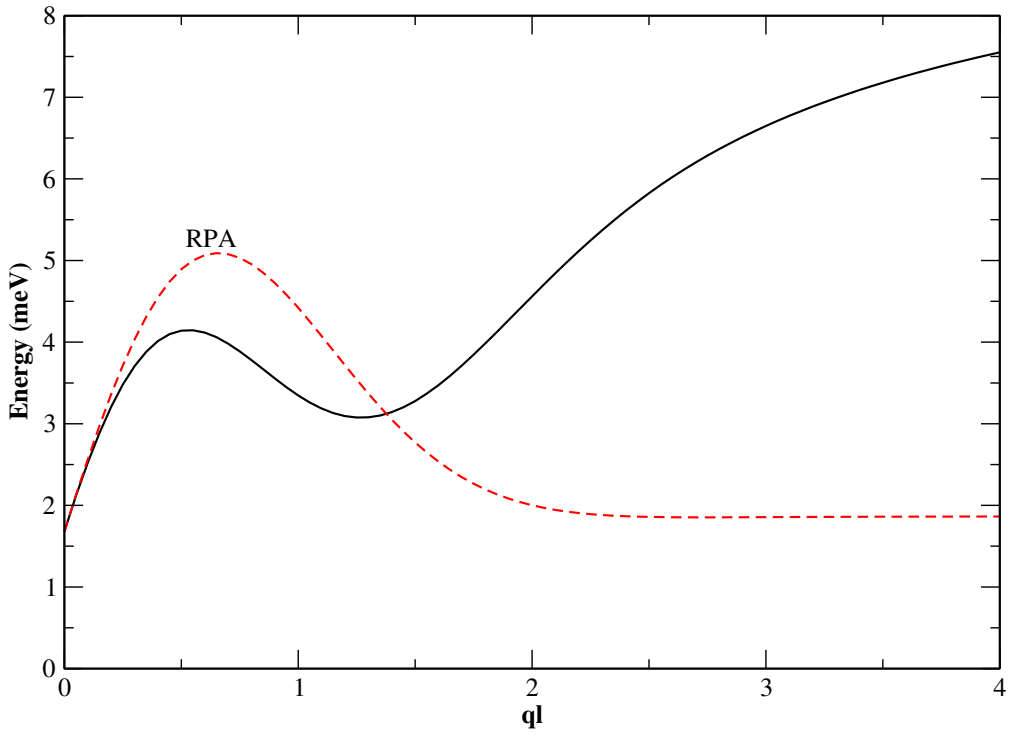

Figure 4.2: (Color online) Energy dispersion $\bar{\Omega}_{\mathbf{q}}$ of the $Y_{\mathbf{q}}$ states, measured with respect to the X_1 energy at ν=1. Solid line: correlated 2DEG. Dotted line: RPA approximation.B=8.7T as in the experiment.

the local field seen by an electron, which at ν =1 correspond to exchange effects. These local field corrections result in a magnetoroton dispersion minimum absent within the RPA, whose detailed momentum dependence is determined by the ground state static structure factor at the corresponding filling factor.[33] Analogous dispersions can be obtained for fractional ν by considering a basis set of 2DEG excitations as in Ref [33].

Fig.5.2 shows $\bar{\Omega}_{\mathbf{q}}$ at ν=1. The energy dispersion of the $Y_{\mathbf{q}}$ continuum basis of states mainly reflects the momentum dependence of the inter–LL excitation energy $\omega_{\mathbf{q}}$, but also depends on the X_{01} dispersion.The origin of the collective excitation dispersion may be seen by first noting that the lowest energy neutral excitations of a non–interacting 2DEG are the N^2 degenerate LL0→LL1 incoherent

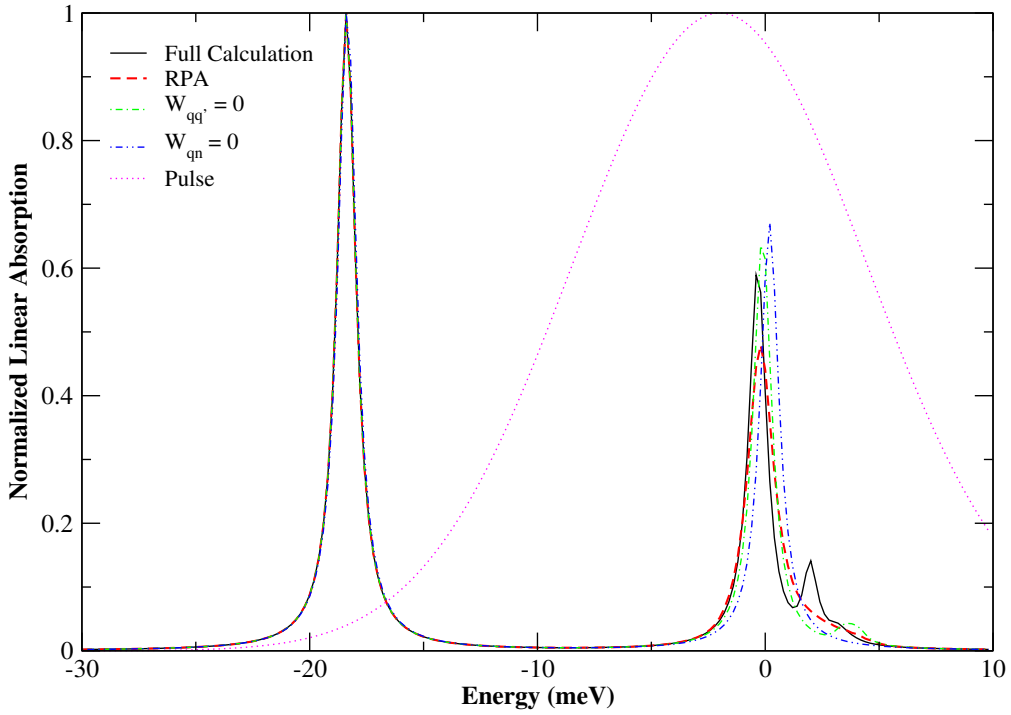

Figure 4.3: (Color online) Linear absorption spectrum.Solid line: full calculation.Dashed–double dotted line: $W_{\mathbf{q}n}$=0.Dashed line: absorption using the RPA dispersion.Dashed–dotted line: $W_{\mathbf{q}\mathbf{q}'}$=0. Also shown is the overlap of the optical pulse with the LL0 and LL1 absorption peaks (dotted line).

pair excitations, which all have energy ω_c^e.This degeneracy is lifted by the electron–electron interaction, which in the case of an incompressible ground state leads to an energy dispersion of the form shown in Fig.5.2. For $q\ell \ll 1$, the momentum dependence of $\bar{\Omega}_{\mathbf{q}}$ is approximately linear, as in the RPA treatment of the 2DEG interactions. However, the RPA fails completely for $q\ell > 1$, where the 2DEG correlations result in a MR dispersion minimum.[24, 25, 31, 33] The drastic change of the $Y_{\mathbf{q}}$ dispersion as compared to the RPA, due to an incompressible ground state, has a significant effect on the X_1–$Y_{\mathbf{q}}$ coupling, since it changes the relative energies(see Fig.5.2). One of our goals here is to study the effects of the inter–LL MR dispersion minimum on the linear and nonlinear optical properties.

Fig.5.3 shows the linear absorption spectrum. By comparing to

the result obtained with $W_{\mathbf{q}n}$=0,which neglects the polaronic effects due to MP coupling, it is clear that the X_1–$Y_{\mathbf{q}}$ coupling gives a third absorption peak above the LL1 exciton peak and not simple broadening. Importantly, this third peak is suppressed if the $Y_{\mathbf{q}}$ energy dispersion is approximated by using the RPA. In the latter case, the coupling of X_1 to the $Y_{\mathbf{q}}$ continuum broadens the LL1 resonance, which suppresses its strength as compared to the full calculation. the differences between the RPA and full dispersion calculations come from the MR minimum, which enhances the X_1–X_{01}+MR coupling. Fig.5.3 also shows the results obtained by treating the X–Y coupling perturbatively (Born approximation), obtained by setting $W_{\mathbf{qq}'}$=0 in Eq.(5.10). The vertex corrections describe rescattering among the continuum of $Y_{\mathbf{q}}$ states and strongly enhance the third absorption peak.

We conclude from Fig.5.3 that the full dynamics of the X+MR excitations and their coupling to X_1 play a crucial role in determining the linear absorption lineshape. We obtain a new resonance close to the LL1 energy.resulting from the coupling of X_1 to {1MR + 1-LL0-e + 1-LL1-h} states in the many–body eigenstates, which is suppressed within the RPA treatment of the 2DEG interactions.An analogy could be drawn between the above resonance at ν=1 and the trion resonances at ν <1 [96, 105, 97, 98](for a review, see Ref.[[95]]). Both come from the coupling of X and Y_n configurations in Eq.(3.30). We note however that X–intra–LL scattering effects are suppressed when the dephasing and disorder characteristic energies are sufficiently strong. For example, in the samples used in the experiments of Refs.[[85, 90]], the LL0 resonance displayed a Lorentzian lineshape while the FWM signal in the case of photoexcitation at the LL0 energy did not produce any unexpected results. On the other hand, these experiments show the emergence, for ν <2, of an asymmetric LL1 resonance with a strong high energy shoulder. In the realistic doped quantum well system,the finite confinement, valence band

mixing, and disorder effects change the exciton energies and X_1–$Y_{\mathbf{q}}$ coupling as compared to our Hamiltonian, which affects the relative magnitudes and energies of the two LL1 peaks.Our calculation a linear absorption lineshape similar the experiment if we consider X_1–$Y_{\mathbf{q}}$ energy splittings smaller than in the ideal 2D system and larger dephasing rates. In this case however, the differences between the RPA and full calculations are suppressed.

4.4 Transient Nonlinear Optical Response

In this section we present our results for the third–order nonlinear polarization.First we use Eq.(3.60) to express the X–X coherence $\langle[\hat{X_m}, \hat{Y_n}]\rangle$ in terms of the two–exciton density matrices $\langle\hat{X}\hat{X}\rangle$ and obtain from Eq.(3.58)

$$\langle X_{-\mathbf{q}10}\hat{X}_{\mathbf{q}10}\rangle = \frac{2V_{10}}{N}P_0^L P_1^L + \langle X_{-\mathbf{q}10}\hat{X}_{\mathbf{q}10}\rangle_c, \tag{4.15}$$

where the first term is the Hartree–Fock X–X contribution.On the other hand, for m=0, n=1 and m=1, n=0.

$$\langle\hat{X}_{-\mathbf{q}mn}\hat{X}_{\mathbf{q}mn}\rangle = \langle\hat{X}_{-\mathbf{q}mn}\hat{X}_{\mathbf{q}mn}\rangle_c \tag{4.16}$$

Since the experimental studies of both doped and undoped quantum wells [83, 84, 110] did not produce any long–lasting FWM signal at negative time delays, which would signify long–lived X–X correlations, [100, 3, 103] we treat for simplicity the X–X interactions within the Hartree–Fock approximation.The interaction matrix element,Eq.(B.42) was obtained by using the commutators Eqs.(3.36,B.7,B.8). The third line on the rhs of Eq.(3.62)was expressed in Appendix B.4 in terms of the Hubbard operator density matrices N_{nm}, $M_{n\mathbf{q}}$, and $N_{\mathbf{q}\mathbf{q}'}$.We thus obtain from Eqs.(**??**, 3.62) after some algebra

$$
\begin{aligned}
i\partial_t P_0 &= (\Omega_0 - i\Gamma_0)P_0 - V_{01}P_1 + d(t)n_0 + V_{01}P_1^L\,(n_0 - 2N_{01}^*) \\
&- V_{01}P_0^L\,(n_1 - 2N_{01}) - P_0^L \sum_{\mathbf{q}} \upsilon_{01}^{01}(\mathbf{q}) \left[\bar{n}_{\mathbf{q}} + \frac{1}{\sqrt{N}}\left(M_{1\mathbf{q}}^* - M_{0\mathbf{q}}\right)\right] \\
&- P_1^L \sum_{\mathbf{q}} \upsilon_{01}^{01}(\mathbf{q}) \left[\bar{n}_{\mathbf{q}} - \frac{1}{\sqrt{N}}\left(M_{1\mathbf{q}} - M_{0\mathbf{q}}^*\right)\right] \\
&- \frac{1}{\sqrt{N}} \sum_{\mathbf{q}} \upsilon_{01}^{01}(\mathbf{q}) P_0^L P_1^L \bar{P}_{\mathbf{q}}^{L*} - \frac{1}{\sqrt{N}} \sum_{\mathbf{q}} \upsilon_{01}^{01}(\mathbf{q}) \bar{P}_{\mathbf{q}}
\end{aligned} \tag{4.17}
$$

$$
\begin{aligned}
i\partial_t P_1 &= (\Omega_1 - i\Gamma_1)P_1 - V_{01}P_0 + d(t)n_1 - V_{01}P_1^L\,(n_0 - 2N_{01}^*) \\
&+ V_{01}P_0^L\,(n_1 - 2N_{01}) + P_0^L \sum_{\mathbf{q}} \upsilon_{01}^{01}(\mathbf{q}) \left[\bar{n}_{\mathbf{q}} + \frac{1}{\sqrt{N}}\left(M_{1\mathbf{q}}^* - M_{0\mathbf{q}}\right)\right] \\
&+ P_1^L \sum_{\mathbf{q}} \upsilon_{01}^{01}(\mathbf{q}) \left[\bar{n}_{\mathbf{q}} - \frac{1}{\sqrt{N}}\left(M_{1\mathbf{q}} - M_{0\mathbf{q}}^*\right)\right] \\
&+ \frac{1}{\sqrt{N}} \sum_{\mathbf{q}} \upsilon_{01}^{01}(\mathbf{q}) P_0^L P_1^L \bar{P}_{\mathbf{q}}^{L*} + \frac{1}{\sqrt{N}} \sum_{\mathbf{q}} \upsilon_{01}^{01}(\mathbf{q}) \bar{P}_{\mathbf{q}}
\end{aligned} \tag{4.18}
$$

The double–peak structure of the linear absorption spectrum close to the LL1 energy implies that the Y and X states couple strongly in the eigenstates of the QHS Hamiltonian, which is described by the coupling between P_n and $\bar{P}_{\mathbf{q}}$.Such linear and nonlinear X–Y couplings are described by the following equation of motion for $\bar{P}_{\mathbf{q}}$, derived in Appendix B.5:

$$
\begin{aligned}
i\partial_t \bar{P}_{\mathbf{q}} &= (\bar{\Omega}_{\mathbf{q}} - i\gamma)\bar{P}_{\mathbf{q}} \frac{\upsilon_{01}^{01}(\mathbf{q})}{\sqrt{N}} \left(P_1 - P_0\right) + \frac{1}{N}\sum_{\mathbf{q}'} W_{\mathbf{q}\mathbf{q}'}\bar{P}_{\mathbf{q}'} + d(t)\left(P_1^{L*} + P_0^{L*}\right)\bar{P}_{\mathbf{q}}^{L} \\
&+ \frac{\upsilon_{01}^{01}(\mathbf{q})}{\sqrt{N}}\left[P_1^L(N_{11} - P_0^{L*}P_0^L - N_{00}) - P_0^L(N_{00} - P_1^{L*}P_1^L - N_{11})\right] \\
&+ \left[\upsilon_{01}^{01}(\mathbf{q}) - V_{01}\right]\left(P_1^L - P_0^L\right)\left(P_1^{L*}\bar{P}_{\mathbf{q}}^L + M_{1\mathbf{q}} - P_0^{L*}\bar{P}_{\mathbf{q}}^L - M_{0\mathbf{q}}\right) \\
&+ \sum_{\mathbf{q}'} \frac{\upsilon_{01}^{01}(\mathbf{q}')}{\sqrt{N}}\bar{P}_{\mathbf{q}'}^L\left(M_{1\mathbf{q}} - M_{0\mathbf{q}}\right) + \frac{\upsilon_{01}^{01}(\mathbf{q})}{\sqrt{N}}\left(P_1^L - P_0^L\right)\left[2N\bar{n}_{\mathbf{q}} - 3\sum_{\mathbf{q}'}\bar{n}_{\mathbf{q}'}\right] \\
&+ \left(P_1^L - P_0^L\right)\sum_{\mathbf{q}'}\frac{\upsilon_{01}^{01}(\mathbf{q}')}{\sqrt{N}}\left[\bar{P}_{\mathbf{q}'}^{L*}\bar{P}_{\mathbf{q}}^L - 4\bar{n}_{\mathbf{q}'\mathbf{q}}\right] + \frac{4}{N}\left(P_1^L - P_0^L\right) \\
&\times \sum_{\mathbf{q}'\mathbf{q}''}\frac{\upsilon_{01}^{01}(\mathbf{q}+\mathbf{q}'-\mathbf{q}'')}{\sqrt{N}}\cos^2\left[\frac{l^2}{2}(\mathbf{q}\times\mathbf{q}' + \mathbf{q}'\times\mathbf{q}'' - \mathbf{q}\times\mathbf{q}'')_z\right]\bar{n}_{\mathbf{q}'\mathbf{q}''} \quad (4.19)
\end{aligned}
$$

The first line on the rhs of Eq.(4.19) describes linear X–Y couplings, similar to the calculation of the linear polarization, while the rest of the terms describe light–induced nonlinear couplings and polarization dephasing.

The nonlinearities in Eqs.(4.17,4.18,4.19) depend on the LLn carrier populations n_n and on the Y–state populations $\bar{n}_{\mathbf{q}}$. As shown in Appendix B.4, the total carrier populations, Eq.(3.31), can be expressed as

$$n_n = 2P_n^L P_n^{L*} + \bar{\nu}_n, \quad (4.20)$$

where the first term is the coherent X_n population and

$$\bar{\nu}_n = 2N_{nn} + \sum_{\mathbf{q}}\bar{n}_{\mathbf{q}}, \quad (4.21)$$

, is the incoherent LLn total electron and hole population, with

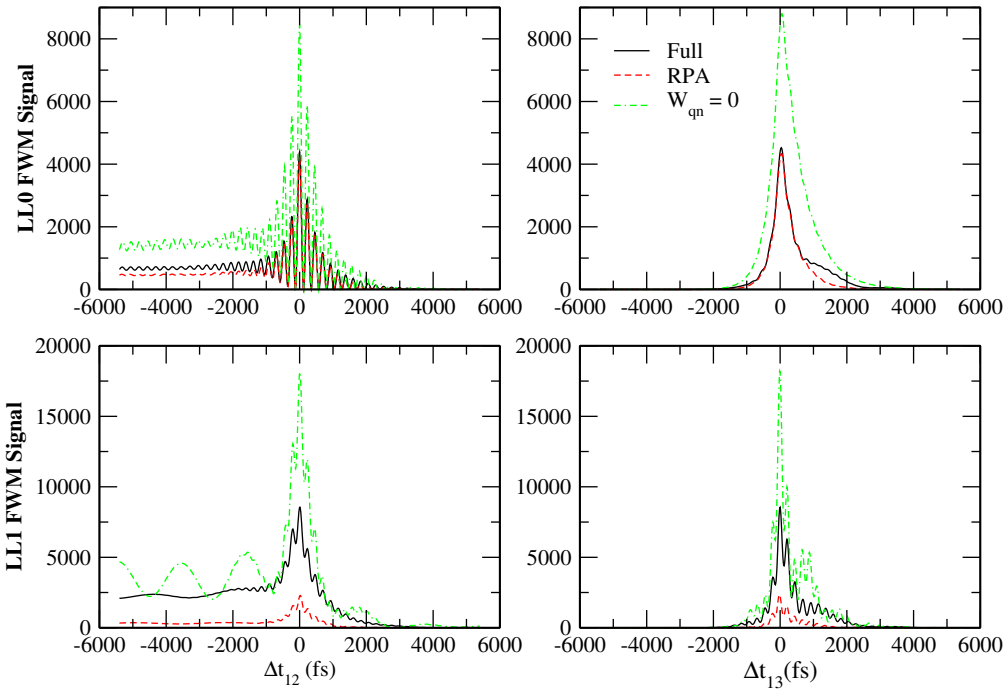

Figure 4.4: (Color online) Interaction effects on the FWM signal along the Δt_{12} and Δt_{13} axes for LL1 photoexcitation. Solid line: Full calculation. Dashed–dotted line: $W_{\mathbf{q}n}$=0, $V_{01} \neq$0 (as in the undoped system). Dashed line: RPA $Y_{\mathbf{q}}$ dispersion.

contributions in the QHS from both the X_n and $Y_{\mathbf{q}}$ configurations, N_{nn} and $\bar{n}_{\mathbf{q}}$ respectively. $\bar{n}_{\mathbf{q}}$= $\bar{n}_{\mathbf{qq}}$, where

$$\bar{n}_{\mathbf{qq'}} = \bar{P}^{L*}_{\mathbf{q}} \bar{P}^{L}_{\mathbf{q'}} + N_{\mathbf{qq'}}, \tag{4.22}$$

The coherences $\bar{n}_{\mathbf{qq'}}$ between Y states with different momenta $\mathbf{q}\neq\mathbf{q'}$ dephase rapidly and are neglected for simplicity. We retain however the $X_n \leftrightarrow Y_{\mathbf{q}}$ coherences $M_{n\mathbf{q}}$, obtained from the equation of motion Eq.(3.52) with dephasing rates $\gamma_{n\mathbf{q}}$=0.5meV without resorting to the adiabatic semiclassical approximation. [17] The total populations n_n were obtained from Eqs.(3.51,3.53) by including the population relaxation rate $\Gamma_{\rm pop}$=$\Gamma_{\mathbf{qq}}$=Γ_{nn}=0.001meV. Our truncation scheme satisfies the total charge conservation condition:

$$\partial_t(n_0 + n_1) = 4\mathrm{Im}[\mathrm{d}^*(\mathrm{t})(\mathrm{P}_0^{\mathrm{L}} + \mathrm{P}_1^{\mathrm{L}})] - \Gamma_{\mathrm{pop}}(\mathrm{n}_0 + \mathrm{n}_1), \qquad (4.23)$$

where the first term on the rhs describes the photoexcited total carrier population.The LL0–LL1 coupling due to the interactions leads to carrier redistribution and coherence between the LLs.Such coupling changes the frequency dependence of the FWM signal as discussed below without however affecting the *total* charge.

4.5 Three–pulse Four Wave Mixing: Numerical Results

We now consider a three–pulse FWM configuration, where the QHS system is excited by three optical pulses

$$d(t) = \mu E_p(t)e^{i(\mathbf{k}_1\cdot\mathbf{r}-\omega_p t)} + \mu E_p(t+\Delta t_{12})e^{i(\mathbf{k}_2\cdot\mathbf{r}-\omega_p t)} + \mu E_p(t+\Delta t_{13})e^{i(\mathbf{k}_3\cdot\mathbf{r}-\omega_p t)},$$

where $E_p(t) = E_0 e^{-(t/t_p)^2}$ is the pulse amplitude and ω_p its central frequency.The optical fields propagate in the spatially distinct directions $\mathbf{k}_1$, $\mathbf{k}_2$, and $\mathbf{k}_3$, with a time delay Δt_{12} (Δt_{13}) between pulses $\mathbf{k}_1$ and $\mathbf{k}_2$ ($\mathbf{k}_3$). For negative time delays, pulse $\mathbf{k}_1$ arrives first. Importantly, *we tune ω_p close to LL1*(see Fig.5.3), which results in small photoexcitation of LL0 transitions as compared to LL1. This choice suppresses the PSF contribution at the LL0 energy and highlights the interaction effects.

We calculated the third–order FWM signal

$$S(\omega, \Delta t_{12}, \Delta t_{13}) = |P_0(\omega) + P_1(\omega)|^2 \qquad (4.24)$$

in the background–free direction $\mathbf{k}_1$+$\mathbf{k}_2$-$\mathbf{k}_3$, as function of frequency and the two time delays. Here we present the time–dependence

along the Δt_{12} axis (Δt_{13}=0) and the Δt_{13} axis (Δt_{12}=0),calculated in all cases at the two frequencies ω corresponding to the peaks of the LL0 and LL1 FWM resonances. For Δt_{13} >0, Δt_{12}=0, pulse $\mathbf{k}_3$ comes first and creates an interband polarization.The latter evolves and decays for a time interval Δt_{13}, when pulses $\mathbf{k}_1$ and $\mathbf{k}_2$ arrive and create the third–order FWM signal.Therefore, the Δt_{13} >0 axis mainly accesses the decoherence of the interband polarization.Along the negative Δt_{13} axis,pulses $\mathbf{k}_1$ and $\mathbf{k}_2$ first create an X–X coherence, which evolves and dephases for a time–interval $|\Delta t_{13}|$ when pulse $\mathbf{k}_3$ arrives. Therefore, the Δt_{13} <0 axis mainly accesses the dephasing of the X–X coherence. Along the negative Δt_{12} axis, pulses $\mathbf{k}_1$ and $\mathbf{k}_3$ arrive first (Δt_{13}=0) and create a second–order X– or Y–state population, or a coherence between different X and Y states. These evolve and relax for a time interval $|\Delta t_{12}|$, at which time pulse $\mathbf{k}_2$ arrives. Therefore, the Δt_{12} <0 axis probes population relaxation and intra–band coherence dephasing and oscillations. Finally, along the positive Δt_{12} axis, pulse $\mathbf{k}_2$ arrives first and creates an interband polarization, which evolves for a time–interval Δt_{12} when pulses $\mathbf{k}_1$ and $\mathbf{k}_3$ arrive. Thus the Δt_{12} >0 axis mainly probes interband polarization dephasing. The dependence of the three–pulse FWM signal on the two time delays gives complementary information on the coherent and relaxation dynamicsof the QHS.

The polarizations P_n, Eqs.(4.17,4.18,4.19),depend on the interactions V_{01}, Eq.(5.4), and $W_{\mathbf{q}n}$, Eq.(4.5).V_{01} gives static LL0–LL1 couplings and X–X interaction nonlinearities similar to the undoped system. $W_{\mathbf{q}n} \propto \upsilon_{01}^{01}(\mathbf{q})$ governs the X–2DEG scattering in the ideal QHS.Next we present numerical results that clarify the role of these two different interaction effects. Fig.5.4 shows the time evolution of the FWM signal at the LL0 and LL1 peak energies for photoexcitation triggered by optical pulses centered close to LL1 as in Fig.5.3. Striking in Fig.5.4 is that, despite the very different photoexcitation of the two LLs, the full calculation with $W_{\mathbf{q}n}\neq 0$ gives LL0 and LL1

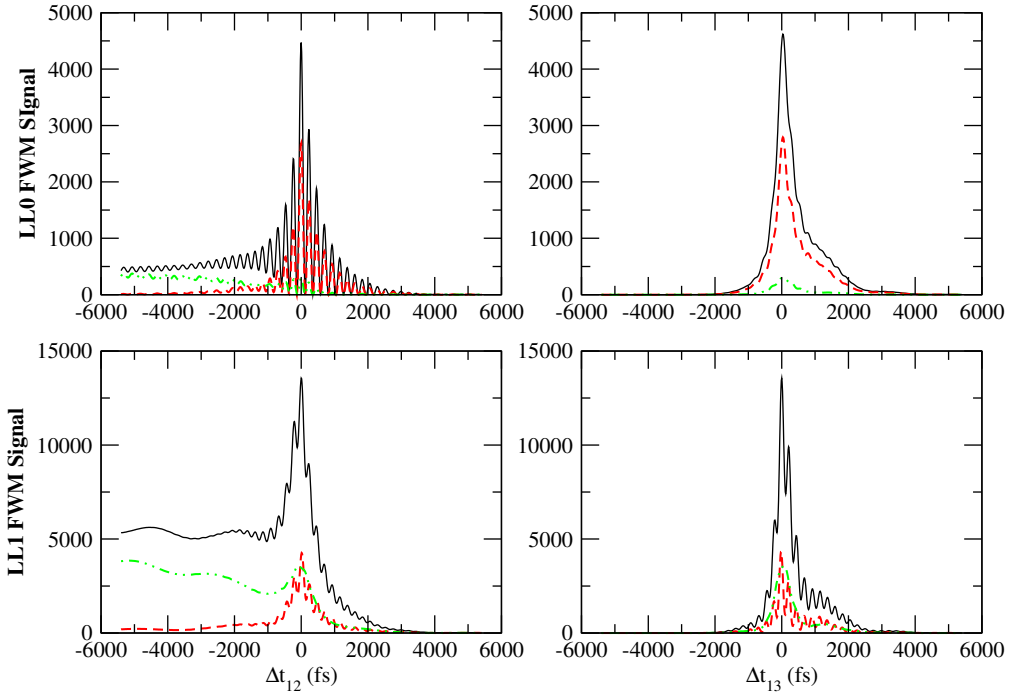

Figure 4.5: (Color online) FWM contribution due to the PSF and X–X interaction nonlinearities(first line on the rhs of Eqs.(4.17,4.18).Solid line: n_n=$2P_n^L P_n^{L*}$ + $2N_{nn}$ + $\sum_{\mathbf{q}} \bar{n}_{\mathbf{q}}$.Dashed line: n_n^X=$2P_n^L P_n^{L*}$ + $2N_{nn}$. Dashed–double dotted line: n_n^Y=$\sum_{\mathbf{q}} \bar{n}_{\mathbf{q}}$.

FWM signals that are *comparable in magnitude*(solid line). This result is consistent with the experiments. [83, 84, 85, 90] On the other hand, for $W_{\mathbf{q}n}$=0, $V_{01}\neq$0, the LL0 signal is *much smaller* than the LL1 signal (dashed–dotted line in Fig.5.4), as expected for LL1 photoexcitation and as observed experimentally in the undoped system.[110] We conclude that the X–2DEG interactions drastically enhance the LL0/LL1 FWM peak ratio.Fig.5.4 also shows that they drastically change the decay and amplitude of the coherent FWM oscillations.

The X–2DEG interactions couple X_1 to the continuum of $Y_{\mathbf{q}}$ states, in a way that depends on the dispersion of their excitation energies $\bar{\Omega}_{\mathbf{q}}$. To study the effect of the MR minimum, which is characteristic of an incompressible quantum liquid, on the FWM signal,

we compare in Fig.5.4 (and in Fig.5.7(a)) our full result to that obtained by treating the 2DEG interactions within the RPA (dashed line). The RPA dispersion broadens the LL1 FWM resonance while having a smaller effect on the LL0 FWM strength, a result consistent with the linear absorption behavior of Fig.5.3. This RPA broadening is suppressed in the case of an incompressible quantum liquid and significantly depresses the LL1/LL0 FWM ratio. We thus conclude that the LL1/LL0 FWM peak ratio depends sensitively on the correlations leading to an incompressible quantum liquid with magnetoroton inter–LL excitations. The RPA also results in a faster decay of the LL0 coherent FWM oscillations along the $\Delta t_{12} < 0$ axis. This oscillation decay is induced by the X–2DEG interaction. Importantly, the full calculation gives a non–exponential decay of the LL0 signal along the $\Delta t_{13} > 0$ axis, absent within the RPA or for $W_{\mathbf{q}n}$=0. This behavior reflects the non–Markovian polarization dephasing due to X–Y coupling in the presence of MR excitations (compare the full and RPA calculations in Fig.5.4 along the $\Delta t_{13} > 0$ axis). We conclude that the temporal profile of the LL0 FWM signal in the case of LL1 photoexcitation may be used to measure the quantum dynamics due to magnetoexciton interactions with an incompressible 2DEG, which differs significantly as compared to the RPA.

The PSF and X–X interaction nonlinearities,previously studied for magnetoexcitons in undoped semiconductors, [**?**, 103, 110]are described by the first line on the rhs of Eqs.(4.17,4.18).Fig.5.5 shows the contribution of these nonlinearities, which have the form $d(t)n_n$ (PSF) and $P_n n_m$, $P_n N_{01}$ (X–X interactions), to the FWM signal and also includes the effects of the linear P_n–$\bar{P}_{\mathbf{q}}$ coupling (first line in Eq.(4.19)), which gives interaction–induced polarization dephasing =similar to the linear response.The above nonlinearities give a large part of the overall FWM signal in the ideal QHS. However, their contribution differs from the full result, Fig.5.4,at the LL1 energy. This difference comes from the light–induced changes in the X energies,

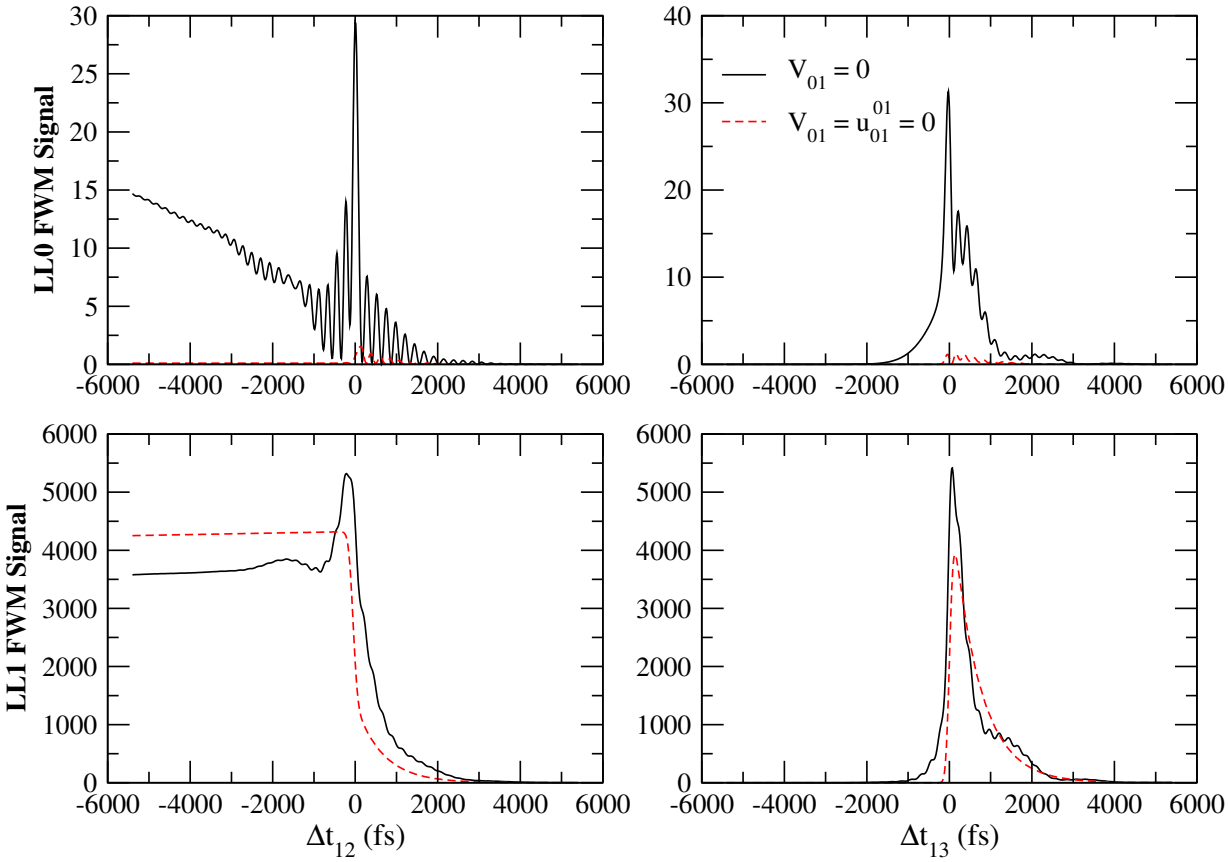

Figure 4.6: (Color online) FWM signal for V_{01}=0. Solid line: Effect of X–2DEG interactions, $W_{\mathbf{q}n} \neq$0.Dashed line: Non–interacting system, $W_{\mathbf{q}n}$=0.

inter–LL couplings, and dephasing described by the rest of the nonlinear terms on the rhs of Eqs.(4.17,4.18,4.19, which are generated by the X–2DEG interaction $v_{01}^{01}(\mathbf{q})$. The PSF and X–X interactions give a large LL1/LL0 FWM peak ratio, similar to the $W_{\mathbf{q}n}$=0 result in Fig.5.4 and the undoped system.[110] The $W_{\mathbf{q}n}$=0, $V_{01} \neq 0$ FWM signal differs from that in Fig.5.5 due to the changes in the population relaxation and the dephasing of the $X_0 \leftrightarrow X_1$ coherence induced by the X–2DEG interactions.

Fig.5.5 also compares the PSF+X–X interaction nonlinear contribution for populations given by (i)n_n=n_n^X+n_n^Y (full result), (ii)

n_n=n_n^X=$2P_n^L P_n^{L*} + 2N_{nn}$ (population of X_n states only), and (iii) n_n=n_n^Y=$\sum_{\mathbf{q}} \bar{n}_{\mathbf{q}}$ (population of the continuum of $Y_{\mathbf{q}}$ states).The excitonic contribution to the LLn population, n_n^X,gives a FWM signal that decays for Δt_{12} <0 and is relatively small.The strong effect of the X–2DEG interaction on this excitonic signal can be seen by comparing it to the $W_{\mathbf{q}n}$=0, $V_{01}\neq$0 result in Fig.5.4 (dashed–dotted line). Importantly, Fig.5.5 demonstrates that the Δt_{12}<0 axis FWM signal reflects the gradual build–up of the Y–state populations n_n^Y, due to the X→Y scattering, and increases slowly with time. We conclude that the population of the Y–state continuum states plays an important role in determining the magnitude and temporal profile of the FWM signal due to PSF+X–X interactions in the QHS.

To elucidate the nonlinear response due to the X–2DEG interaction,we show in Fig.5.6 the FWM results obtained by setting V_{01}=0 and compare them to the non–interacting system for optical pulses tuned as in Fig.5.3. For V_{01}=0, the X–X interactions and static LL0–LL1 couplings vanish, which affects both the linear and nonlinear polarizations. The nonlinearities then result from PSF and X–2DEG interactions. The latter interactions introduce the nonlinear terms in the last two lines on the rhs of Eqs.(4.17,4.18) and on the rhs of Eq.(4.19). They also change the carrier relaxation, which affects the PSF contribution. We see in Fig.5.6 that the LL0 FWM signal of the non–interacting system is very small, as expected for LL1 photoexcitation, and is determined by PSF alone. For $W_{\mathbf{q}n} \neq 0$, the X–2DEG interactions generate a LL0 signal that increases slowly with time along the LL0 $\Delta t_{12} < 0$ axis,which reflects the population dynamics. However, this LL0 signal is still small in the case of LL1 pohotoexcitation of the ideal QHS as in Fig.5.3. We thus conclude that the LL0 signal in Fig.5.4 is mainly generated by X–X interactions modified by X–2DEG scattering. The nonlinearities generated by the X–2DEG interaction give the $\Delta t_{13} < 0$ FWM signal in Fig.5.6, which cannot arise from PSF, and lead to non–exponential decay along the

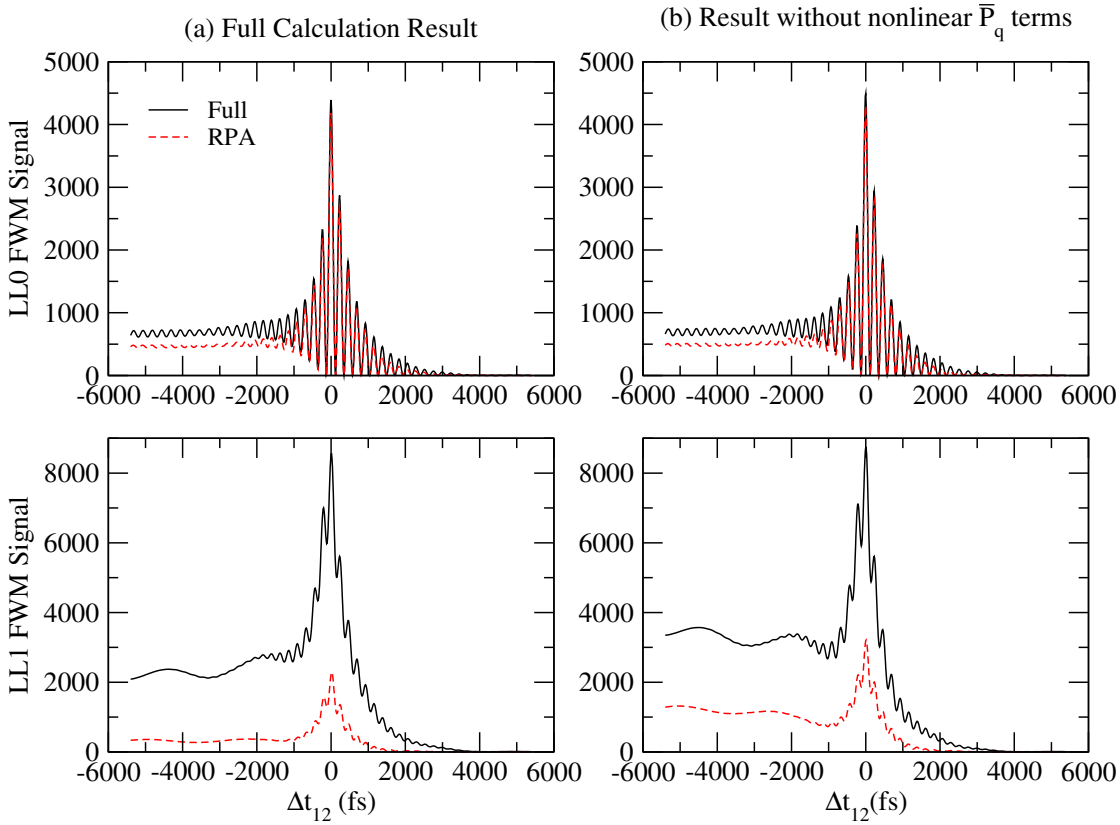

Figure 4.7: (Color online) Effect of nonlinear contributions and 2DEG correlations on $\bar{P}_{\mathbf{q}}$. (a) Full calculation (b) First line on the rhs of Eq.(4.19).Solid line: full dispersion $\bar{\Omega}_{\mathbf{q}}$.Dashed line: results using the RPA dispersion.

$\Delta t_{13} > 0$ axis. The overall FWM behavior results from the interplay between the X–X and X–Y interactions, whose relative contribution depends on the particularities of the realistic system.

Next we consider the coupling between the nonlinear coherences P_n and $\bar{P}_{\mathbf{q}}$,due to the X–2DEG interaction. As already seen by the emergence of the extra absorption peak in Fig.5.3, the linear P_1^L–$\bar{P}_{\mathbf{q}}^L$ coupling changes drastically the 1h eigenstates, in a way that depends critically on the dispersion of the $Y_{\mathbf{q}}$ states. The X and $Y_{\mathbf{q}}$ states are not eigenstates of the system, as demonstrated by the comparison of to the results obtained for $W_{\mathbf{q}n}$=0, in which case X_n

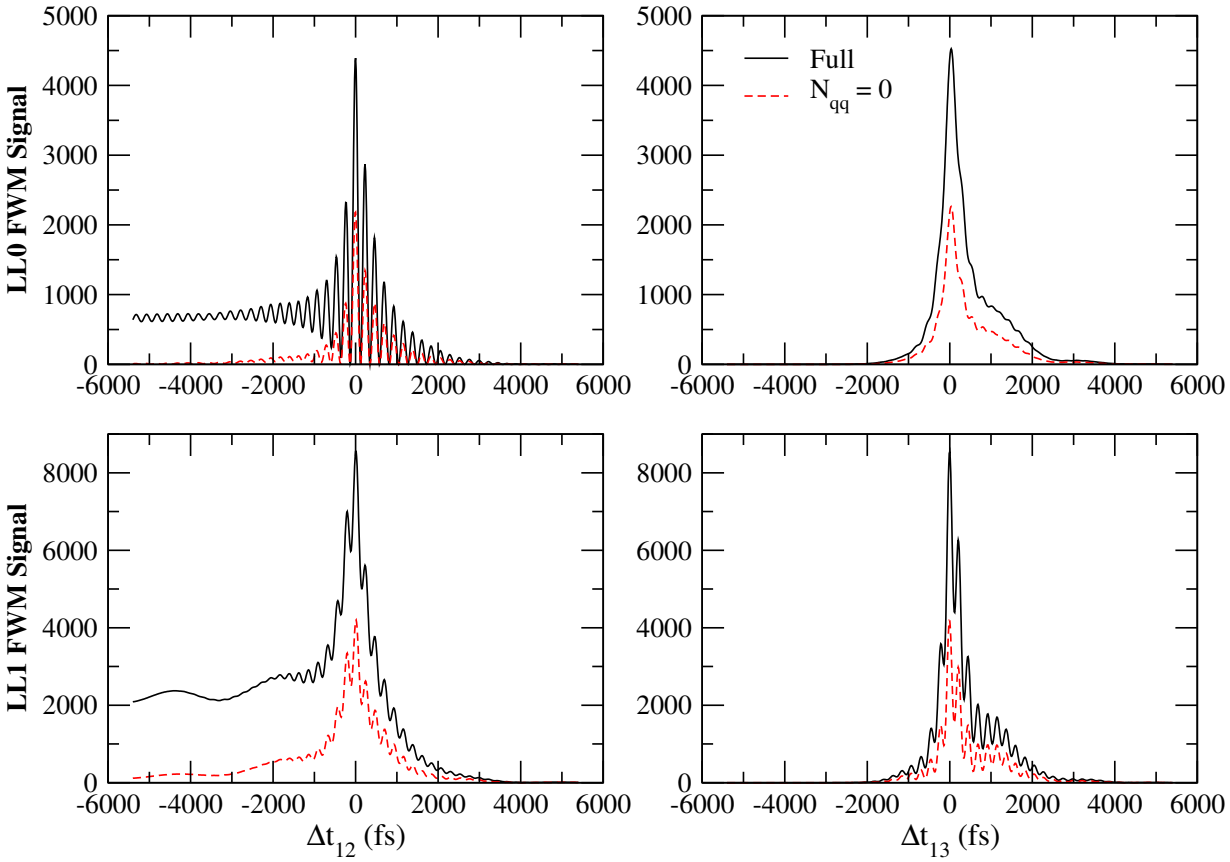

Figure 4.8: (Color online) The role of the Y–state populations $N_{\mathbf{qq}}$. Solid line: full FWM calculation. Dashed line: FWM signal with $N_{\mathbf{qq}}$=0.

are approximate eigenstates in our calculation. Rather, the equations of motion Eqs.(4.17,4.18,4.19)describe polaronic effects in the time domain that lead to eigenstates consisting of a coherent superposition of X_1 and $Y_{\mathbf{q}}$ configurations. Fig.5.7(b)shows the result obtained by only retaining the first line on the rhs of Eq.(4.19), which treats the above coupling similar to the linear polarization calculation. The comparison of Fig.5.7(b)to the full calculation, Fig.5.7(a), shows that the nonlinear contributions to $\bar{P}_{\mathbf{q}}$ (last four lines on the rhs of Eq.(4.19)) mainly decrease the Δt_{12} <0 LL1 signal but do not change the overall qualitative behaviour. Fig.5.7 also compares the full and RPA dispersion calculations and shows more clearly that

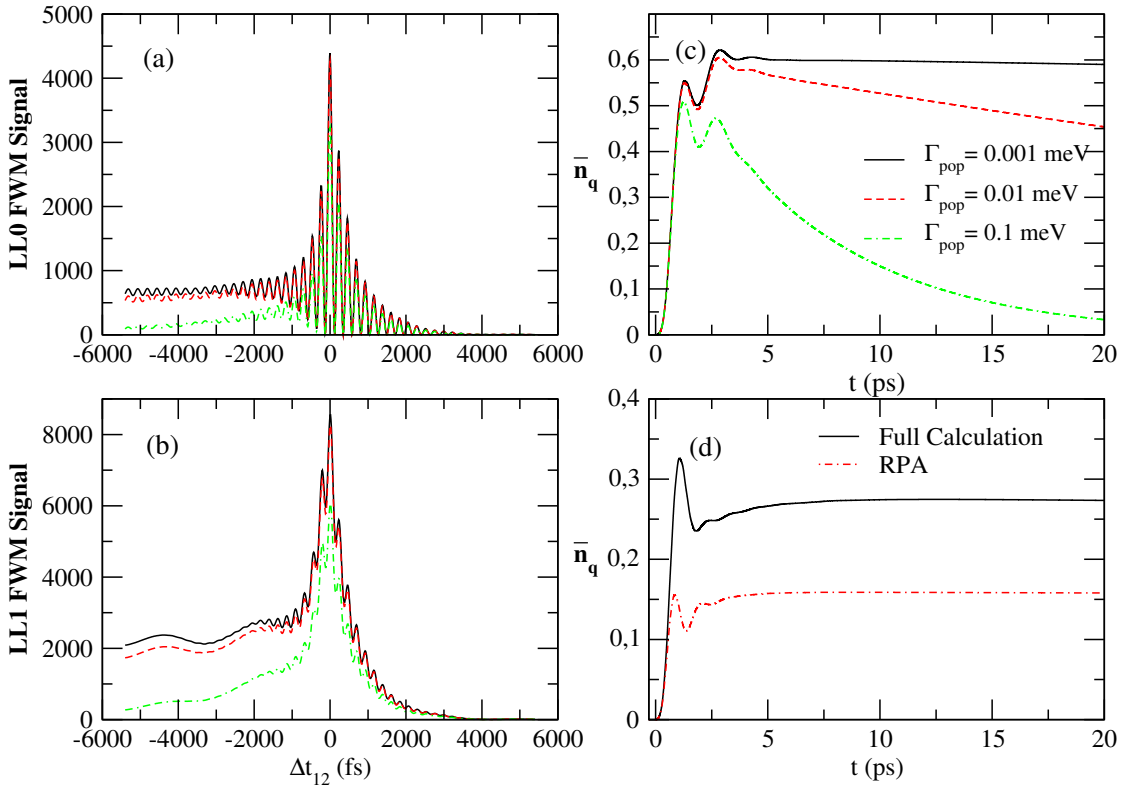

Figure 4.9: (Color online) Dependence of the Δt_{12} axis FWM signal on the population relaxation rate Γ_{pop}=$\Gamma_{\mathbf{qq}}$=Γ_{nn}. (a) LL0 signal. (b) LL1 signal. (c) Time–dependence of the Y–state population $\bar{n}_{\mathbf{q}}(t)$ for ql=1. (d) Comparison of $\bar{n}_{\mathbf{q}}(t)$ for ql=2 between full (solid line) and RPA (dashed–dotted line) Y–state dispersions.

the RPA dispersion depresses the LL1 nonlinear signal and enhances the decay of the LL0 coherent FWM oscillations. The RPA broadening comes from the X_1 coupling to the entire $Y_{\mathbf{q}}$ continuum, given by the first line on the rhs of Eq.(4.19), which is suppressed in the full calculation due to the MR excitation energy minimum of the incompressible quantum liquid.

We now turn to the FWM signal generated by the Y–state populations $\bar{n}_{\mathbf{q}}(t)$, Eq.(5.16). In Fig.5.8 we compare the full FWM calculation with the result obtained by setting $N_{\mathbf{qq}}$=0, in which case $\bar{n}_q$=$\bar{P}^{L*}_{\mathbf{q}}\bar{P}^{L}_{\mathbf{q}}$ is given by the Y–state coherences. Fig.5.8 demonstrates

that the long–lived Y–state populations $N_{\mathbf{qq}}$ give a LL0 FWM signal that *rises* with Δt_{12} <0 following the initial coherent regime. This can be seen by comparing the full and $N_{\mathbf{qq}}$=0 results in Figs.5.8(a) and (b).For $N_{\mathbf{qq}}$=0, the FWM signal decays fast along the Δt_{12} <0 axis. The full calculation signal builds up gradually and then decays as determined by the population relaxation rate Γ_{pop}=Γ_{nn}=$\Gamma_{\mathbf{qq}}$. This is seen more clearly in Figs.4.9(a) and (b), where we compare the LL0 and LL1 FWM for the different relaxation rates given in the inset of Fig.4.9(c). The rise time of the LL0 signal for Δt_{12} <0 reflects the slow build–up of $\bar{n}_{\mathbf{q}}(t)$, shown in Figs.4.9(c) and (d) at different momenta, as the X states de–populate due to irreversible X→X+MP scattering.Fig.4.9 shows that the dynamics of this X–2DEG interaction process can be resolved with femtosecond pulses. The strong coupling of the X+MR final states, missed by the RPA, is demonstrated by Fig.4.9(d), which compares the populations of the $Y_{\mathbf{q}}$ states with ql=2 for the full or RPA dispersion. At such momenta, the two dispersions deviate strongly (see Fig.5.2).Fig.4.9(d) shows that the MR excitations characteristic of the incompressible 2DEG result in larger X+MR populations as compared to the RPA, which implies stronger coupling of X_1 to the $Y_{\mathbf{q}}$ states with MR momenta.

The above results indicate the important role of carrier relaxation due to X–2DEG scattering on the three–pulse FWM signal, in addition to the non–Markovian polarization dephasing effects. Figs.4.10(a) and (b) show the time–dependence of the total LLn carrier populations, n_n,for LL1 photoexcitation by a single pulse as in Fig.5.3. The role of the X–2DEG interaction is seen by comparing to the populations obtained for $W_{\mathbf{q}n}$=0, V_{01} ≠0 as in the undoped system. The LLn electron and hole populations, given by Eqs.(5.15,4.21),include coherent and incoherent contributions rom both the X_n and $Y_{\mathbf{q}}$ states, which are shown in Figs.4.10(c) and (d).

In the initial coherent temporal regime,n_n∼$2P_n^{L*}P_n^L$. The time

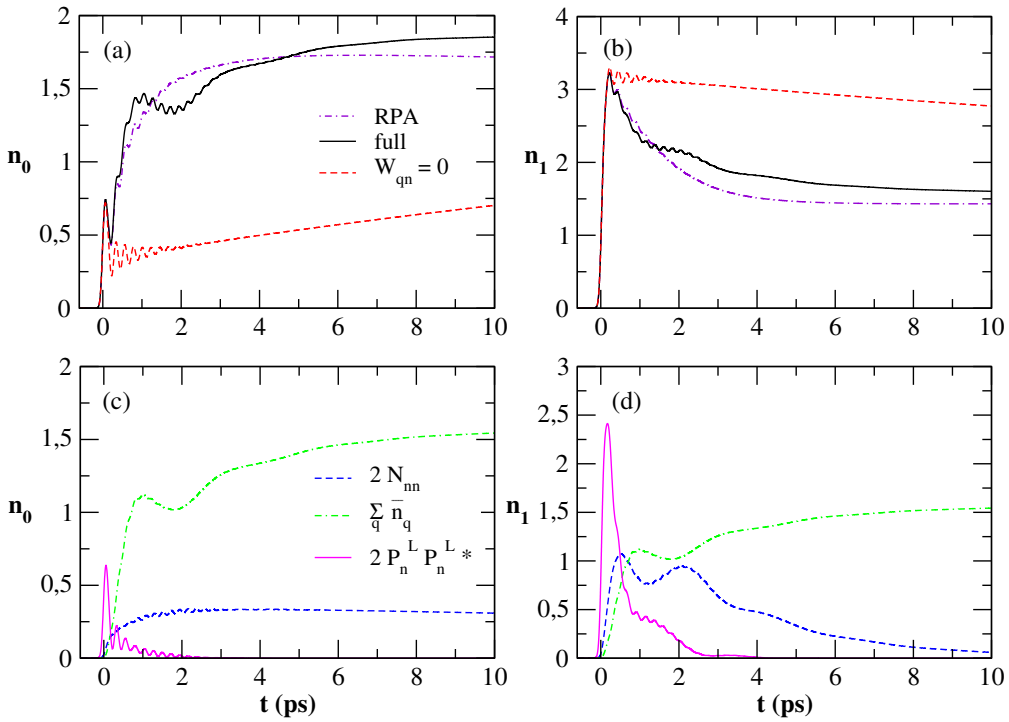

Figure 4.10: (Color online) Time evolution of the total carrier populations $n_n(t)$. Solid line: full calculation.Dashed line: $W_{\mathbf{q}n}$=0, $V_{01}\neq 0$. Dashed–dotted line: RPA dispersion. (c) and (d): coherent and incoherent contributions, Eqs.(5.15,4.21), to the LLn total electron and hole populations.

evolution of these coherent exciton populations is shown in Figs.4.10 (c) and (d).The non–exponential time evolution of the LL1 populations in Fig.4.10(d) is due to the emergence of the two LL1 peaks (Fig.5.3) as a result of the MR dispersion minimum.By comparing to the RPA,Figs.4.10 (a) and (b) show that these quantum kinetic effects manifest themselves on the carrier relaxation. We also note that n_1/n_0 ∼4 in the coherent regime, due to the different photoexcitation of the two LLs.It is clear that the early time LL1/LL0 FWM ratio in Fig.5.4 does not simply reflect the photoexcited carrier ratio n_1/n_0, in agreement with the experiment.[83, 85]

Figs.4.10(a) and (b) clearly show that, following the initial coherent temporal regime, the X–2DEG interaction drastically changes

the carrier relaxation and n_0/n_1 population ratio as compared to the undoped system. The LL0 population increases sharply for intermediate timescales (Fig.4.10(a)), while simultaneously the LL1 population drops (Fig.4.10(b)) and the Y–state populations build up (Figs.4.9(c) and (d)). The above dynamics is due to the $X_1 \rightarrow X_{01}$ +MP interaction process of Fig.5.1(a), which involves inter–LL 2DEG excitations and couples the two LLs.The population time–dependence differs markedly for $W_{\mathbf{q}n}$=0, in which case the coupling of the X_0 and X_1 populations comes from the nonresonant e–h interaction process described by the $X_0 \leftrightarrow X_1$ coherence $N_{01}(t)$ in Eq.(3.51). In the QHS,the population relaxation is governed instead by the resonant $X_1 \rightarrow$Y interactions and the $X_1 \leftrightarrow Y_{\mathbf{q}}$ coherence. The population time–dependence becomes similar to the undoped system if we set $M_{n\mathbf{q}}$=0 in Eqs.(3.51,3.53).The LL0 population rise–time in Fig.4.10(a) is mainly determined by the dynamics of $M_{1\mathbf{q}}$(t). At sufficiently long times, when the scattering is complete, the carrier populations n_n are determined by the total population of the continuum of {1MP + 1-LL0-e + 1-LL1-h} states, $n_n^Y = \sum_{\mathbf{q}} \bar{n}_{\mathbf{q}}$, whose time–dependence and slow rise is shown in Figs.4.10(c) and (d) (dashed–dotted line). As a result, $n_0 \sim n_1$ at long times, in contrast to the $W_{\mathbf{q}n}$=0 result, which gives $n_1 > n_0$ as in the undoped system.[110] Figs.4.10(c) and (d) also show the time–dependence of the incoherent exciton populations $N_{nn}(t)$ (dashed line). N_{00} relaxes very slowly, as determined by Γ_{pop}. In contrast, the relaxation of N_{11} is fast in the QHS and occurs on a time scale of a few picoseconds, which coincides with the build–up of n_n^Y. This rapid relaxation of the LL1 excitonic population due to inter–LL MP scattering is absent for $W_{\mathbf{q}n}$=0 and changes the temporal profile of the 2DEG FWM.

4.6 Conclusions

In conclusion, we discussed in full detail a non–equilibrium many–body theory that describes the ultrafast coherent non-linear optical response of magnetoexcitons interacting with an incompressible quantum liquid. For this, we developed a density matrix quantum kinetic description of dephasing/decoherence and relaxation in systems with a strongly correlated ground state, which recovers established results in undoped semiconductors and does not adopt the semiclassical or Boltzmann pictures of instantaneous interactions, structureless 2DEG bath, and quasi–equilibrium free energy.

Our main motivation for developing this theory was to identify the signatures of an incompressible quantum liquid in nonlinear optical spectroscopies and compare to recent experiments. [83, 84, 85, 90] We note that photoexcitation with three time–delayed femtosecond optical pulses accesses a much larger phase space than the more conventional one–dimensional four–wave–mixing or linear spectroscopic techniques. The main question down the road is how two–dimensional correlation spectroscopy [113] can be used to resolve the detailed dynamics of the fundamental many–body interaction processes in strongly correlated systems.

Our goal here was to identify generic temporal and spectral features due to exciton coupling with an incompressible quantum liquid. For this we presented numerical results obtained for an ideal two–dimensional 2DEG at filling factor ν=1. This is the simplest system for studying the generic effects of inter–LL magnetoroton collective excitations, which are signatures of the many–body corrections in the local field of an incompressible quantum liquid, and their coupling to Xs. We studied the differences between the full calculation of the third–order nonlinear polarization and the results obtained by treating the 2DEG interactions within the RPA. The latter approximation only gives MP long–wavelength collective excitations but

misses the magnetoroton minimum. We described the effects of the dynamical coupling between the X and X+MP or X+MR configurations by spectrally resolving the FWM signal and then comparing its strength and time evolution along two time axes at the LL0 and LL1 energies. We showed that it is usefull for drawing conclusions to excite the system close to the LL1 energy, so that the LL0/LL1 ratio of photoexcited carrier populations is kept small and the Phase Space Filling nonlinearities at the LL0 energy are suppressed. A non–interacting multi–level system calculation then predicts a correspondingly small ratio of LL0/LL1 FWM signals. This also holds true in the undoped system, [110] despite the coupling of the LL0 and LL1 magnetoexcitons by the exciton–exciton interaction nonlinearities. The experimental measurements in the 2DEG revealed comparable LL0 and LL1 FWM signals for ν <2 even though the photoexcited LL1 carriers far exceeded the photoexcited LL0 carriers, in sharp contrast to an undoped quantum well system under the same photoexcitation conditions. [83, 85, 84] These experiments also revealed the emergence of a strong high energy shoulder above the LL1 exciton peak for ν <2, as empty LL0 states become available for LL1→LL0 scattering.[85] Our calculations offer a possible microscopic explanation of these experimental features, which clearly distinguish the dynamics of magnetoexcitons interacting with a 2DEG at filling factors ν <2 from that of magnetoexcitons in an undoped semiconductor system. Here we also predict the experimental signatures of an incompressible 2DEG.

By treating the full quantum kinetics of the coupling between the LL1 magnetoexciton and the continuum of {1-LL0-e + 1-LL1-h + LL0→LL1 MP } configurations, we obtained n a double–peak spectral lineshape close to the LL1 energy. This double resonance is suppressed by the RPA treatment of the 2DEG interactions, which misses the magnetoroton excitations and simply broadens the LL1 excitonic resonance. Such broadening is suppressed in our full calcu-

lation, which gives indicates polaronic effects due to the coupling of MRs. The above result may explain the experimental observation, for ν <2, of a strong high energy shoulder right above the LL1 energy, while at the same time the LL0 resonance remains Lorentzian. [85] This difference in resonance lineshape results from the suppression of the X_0–2DEG coupling.

Our calculations show that the ratio of the LL1 and LL0 FWM resonance strengths does not simply reflect the photoexcited carrier populations, as in an atomic–like noninteracting system, but depends on interaction–induced nonlinearities and couplings in the presence of an interacting 2DEG. By only including the X–X interactions, or in a completely non–interacting system, we obtain a LL1 peak FWM signal that far exceeds the LL0 peak signal. In contrast, the full calculation gives comparable FWM peaks, despite the different LL0 and LL1 photoexcitation. This result is consistent with the experimental observations [83, 85, 84] and comes from the gradual population of {1-LL0-e + 1-LL1-h + LL0 $\rightarrow$ LL1 MP } configurations in the many–body igenstates and from their coherent dynamical coupling to the discrete X states.

Our quantum kinetic calculation shows that femtosecond optical pulses can be used to resolve the details of this non–instantaneous interaction process, whose dynamics is described by the time evolution of the X and $Y_{\mathbf{q}}$–state populations coupled by a X $\leftrightarrow$ $Y_{\mathbf{q}}$ coherence.

The comparison between our full calculation and the RPA results show that the optical spectra and their time evolution are sensitive to the magnetoroton minimum in the excitation dispersion of an incompressible liquid. The latter changes the exciton coupling to the continuum of X+MP configurations. In particular, the RPA dispersion broadens the LL1 resonance, while this broadening is suppressed in the full calculation. This drastic effect of the 2DEG correlations strongly affects the LL1/LL0 FWM peak ratio and reflects on the time evolution of the FWM lineshape. Along the Δt_{13} axis, the

incompressible quantum liquid gives a non–exponential FWM decay that reflects the non–Markovian interaction–induced exciton dephasing. Along the Δt_{12} axis, the incompressible quantum liquid determines the decay time of the LL0 coherent FWM oscillations Another experimental signature is the rise–time of the $\Delta t_{12} < 0$ LL0 FWM signal, which is determined by the X–Y coupling described by the dynamics and dephasing of the $X \leftrightarrow Y$ coherences. A comparison to the experimental results of [83, 85, 84] will be presented elsewhere.

The numerical calculations discussed here did not explore the full phase space accessible with two–dimensional correlation spectroscopy. [113] Nevertheless, they clearly show that these experiments can isolate the different physical processes and measure the details of the magnetoexciton coupling to an incompressible quantum liquid at different filling factors and ground states. In the realistic system, the relative magnitude of the different competing contributions also depend on the valence bandstructure, disorder, finite quantum well confinement, doping asymmetry, and dephasing rates, which are clearly important for a detailed description of the experiments. For example, here we did not address the formation of trion states and their nonlinear response, or quasiexcitons at fractional filling factors. Future experimental and theoretical studies promise to elucidate the dynamics of both spin and charge elementary excitations and their interactions in strongly correlated systems.

Chapter 5

Inter-LL Dynamical couplings

In this chapter we corroborate, by comparing our microscopic calculation and experiment, our earlier claim that the dynamical coupling of the two lowest magnetoexcitons by inter–LL MP and MR excitations is an important nonlinearity in the QHS.For this we present numerical results obtained by calculating the parameters that enter the theory using the ν=1 QH ground state and a Hamiltonian that captures the essential physical processes.

5.1 Description of the model

We consider a two–band Hamiltonian describing two–dimensional electrons and holes subject to a perpendicular magnetic field. [21]. We also consider right–circularly polarized light, which excites a single interband transition that creates spin–$\downarrow$ electrons and results in a single LL0 peak. [85] We use the Landau gauge and label the single–particle states by $\alpha = (k, n, \sigma)$, where k is proportional to the cyclotron orbit center x–coordinate, n is the LL index, and s denotes the carrier spin. $\varepsilon_\alpha^{e,h}=\omega_c^{e,h}(n+1/2)$,where $\omega_c^{e,h} = eB/m_{e,h}$ are the electron and hole cyclotron energies ($\hbar$=1). Although this discrete LL energy structure resembles an atomic system, each level has a macroscopic degeneracy N. Some particularities of the realistic system

missed by our model, such as finite quantum well height and width, symmetric vs asymmetric doping and confining potential profiles, spin–orbit interaction,etc lift the optical selection rules due to invariance under magnetic translations ("geometric symmetry") [105] and electron–hole symmetry ("hidden symmetry"). [106, 107, 95] This is important, e.g., for trion formation and for the observation of skyrmion and composite fermion effects.[99] Nevertheless, our predicted spectral and temporal features, due to LL0–LL1 dynamical coupling,are ubiquitous and largely independent of such particularities.

At ν=1, the 2DEG in the ground state Laughlin wavefunction [27] populates all N of the spin–$\uparrow$ LL0 states, while all spin–$\downarrow$ LL0 states and all higher LLs are empty.Signatures of such spin polarization [25, 108] were observed in linear absorption experiments at temperatures as high as a few Kelvin. [109] The lowest 2DEG neutral excitations are LL0$\rightarrow$LL1 excitations, while screening is suppressed by the LL0–LL1 energy gap.[31] Due to the hidden symmetry,[106] $\langle \hat{Y}_n \rangle$ in Eq(3.30) vanishes if we project within a single LL, in which case the optical response resembles that of a non–interacting system. We break the hidden symmetry by photoexciting both LL0 and LL1 states and by considering LL0–LL1 mixing due to inter–LL 2DEG excitations.We neglect states with energy comparable to LL2 or higher, such as higher excitons and states with two or more inter–LL excitations, whose FWM contribution is suppressed due to their small energetic overlap with the optical pulses and their enhanced dephasing. We note that a similar approximation in the many–body eigenstates is used in the literature since, in most cases, it describes the 2DEG excitation spectrum well.[33, 72] It even becomes exact for very large magnetic fields, when the Coulomb-to-cyclotron energy ratio $e^2/(\epsilon l \omega_c^e)$ becomes smaller than 1 (ϵ is the dielectric constant). We note however that, in GaAs at 10T, ω_c $\sim$18meV for electrons, while the characteristic Coulomb energy $e^2/\epsilon l$ $\sim$14meV. Therefore,

for quantitative fits to experiments, one must include higher LLs.

Here we solve a *polaronic problem* where the LL0 (X_0) and LL1 (X_1) magnetoexcitons couple to a continuum of {1-LL0-e + 1-LL1-h + LL0→LL1 MP} four–particle excitations ($Y_{\mathbf{q}}$). In the case of X_1, the e–2DEG interaction scatters the LL1 electron to LL0 by emitting a LL0→LL1 2DEG excitation at small total energy cost. This resonant interaction process couples $|X_1\rangle$ to the continuum of orthonormal states [21]

$$|Y_{\mathbf{q}}\rangle = \hat{Y}^{\dagger}_{\mathbf{q}}|G\rangle = \hat{X}^{\dagger}_{\mathbf{q}01}\hat{\rho}^{e}_{-\mathbf{q}10\uparrow}|G\rangle, \tag{5.1}$$

where

$$\rho^{e}_{\mathbf{q}10\sigma} = \frac{1}{\sqrt{N}}\sum_{k} e^{iq_x k\ell^2}\hat{e}^{\dagger}_{k+q_y/21\uparrow}\hat{e}_{k-q_y/20\uparrow} \tag{5.2}$$

creates a LL0 → LL1 magnetoplasmon or magnetoroton [32, 33] and

$$\hat{X}^{\dagger}_{\mathbf{q}01} = \frac{1}{\sqrt{N}}\sum_{k} e^{ikq_x\ell^2}\hat{e}^{\dagger}_{k+q_y/20\downarrow}\hat{h}^{\dagger}_{-k+q_y/21\downarrow} \tag{5.3}$$

creates a {1-LL0-e + 1-LL1-h} interband excitation.In $Y_{\mathbf{q}}$, the X_{01} and MP degrees of freedom have opposite momenta $\mathbf{q}$ and are strongly correlated.The analogy to the X–X correlation in undoped semiconductors [100] is clear. As we shall see, the dephasing of $Y_{\mathbf{q}}$ has an important effect on the optical response. X_0 also couples to the $|Y_{\mathbf{q}}\rangle$ when its LL0 hole scatters to LL1.However, $Y_{\mathbf{q}}$ have higher energy than X_0 and thus the X_0–2DEG interactions are suppressed as compared to the X_1–2DEG interactions. This asymmetry between the two magnetoexcitons in the case of inter–LL MPs is important for understanding the experimentally–observed dynamics.

5.2 Equations of motion

We calculate the full dynamics within the subspace spanned by the 1–h+(N_e+1)–e states $|X_n\rangle$, n=0,1, and $|Y_{\mathbf{q}}\rangle$, Eq.(5.1). Different many–body effects are determined by the interaction matrix elements V_{nm}, $W_{\mathbf{q}n}$, and $W_{\mathbf{qq}'}$.

$$V_{nm} = \int \frac{d\mathbf{q}}{(2\pi)^2} v_q |\phi_{nm}(\mathbf{q})|^2 \tag{5.4}$$

determine the exciton binding energies (V_{nn}), static inter–LL coupling (V_{01}), and mean–field X–X interaction (V_{01}). The coupling between the X and Y states is determined by

$W_{\mathbf{q}n} \propto v_{01}^{01}(\mathbf{q})$,

where

$$v_{nn'}^{mm'}(q) = \frac{1}{2\pi l^2} v_q \phi_{mm'}^*(\mathbf{q}) \phi_{nn'}(\mathbf{q}). \tag{5.5}$$

By setting $W_{\mathbf{q}n}$=0 in our calculation, we decouple the Xs from the 2DEG and obtain an optical response similar to the undoped system.

$$W_{\mathbf{qq}'} = 2v_{11}^{00}(\mathbf{q}'-\mathbf{q}) \cos\left[(\mathbf{q}\times\mathbf{q}')_z \ell^2\right] - v_{11}^{11}(\mathbf{q}'-\mathbf{q}) - v_{00}^{00}(\mathbf{q}'-\mathbf{q}) \tag{5.6}$$

describes rescattering among the continuum of $Y_{\mathbf{q}}$ states, which corresponds to non–perturbative vertex corrections beyond the Born approximation.

The linear polarizations, as discussed in 4 are obtained from Eqs(**??**): [21]

$$i\partial_t P_0^L = (\Omega_0 - i\Gamma_0) P_0^L - V_{01} P_1^L - d(t) - \frac{1}{\sqrt{N}} \sum_{\mathbf{q}} v_{01}^{01}(\mathbf{q}) \bar{P}_{\mathbf{q}}^L \tag{5.7}$$

for the LL0 polarization and

$$i\partial_t P_1^L = (\Omega_1 - i\Gamma_1)P_1^L - V_{10}P_0^L - d(t) + \frac{1}{\sqrt{N}}\sum_{\mathbf{q}} \upsilon_{01}^{01}(\mathbf{q})\bar{P}_{\mathbf{q}}^L \quad (5.8)$$

for the LL1 polarization, where the exciton dephasing rates, Γ_0=Γ_1=0.5meV, are chosen similar to the undoped system and the exciton energies are

$$\Omega_n = E_g + \left(n + \frac{1}{2}\right)\left(\omega_c^e + \omega_c^h\right) - V_{nn}. \quad (5.9)$$

The equations of motion for the coherences between the ground state and the {1-LL0-e + 1-LL1-h + LL0→LL1 MP} $Y_{\mathbf{q}}$ states are obtained from Eq.(3.47):[21]

$$i\partial_t \bar{P}_{\mathbf{q}}^L = (\bar{\Omega}_{\mathbf{q}} - i\gamma)\bar{P}_{\mathbf{q}}^L + \frac{\upsilon_{01}^{01}(\mathbf{q})}{\sqrt{N}}\left(P_1^L - P_0^L\right) + \frac{1}{N}\sum_{\mathbf{q}'\neq\mathbf{q}} W_{\mathbf{q}\mathbf{q}'}\bar{P}_{\mathbf{q}'}^L. \quad (5.10)$$

$\bar{\Omega}_{\mathbf{q}} = \Omega_{\mathbf{q}01} + \omega_{-\mathbf{q}}$ is the $Y_{\mathbf{q}}$ dispersion, where $\Omega_{\mathbf{q}01}$ is the X_{01} excitation energy, shifted here by ∼1meV as compared to its value in the ideal 2D system to obtain a better fit to the experimental linear absorption, and $\omega_{\mathbf{q}}$ is the LL0→LL1 2DEG excitation energy, given at ν=1 by [31]

$$\begin{aligned}\omega_{\mathbf{q}} - \omega_c^e \;=\; & \frac{e^2}{\epsilon\ell}\frac{q\ell}{2}e^{-q^2\ell^2/2} + \frac{e^2}{\epsilon\ell}\frac{1}{2}\sqrt{\frac{\pi}{2}}\{1 - \\ & e^{-q^2\ell^2/4}\left[\left(1 + \frac{q^2\ell^2}{2}\right)I_0\left(\frac{q^2\ell^2}{4}\right) - \frac{q^2\ell^2}{2}I_1\left(\frac{q^2\ell^2}{4}\right)\right]\},\end{aligned} \quad (5.11)$$

where I_n is a modified Bessel function of the first kind.The first term on the rhs of the above equation corresponds to the RPA treatment of the 2DEG interactions.The second term results from the

many–body corrections to the local field seen by an electron.These local field corrections result in a *magnetoroton dispersion minimum* absent within the RPA, whose detailed momentum dependence is determined by the ground state static structure factor [33]

Next we present the equations of motion for the third–order non-linear polarizations.Since the experimental studies of both doped and undoped quantum wells [83, 84, 110] did not produce any long–lasting FWM signal at negative time delays, which would signify long–lived X–X correlations, [100, 3, 103] we treat for simplicity the X–X interactions within the Hartree–Fock approximation.Within the chosen subspace of many–body states, the third–order polarization is described by the following closed system of equations of motion, derived in Ref.[21]:

$$\begin{aligned} i\partial_t P_0 &= (\Omega_0 - i\Gamma_0)P_0 - V_{01}P_1 + d(t)n_0 + V_{01}P_1^L\,(n_0 - 2N_{01}^*) \\ &- V_{01}P_0^L\,(n_1 - 2N_{01}) - P_0^L \sum_{\mathbf{q}} \upsilon_{01}^{01}(\mathbf{q}) \left[\bar{n}_{\mathbf{q}} + \frac{1}{\sqrt{N}}\left(M_{1\mathbf{q}}^* - M_{0\mathbf{q}}\right)\right] \\ &- P_1^L \sum_{\mathbf{q}} \upsilon_{01}^{01}(\mathbf{q}) \left[\bar{n}_{\mathbf{q}} - \frac{1}{\sqrt{N}}\left(M_{1\mathbf{q}} - M_{0\mathbf{q}}^*\right)\right] \\ &- \frac{1}{\sqrt{N}} \sum_{\mathbf{q}} \upsilon_{01}^{01}(\mathbf{q}) P_0^L P_1^L \bar{P}_{\mathbf{q}}^{L*} - \frac{1}{\sqrt{N}} \sum_{\mathbf{q}} \upsilon_{01}^{01}(\mathbf{q}) \bar{P}_{\mathbf{q}} \end{aligned} \tag{5.12}$$

$$\begin{aligned} i\partial_t P_1 &= (\Omega_1 - i\Gamma_1)P_1 - V_{01}P_0 + d(t)n_1 - V_{01}P_1^L\,(n_0 - 2N_{01}^*) \\ &+ V_{01}P_0^L\,(n_1 - 2N_{01}) + P_0^L \sum_{\mathbf{q}} \upsilon_{01}^{01}(\mathbf{q}) \left[\bar{n}_{\mathbf{q}} + \frac{1}{\sqrt{N}}\left(M_{1\mathbf{q}}^* - M_{0\mathbf{q}}\right)\right] \\ &+ P_1^L \sum_{\mathbf{q}} \upsilon_{01}^{01}(\mathbf{q}) \left[\bar{n}_{\mathbf{q}} - \frac{1}{\sqrt{N}}\left(M_{1\mathbf{q}} - M_{0\mathbf{q}}^*\right)\right] \\ &+ \frac{1}{\sqrt{N}} \sum_{\mathbf{q}} \upsilon_{01}^{01}(\mathbf{q}) P_0^L P_1^L \bar{P}_{\mathbf{q}}^{L*} + \frac{1}{\sqrt{N}} \sum_{\mathbf{q}} \upsilon_{01}^{01}(\mathbf{q}) \bar{P}_{\mathbf{q}} \end{aligned} \tag{5.13}$$

$\langle \hat{Y}_{\mathbf{q}} \rangle_{corr}$ is determined by the equation of motion

$$\begin{aligned} i\partial_t \bar{P}_{\mathbf{q}} &= (\bar{\Omega}_{\mathbf{q}} - i\gamma)\bar{P}_{\mathbf{q}} + \frac{\upsilon_{01}^{01}(\mathbf{q})}{\sqrt{N}}(P_1 - P_0) + \frac{1}{N}\sum_{\mathbf{q}'} W_{\mathbf{q}\mathbf{q}'}\bar{P}_{\mathbf{q}'} \\ &+ d(t)\left(P_1^{L*} + P_0^{L*}\right)\bar{P}_{\mathbf{q}}^{L} \\ &+ \frac{\upsilon_{01}^{01}(\mathbf{q})}{\sqrt{N}}\left[P_1^L(N_{11} - P_0^{L*}P_0^L - N_{00}) - P_0^L(N_{00} - P_1^{L*}P_1^L - N_{11})\right] \\ &+ \left[\upsilon_{01}^{01}(\mathbf{q}) - V_{01}\right]\left(P_1^L - P_0^L\right)\left(P_1^{L*}\bar{P}_{\mathbf{q}}^L + M_{1\mathbf{q}} - P_0^{L*}\bar{P}_{\mathbf{q}}^L - M_{0\mathbf{q}}\right) \\ &+ \sum_{\mathbf{q}'}\frac{\upsilon_{01}^{01}(\mathbf{q}')}{\sqrt{N}}\bar{P}_{\mathbf{q}'}^L(M_{1\mathbf{q}} - M_{0\mathbf{q}}) + \frac{\upsilon_{01}^{01}(\mathbf{q})}{\sqrt{N}}\left(P_1^L - P_0^L\right)\left[2N\bar{n}_{\mathbf{q}} - 3\sum_{\mathbf{q}'}\bar{n}_{\mathbf{q}'}\right] \\ &+ \left(P_1^L - P_0^L\right)\sum_{\mathbf{q}'}\frac{\upsilon_{01}^{01}(\mathbf{q}')}{\sqrt{N}}\bar{P}_{\mathbf{q}'}^{L*}\bar{P}_{\mathbf{q}}^L \end{aligned} \tag{5.14}$$

where we neglected $Y_{\mathbf{q}} \leftrightarrow Y_{\mathbf{q}'}$ coherences by assuming that they dephase rapidly. We retain, however, the $X_n \leftrightarrow Y_{\mathbf{q}}$ coherences $M_{n\mathbf{q}}$ and the $X_0 \leftrightarrow X_1$ coherence N_{01}, obtained from Eqs(3.52,3.51) with dephasing rates of 0.5meV. The nonlinearities in Eqs**??** depend on the total LLn carrier populations n_n and the Y–state populations $\bar{n}_{\mathbf{q}}$:

$$n_n = 2P_n^L P_n^{L*} + 2N_{nn} + \sum_{\mathbf{q}} \bar{n}_{\mathbf{q}}, \tag{5.15}$$

where the first term is the coherent X_n population and the rest of the terms describe the incoherent LLn carrier population, with contributions N_{nn} and$\bar{n}_{\mathbf{q}}$ from the X_n and $Y_{\mathbf{q}}$ states, respectively, where

$$\bar{n}_{\mathbf{q}} = \bar{P}_{\mathbf{q}}^{L*}\bar{P}_{\mathbf{q}}^L + N_{\mathbf{q}\mathbf{q}}. \tag{5.16}$$

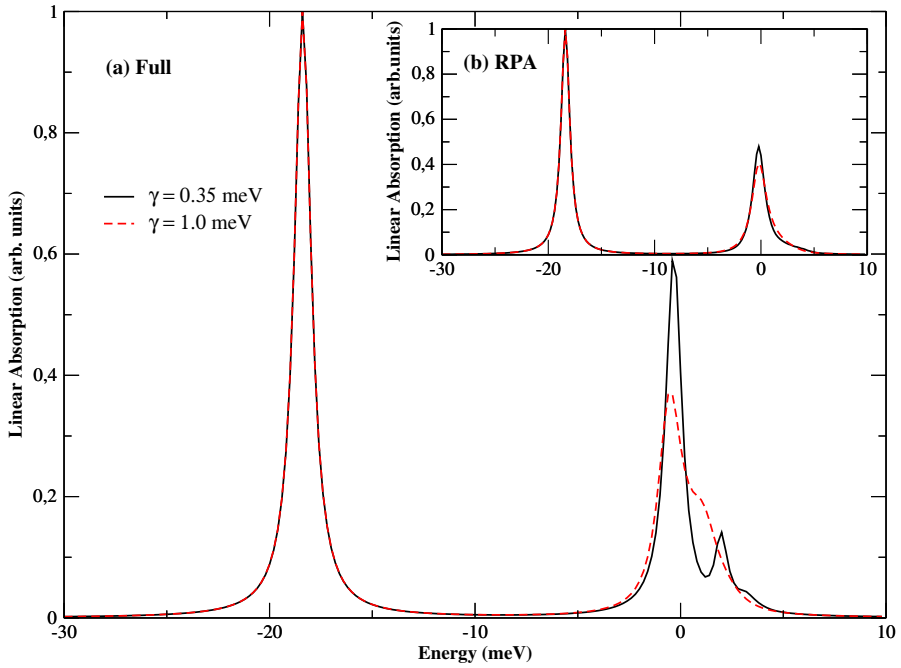

Figure 5.1: (Color online) Linear absorption calculation using the full Y–state dispersion for two values of the Y–state dephasing rate γ. Inset: Same for the RPA Y–state dispersion.

N_{nn} and $N_{\mathbf{qq}}$ were obtained from Eqs(3.51,3.53) with population relaxation rate $\Gamma_{\mathbf{qq}}$=Γ_{nn}=0.001meV.

5.3 Numerical results and comparison to experiment

In this section we present our numerical results, obtained for a magnetic field ∼9T at ν=1, and compare them to the experiment.5.1 compares the linear absorption spectra calculated by using the full and RPA dispersions $\bar{\Omega}_{\mathbf{q}}$. It also compares the results obtained for a small, γ=0.35meV, and a large,γ=2Γ_1=2Γ_0=1meV, dephasing rate of the $Y_{\mathbf{q}}$ four–particle coherence, with amplitude $\bar{P}_{\mathbf{q}}$.5.1 demonstrates that the linear absorption lineshape is sensitive to the $Y_{\mathbf{q}}$ dispersion. In particular, a second absorption peak,absent within

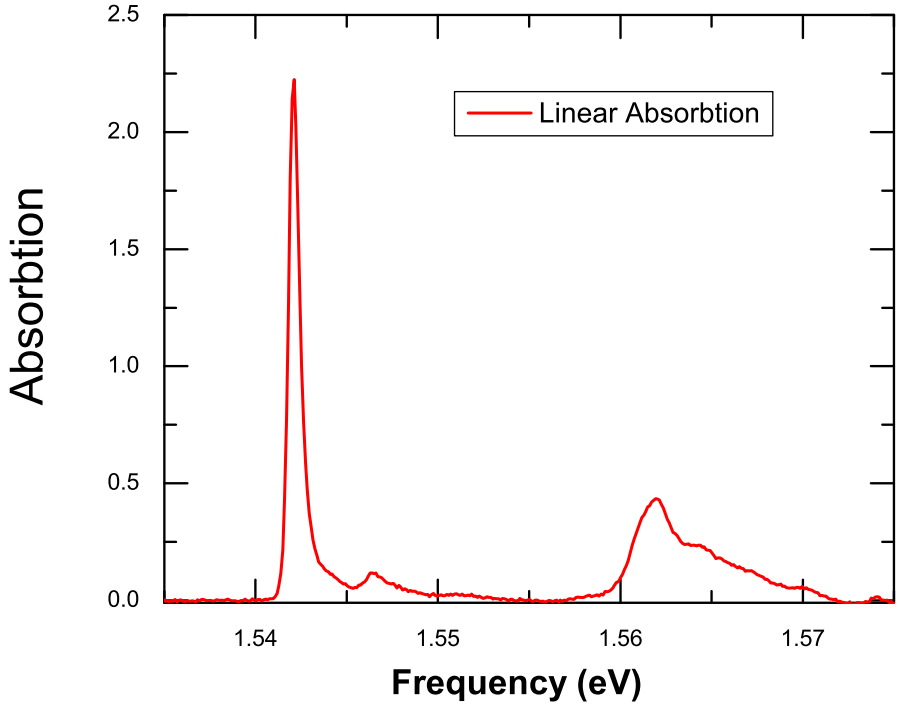

Figure 5.2: (Color online) Experimental linear absorption

the RPA, develops above the LL1 exciton resonance when the full $Y_{\mathbf{q}}$ dispersion is used. The latter displays a magnetoroton minimum, absent in the RPA dispersion, that is characteristic of incompressibility. [24, 25, 31, 32, 33] We note in 5.1 that the double–peak LL1 resonance lineshape depends sensitively on the dephasing of the {1-LL0-e + 1-LL1-h + LL0→LL1 MP} four–particle correlation, characterized by γ. As γ increases, these correlations become short–lived and the two LL1 absorption peaks merge into one broad but asymmetric LL1 resonance. This result agrees with the experimental observation, shown in 5.2.In contrast, the LL0 resonance is insensitive to the Y–state dynamics, consistent with the experiment(its precise lineshape may however depend on intra–LL excitations [82, 86]). γ can be large in the realistic system, due to e.g. sample–dependent disorder– and

phonon–induced scattering of the MP and X_{01} excitations, which have opposite momenta in $Y_{\mathbf{q}}$. On the other hand, the RPA lineshape is less sensitive to γ, as seen in the inset of 5.1, due to the absence of magnetorotons.

Next we turn to the ultrafast nonlinear response to three time–delayed optical pulses,

$$d(t) = \mu E_p(t)e^{i(\mathbf{k}_1\cdot\mathbf{r}-\omega_p t)}+\mu E_p(t+\Delta t_{12})e^{i(\mathbf{k}_2\cdot\mathbf{r}-\omega_p t)}+\mu E_p(t+\Delta t_{13})e^{i(\mathbf{k}_3\cdot\mathbf{r}-\omega_p t)}, \tag{5.17}$$

where $E_p(t) = E_0 e^{-(t/t_p)^2}$ is the pulse amplitude and ω_p its central frequency.Theoptical fields propagate in the directions $\mathbf{k}_1$, $\mathbf{k}_2$, and $\mathbf{k}_3$, with a time delay Δt_{12} (Δt_{13}) between pulses $\mathbf{k}_1$ and $\mathbf{k}_2$ ($\mathbf{k}_3$). For negative time delays, pulse $\mathbf{k}_1$ arrives first. We calculate the FWM spectrum

$$S(\omega, \Delta t_{12}, \Delta t_{13}) = |P_0(\omega) + P_1(\omega)|^2 \tag{5.18}$$

in the background–free direction $\mathbf{k}_1$+$\mathbf{k}_2$-$\mathbf{k}_3$.By tuning ω_p close to LL1, the LL0/LL1 photoexcited carrier ratio n_0/n_1 is small. This suppresses the PSF contribution at the LL0 energy and highlights the interaction effects that distinguish the many–body system from a multi–level atomic–like system. Below we discuss the time–dependence obtained along the $\Delta t12$ axis ($\Delta t13$=0) and the Δt_{13} axis (Δt_{12}=0),calculated in all cases at the two frequencies ω corresponding to the peaks of the LL0 and LL1 FWM resonances.For Δt_{13} >0, Δt_{12}=0, pulse $\mathbf{k}_3$ comes first and creates an interband polarization.The latter evolves and decays for a time interval Δt_{13}, when pulses $\mathbf{k}_1$ and $\mathbf{k}_2$ arrive and create the third–order FWM signal. Therefore, the Δt_{13} >0 axis mainly accesses the polarization dephasing.Along the Δt_{13} <0 axis,pulses $\mathbf{k}_1$ and $\mathbf{k}_2$ first create an X–X coherence,which evolves and dephases for a time–interval $|\Delta t_{13}|$ when pulse $\mathbf{k}_3$ arrives. Therefore, the Δt_{13} <0 axis mainly accesses the dephasing of the X–X coherence.Along the

negative Δt_{12} axis, pulses $\mathbf{k}_1$ and $\mathbf{k}_3$ arrive first (Δt_{13}=0) and create a LL population, or a coherence between different X and Y states. These evolve and relax for a time interval $|\Delta t_{12}|$, at which time pulse $\mathbf{k}_2$ arrives. Therefore, the Δt_{12} <0 axis probes population relaxation and intra–band coherence dephasing and oscillations. Finally, along the positive Δt_{12} axis, pulse $\mathbf{k}_2$ arrives first and creates an interband polarization, which evolves for a time–interval Δt_{12} when pulses $\mathbf{k}_1$ and $\mathbf{k}_3$ arrive. Thus the Δt_{12} >0 axis mainly probes polarization dephasing. The FWM dependence on the two time delays gives complementary information on the coherent and relaxation dynamicsof the QHS.

5.3 shows the three–pulse FWM signal, calculated at the LL0 and LL1 FWM peak energies, for linear absorption as in 5.1.We compare the results obtained for small and large dephasing rate γ of the {1-LL0-e + 1-LL1-h + LL0→LL1 MP} correlations as in 5.1. Despite tuning the frequency ω_p close to LL1, for small γ the LL0 and LL1 FWM peaks have comparable height. By increasing γ, the LL1/LL0 FWM peak ratio decreases sharply, as the two LL1 linear absorption peaks begin to merge into a single broad resonance. On the other hand, the LL0 peak remains relatively insensitive to γ and $\bar{P}_{\mathbf{q}}$.Regarding the time–dependence, along the Δt_{12} axis the LL0 FWM signal displays strong temporal coherent oscillations, with a frequency determined by the LL0–LL1 energy splitting.Importantly, the decay of these oscillations is enhanced by increasing γ, which indicates that it is determined by dephasing due to X–2DEG interactions. Along the Δt_{13} >0 axis, for small γ the FWM temporal profile displays a small oscillation. With increasing γ however, the LL0 temporal profile becomes symmetric around Δt_{13}=0, as the two linear absorption LL1 peaks merge into a single broad resonance, while the LL1 temporal profile remains asymmetric. The dependence of the above features on the {1-LL0-e + 1-LL1-h + LL0→LL1 MP} dephasing rate γ indicates that they arise from non–Markovian mem-

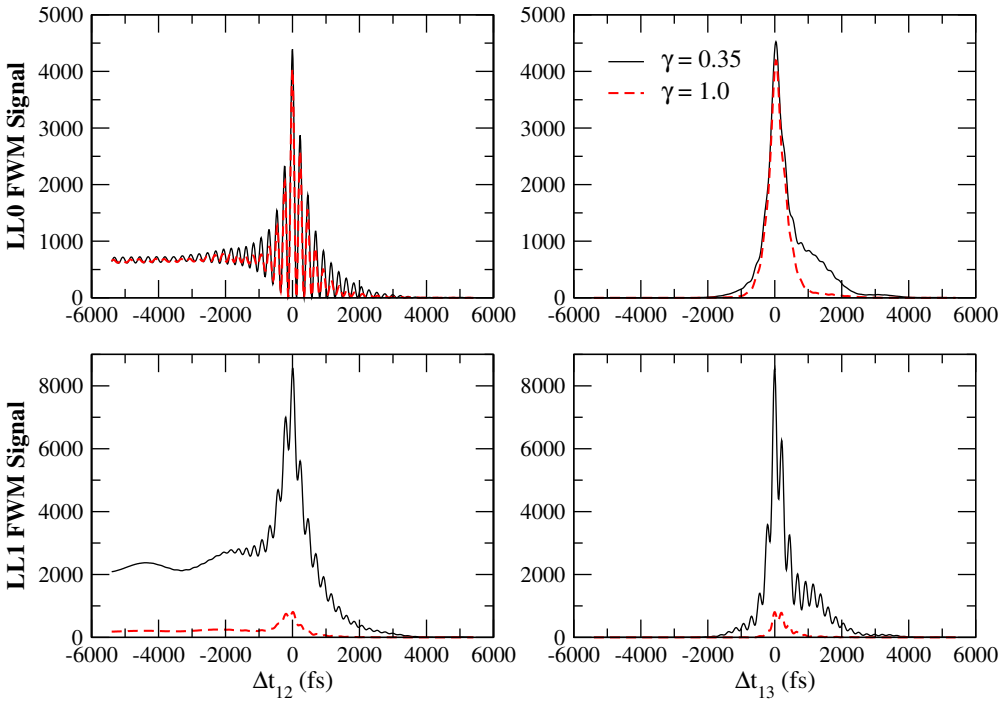

Figure 5.3: (Color online) Calculated three–pulse FWM signal and its dependence on the {1-LL0-e + 1-LL1-h + LL0→LL1 MP} correlation dephasing.

ory effects due to the four–particle correlations and their dynamics. Furthermore, along the Δt_{12} <0 axis, the FWM signal reflects the relaxation of the incoherent carrier populations and decreases drastically if we neglect the long–lived incoherent Y–state populations $N_{\mathbf{qq}}$.[21] The FWM spectral and temporal profile can be controlled by tuning ω_p towards the LL0 frequency, which suppresses the LL1 FWM peak.

We now compare our predictions to the FWM experiments discussed in Refs.[83, 84, 110] We take γ=1meV, which gives good agree-

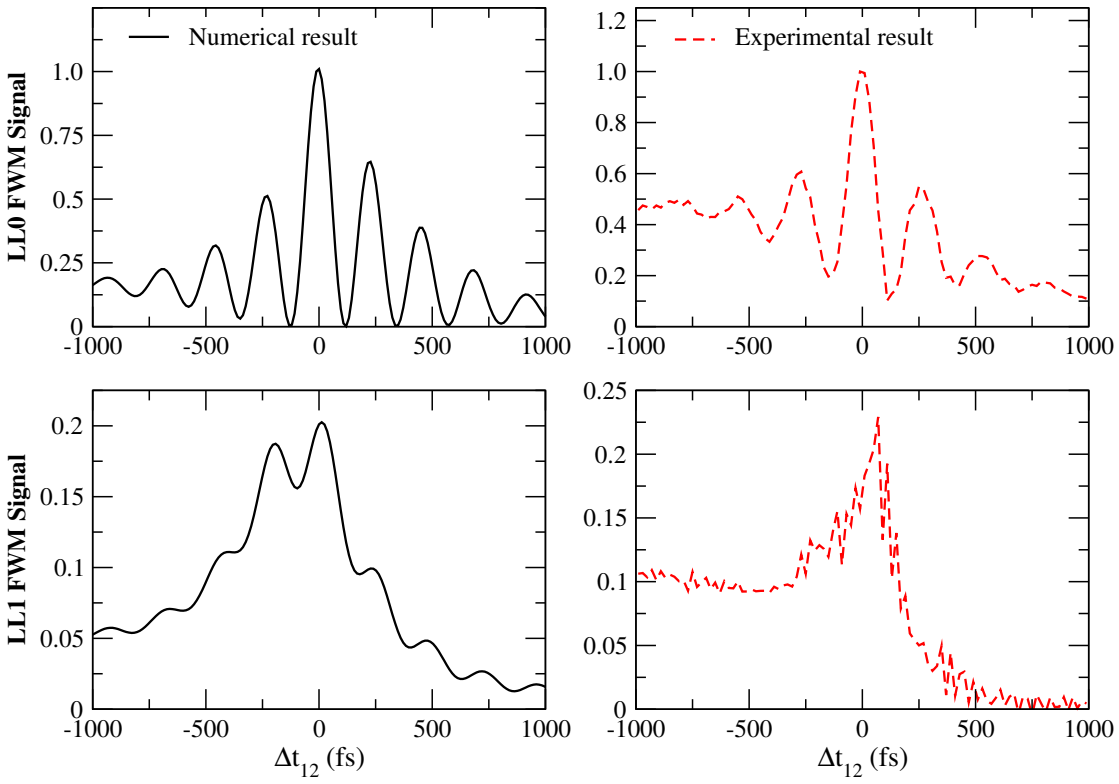

Figure 5.4: (Color online) Three–pulse FWM: comparison between theory and experiment along the Δt_{12} axis for γ=1meV.

ment between the theoretical and experimental linear absorption if we ignore the extra peaks due to the valence bandstructure(compare 5.1 and 5.2). 5.4 compares the FWM time evolution along the Δt_{12} axis.Our theory captures the main experimental features: strong LL0 temporal oscillations due to LL0–LL1 coherence, Δt_{12} <0 signal reflecting incoherent population relaxation, and unusually large LL0/LL1 peak ratio despite predominantly exciting LL1 transitions. 5.5 compares the calculated and experimental temporal evolution along the Δt_{13} axis. We capture the symmetric LL0 temporal profile seen in the experiment, absent in the undoped system, [110] while the time–dependence of the LL1 FWM is asymmetric around Δt_{13}=0. Our theory predicts the experimentally–observed FWM features of

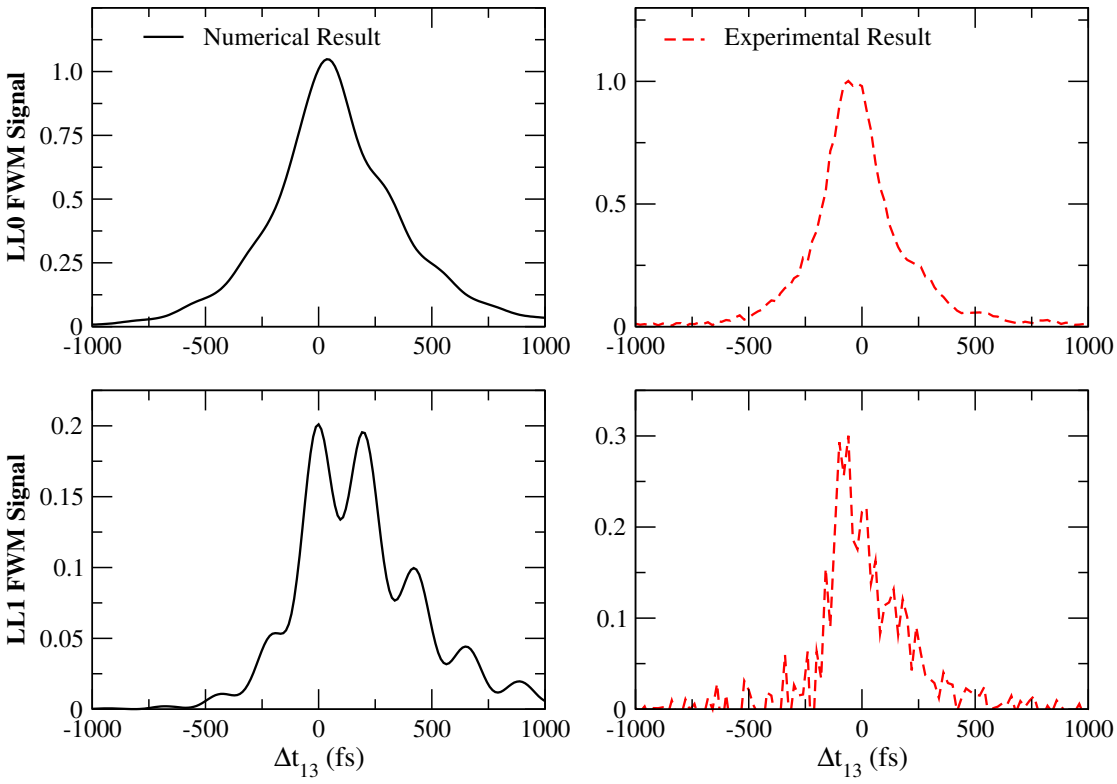

Figure 5.5: (Color online) Three–pulse FWM: comparison between theory and experiment along the Δt_{12} axis for γ=1meV.

the 2DEG which are absent in an atomic–like or an undoped semiconductor system.

Next we discuss the origin of the above effects. 5.6 compares our full calculation to the result obtained by setting $W_{\mathbf{q}n}$=0, in which case the X states decouple from the 2DEG.While the full calculation gives a large LL0/LL1 FWM ratio (LL0/LL1 ∼5), this ratio is strongly suppressed if we set $W_{\mathbf{q}n}$=0 (LL0/LL1∼1/2). This rather drastic effect of the X–2DEG coupling is consistent with the observed differences between the 2DEG and undoped samples.[83, 84, 110] Furthermore, for $W_{\mathbf{q}n}$=0, the LL0 FWM temporal profile along the Δt_{13} axis becomes asymmetric, as observed in the undoped system. [110] Along the Δt_{12} axis, coherent oscillations are also present for

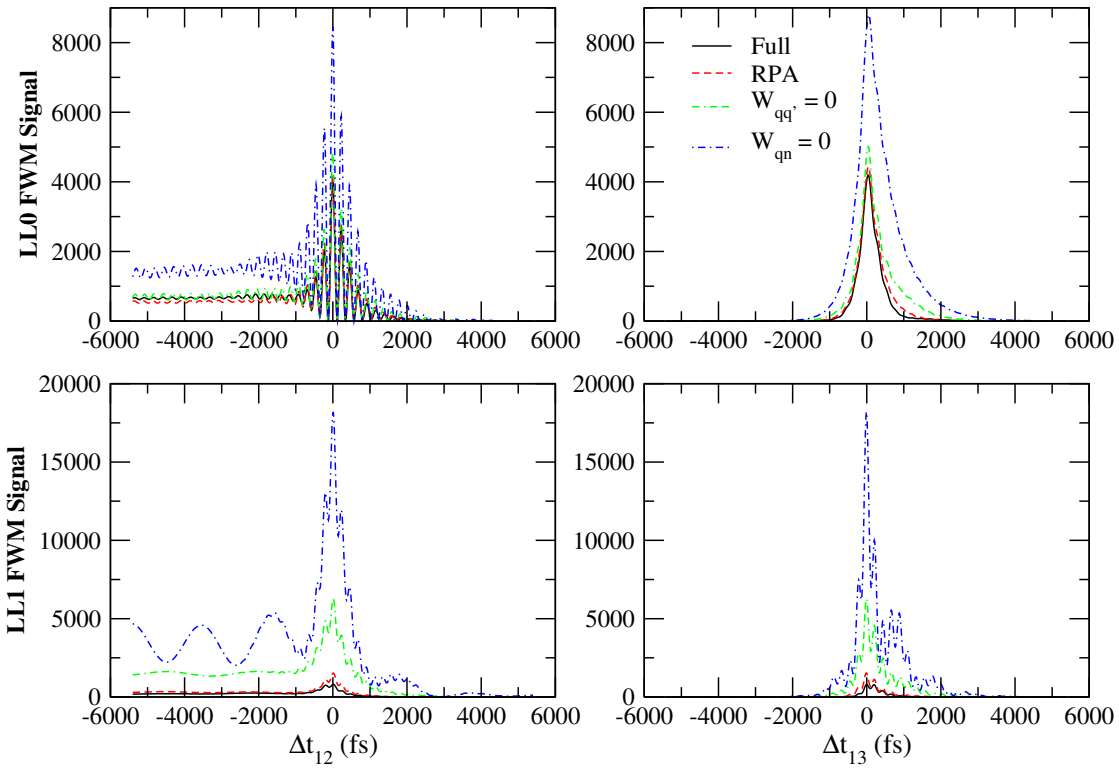

Figure 5.6: (Color online) Interaction effects on the three–pulse FWM for γ=1meV.

$W_{\mathbf{q}n}$=0, attributed to the X–X interactions. [110]However, while in the undoped system the oscillation decay is determined by the exciton dephasing rates Γ_n, in the 2DEG it mainly comes from X–2DEG interactions and the dynamics of the Y–states. While the profound role of the X–2DEG coupling in interpreting the experiment is clear from the results of 5.6, we note that, with increasing γ, the differences [21] between the RPA and the full $Y_{\mathbf{q}}$ dispersion FWM calculations decrease. This result suggests that the incompressibility of the 2DEG does not strongly affect the FWM in the samples studied here due to strong dephasing of the {1-LL0-e + 1-LL1-h + LL0→LL1 MP} correlation.

To interpret the unusual temporal profile along the Δt_{13} axis and its dependence on γ, let us consider the PSF and X–X interaction

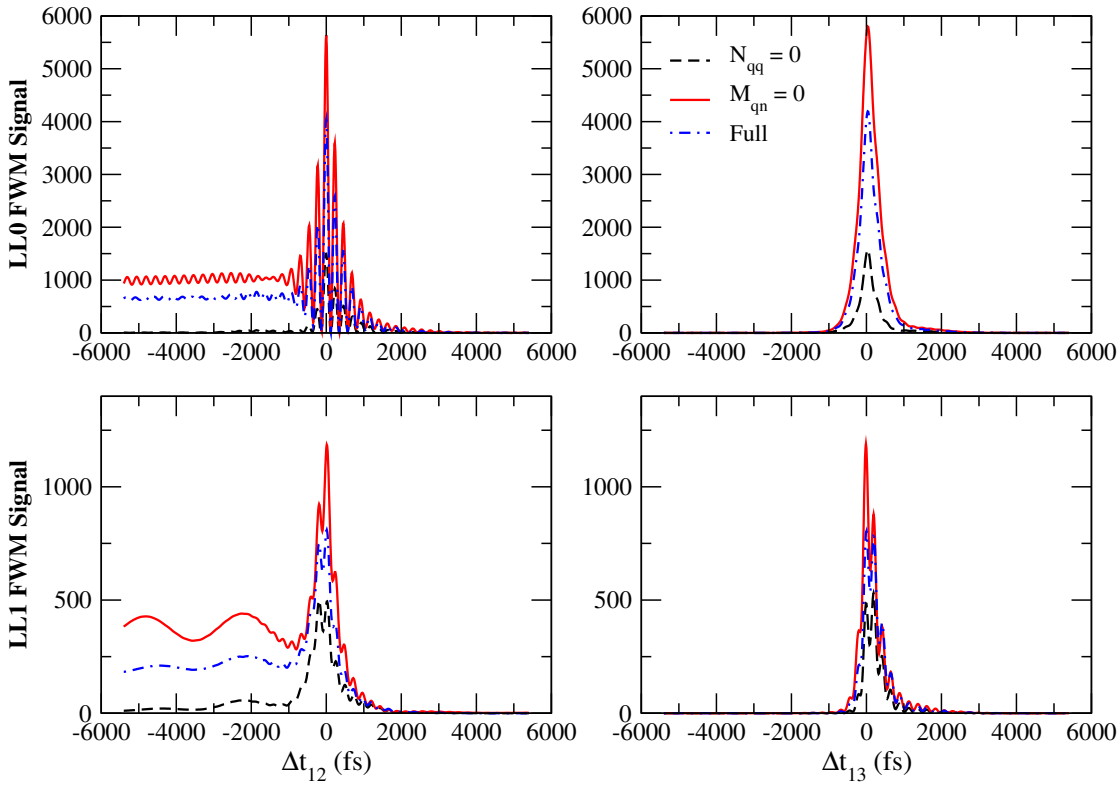

Figure 5.7: (Color online) The M_{qn} and N_{qq} role on the three–pulse FWM for γ=1meV.

contributions to Eqs(**??**). The PSF contribution, $d(t)n_n$ at LLn, always gives an asymmetric Δt_{13} temporal profile, with Δt_{13} <0 contribution that follows the optical pulse. [12, 5] At LL0, the resonant X–X interaction contribution in Eq(A.3) has the form $P_0^L n_1$ and $P_1^L N_{01}^*$, which couples the two LLs via light-induced nonlinear coherence. The Δt_{13} >0 decay of the LL0 FWM signal then reflects the dephasing of X_1, while its Δt_{13} <0 decay reflects the dephasing of the X_1+X_0 coherence. X_1 couples strongly to the $Y_{\mathbf{q}}$ states in the QHS and thus dephases more strongly than X_0. If γ is sufficiently large, so that the LL1 resonance is broad, the Δt_{13} temporal profile is dominated by the dephasing of P_1^L. If on the other hand γ is small, P_1^L is long–lived and the temporal profile becomes asym-

metric, with memory effects due to the multi–peak structure in 5.1. When $W_{\mathbf{q}n}$=0, both X_0 and X_1 have similar dephasing rates and thus the Δt_{13} temporal profile is again asymmetric. In contrast, at the LL1 energy, the X–X interaction resonant contribution has the form $P_1^L n_0$ and $P_0^L N_{01}$.Therefore, while the Δt_{13} <0 FWM decay again reflects the X_0+X_1 dephasing, the Δt_{13} >0 FWM signal is determined by the dephasing of X_0 and thus decays more slowly than the LL0 FWM, since X_0 couples weakly to inter–LL MPs. We conclude that the observation of a symmetric LL0 Δt_{13} profile reflects the asymmetry in the dephasing of the LL0 and LL1 excitons due to coupling with inter–LL MPs. Even though the X–X interaction+PSF nonlinear contribution gives a large part of the 2DEG FWM [21], it still gives a LL1/LL0 ratio much larger than the full calculation, while its dynamics changes drastically when $W_{\mathbf{q}n} \neq 0$.

The question now arises whether a perturbative Born approximation treatment of the X–2DEG interactions and the corresponding exciton self–energy is enough to describe the above effects.5.6 compares our full calculation to the Born approximation result, obtained by setting $W_{\mathbf{qq'}}$=0 in Eq(A.3).This approximation neglects the scattering between the X_{01} and MP excitations that make $Y_{\mathbf{q}}$. This X_{01}–MP dynamics is similar to that due to X–X scattering in the undoped system, which governs the dynamics of the four–particle 2–h+2–e correlation and the Δt_{13} <0 FWM signal. [100, 103] 5.6 shows that the perturbative treatment of the X–2DEG scattering significantly overestimates the strength of the LL1 peak, by a factor of more than ∼5 as compared to the full calculation. Importantly, it gives a more asymmetric Δt_{13} temporal profile and also changes the decay of the Δt_{12} <0 LL0 temporal oscillations. We conclude that the vertex (rescattering) corrections affect the FWM profile in a significant way.In particular, the non–exponential time–dependence of the {1-LL0-e + 1-LL1-h + LL0→LL1 MP} correlation manifests itself in the symmetric temporal profile of the Δt_{13} signal, which is not

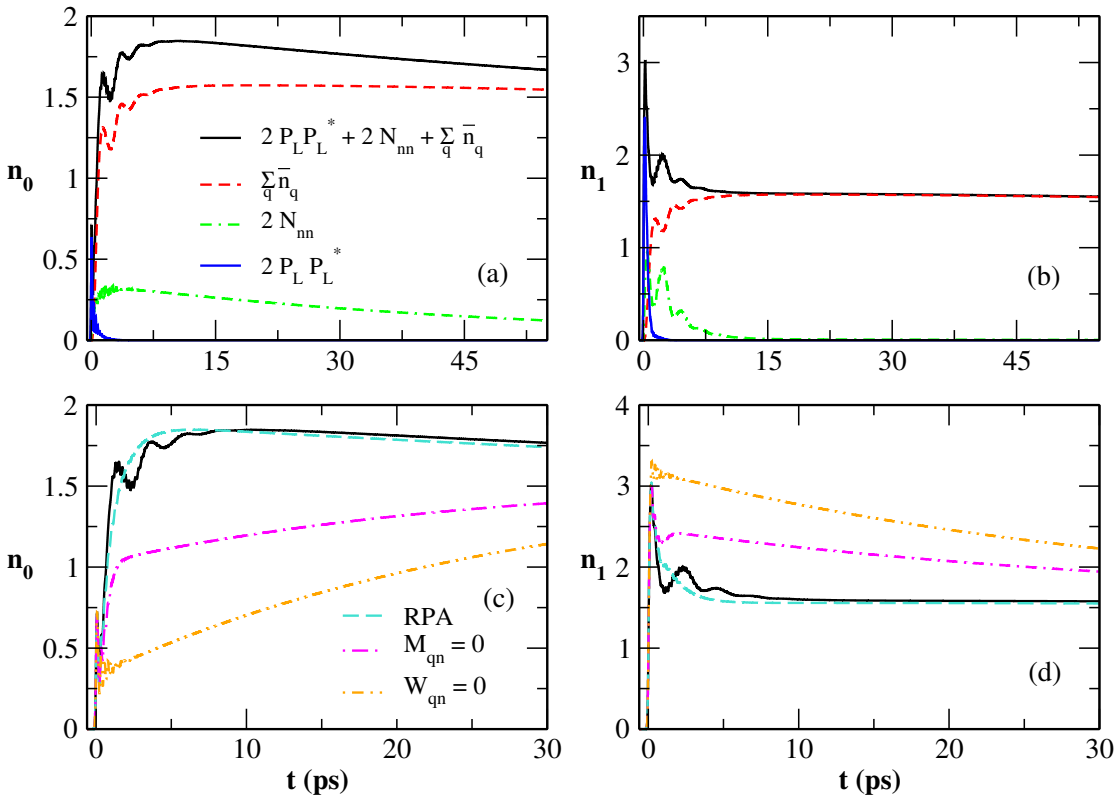

Figure 5.8: (Color online) LL0 and LL1 total carrier population relaxation for photoexcitation close to LL1 by a single pulse and γ=1meV. Upper panel: time evolution of the different coherent and incoherent contributions.Lower panel: comparison between populations obtained with the full calculation, RPA dispersion, and by neglecting the linear or nonlinear X–Y couplings.

adequately described by the Born approximation or by the average polarization model used to inerpret the 2DEG FWM experiments. [20, 84, 88, 89, 90, 91]

We now turn to the population relaxation. 5.7(a) and (b) show the time evolution of the LL0 (n_0) and LL1 (n_1)total carrier populations, photoexcited at t=0 by a single optical pulse, and their different contributions, 5.15.The coherent contribution to n_n, $2P_n^L P_n^{L*}$, decays rapidly,as determined by the polarization dephasing. When ω_p is tuned close to the LL1 energy, the coherent n_1 exceeds n_0, by

a factor ∼4 in 5.7. Nevertheless, it is clear from our results that the LL0/LL1 FWM ratio does not simply reflect the ratio n_0/n_1, in contrast to the predictions of a multi–level atomic–like model. Following the coherent regime, the X–2DEG interaction drastically changes the carrier relaxationand enhances n_0/n_1 as compared to the undoped system.The LL0 population increases sharply during intermediate timescales of a few picoseconds, while simultaneously the LL1 population drops and the Y–state populations build up.This incoherent dynamics comes from the $X_1 \rightarrow Y_{\mathbf{q}}$ scattering processes. It is described by Eqs(3.51, 3.52, 3.53) and should be contrasted to the coherent dynamics due to the same interaction process, discussed above. The rise time of the LL0 FWM signal for Δt_{12} <0 mainly reflects the slow build–up of the Y–state populations $\sum_{\mathbf{q}} \bar{n}_{\mathbf{q}}(t)$ as X_1 de–populates. 5.7(a) and (b) also show the time–dependence of the incoherent exciton populations $N_{nn}(t)$. N_{00} relaxes slowly, as determined by the population relaxation time, since the X_0+2DEG scattering is suppressed for inter–LL MPs. In contrast, the relaxation of N_{11} is fast and occurs on a time scale of a few picoseconds, which coincides with the build–up of $\bar{n}_{\mathbf{q}}$.After sufficiently long times, when the above scattering is complete, n_n are determined by the total population of the continuum of {1MP + 1-LL0-e + 1-LL1-h} states and by the long–lived LL0 population N_{00}. Finally, 5.7(c) and (d) compare the n_n obtained by using the full or the RPA $Y_{\mathbf{q}}$ dispersions and show rather small differences between them.In contrast, by neglecting the linear or nonlinear X–Y couplings, i.e by setting $W_{\mathbf{q}n}$=0 or $M_{\mathbf{q}yn}$=0, we obtain drastically different population relaxation and time–dependence of n_0/n_1.

5.4 Conclusions

In conclusion, we developed a density matrix quantum kinetic description of dephasing/decoherence and relaxation processes in pho-

toexcited systems with strongly correlated ground state electrons. Similar to the description of the strongly correlated QH ground state and its excitations (composite fermions etc),[72, 99, 75] in the absence of a small interaction parameter we obtain the exact dynamics of "Hubbard operator" density matrices within a subspace of almost degenerate many–body states strongly coupled by the interactions, after introducing an appropriate density matrix decomposition that separates different correlation effects. Our main motivation for developing this theory is to address the timely, both from non–equilibrium many–body physics and from applications points of view, problem of nonlinear dynamics induced by the strong coupling of different degrees of freedom triggered by coherent photoexcitation. We compared the predictions of our theory to three–pulse FWM experiments, performed on a 2DEG subjected to a magnetic field. This comparison corroborates our earlier claims that the dynamical coupling of the two lowest Landau level states by inter–LL magnetoplasmon (MP) and magnetoroton (MR) 2DEG excitations is an important and robust nonlinear process in the QHS, with possible implications for coherent control and quantum computation schemes involving many–body qubits. Importantly, we showed that the spectral and temporal behavior of the FWM signal depends sensitively on the dephasing and dynamics of {1-LL0-e + 1-LL1-h + LL0→LL1 MR} four–particle correlations, which couple to the exciton degrees of freedom. For long–lived correlations, the incompressibility of the 2DEG, which leads to magnetorotons and a double–peak LL1 resonance, manifests itself in the FWM profile. For short–lived correlations, the dephasing of the LL1 coherence is strong, leading to an unusually symmetric temporal profile, determined by the dynamics of the above four–particle correlations, and a depressed LL1 FWM peak. These correlations also affect the decay of the inter–LL coherence that gives FWM temporal oscillations, which in the undoped system is determined by the exciton dephasing rates. A question down the road is how two–dimensional correlation spectroscopy, [113] which accesses

a much larger phase space than the conventional one–dimensional spectroscopic techniques, can be used to resolve the dynamics of such fundamental many–body processes. Future experimental and theoretical studies also promise to elucidate the dynamics of strongly coupled spin, charge, and lattice degrees of freedom that is triggered by coherent photoexcitation of selected modes. In addition to accessing "hidden states" and photo–induced phase transitions in strongly correlated materials, such studies of the QHS can address, for example, the formation and nonlinear response dynamics of trions, composite fermions, and fractional quasi–excitons.[75, 99, 95]

Appendices

Appendix A

Two Dimensional Fourier Transform Spectroscopy

A.1 Introduction

Optical two Dimensional Fourier transform spectroscopy is a powerful technique for studying resonant light-matter interactions, determing the transition structure and monitoring dynamics of optically created excitations. Multidimensional Fourier transform spectroscopy was originally developed in nuclear magnetic resonance. Much of this work has focused on electronic and vibrational transitions in molecules and only considers two frequency variables , thus is known as 2-D Fourier transform (2–DFTS) spectroscopy.

2–DFT spectroscopy has proven to be a powerful tool for unraveling the complex coherent response of exciton resonances in semiconductors.2DFTS can also clearly separate the homogeneous broadening of individual oscillators from inhomogeneous broadening due to sample irregularities in semiconductors.A glance at a 2DFT spectrum can give a qualitative sense of the inhomogeneity in a system. For a given resonance the linewidth in the cross diagonal direction is associated with homogeneous broadening while the diagonal linewidth is related to inhomogeneous broadening. However, acquiring quantita-

tive information about the homogeneous and inhomogeneous broadenings is more difficult because they are coupled along the diagonal and cross diagonal directions of the spectrum.

A.2 Method

In order to calculate the 2D frequency domain lineshapes, we first consider the signal in the time domain. We consider a three time delayed optical pulses:

$$d(t) = \mu E_p(t)e^{i(\vec{k}_1\cdot\vec{r}-\omega_p t)}+\mu E_p(t+\Delta t_{12})e^{i(\vec{k}_2\cdot\vec{r}-\omega_p t)}+\mu E_p(t+\Delta t_{13})e^{i(\vec{k}_3\cdot\vec{r}-\omega_p t)}, \tag{A.1}$$

where $E_p(t) = E_0 e^{-(t/t_p)^2}$ is the pulse amplitude and ω_p its central frequency.

The optical fields propagate in the directions $\mathbf{k}_1$, $\mathbf{k}_2$, and $\mathbf{k}_3$, with a time delay Δt_{12} (Δt_{13}) between pulses $\mathbf{k}_1$ and $\mathbf{k}_2$ ($\mathbf{k}_3$). For negative time delays, pulse k_1 arrives first.

The pulse is centered in the LL1 energy as we see in the Linear Absorption figure $A.2$ below:

We calculate the third order polarization P_n in the background–free direction $\mathbf{k}_1$+$\mathbf{k}_2$-$\mathbf{k}_3$ with a Runge-Kutta method.

We want to calculate the 2D signal in the frequency domain by a fourier transform in the third order polarization $P_n(t, \Delta t_{12}, \Delta t_{13})$.

$$S(\omega_\tau, \omega_t, \Delta t_{12} = 0) = \int_0^{\Delta t_{13max}} \int_{-\Delta t_{13}}^{\infty} d(\Delta t_{13}) dt f(t, \Delta t_{13}) e^{i\omega_t t} e^{i\omega_\tau \Delta t_{13}} \tag{A.2}$$

Where $f(t, \Delta t_{13}) = P_1 + P_0$

We assume that $\Delta t_{12} = 0$ and $\Delta t_{13} > 0$. First arrives pulse $-k_3$ and after $|\Delta t_{13}|$ arrives together k_1 , k_2.

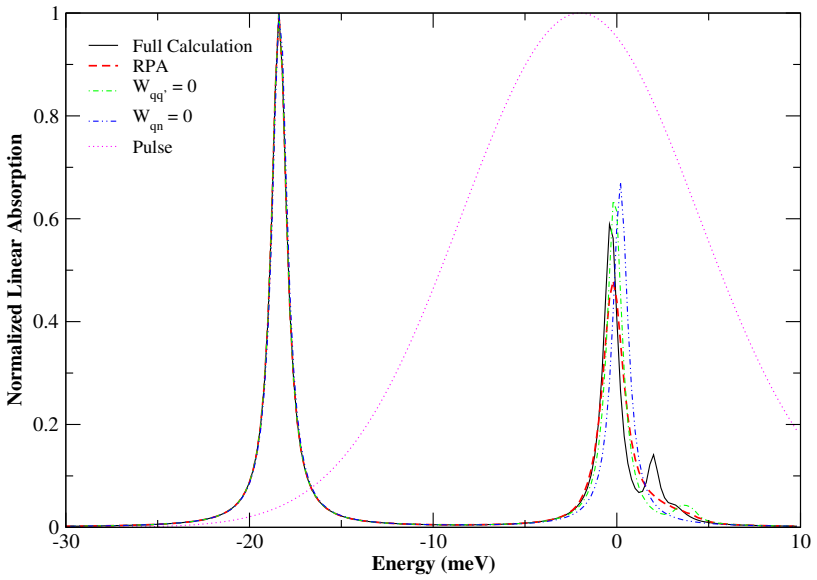

Figure A.1: Linear Absorption calculation

Equations of motion

The third order polarization is described by the following closed system of equations of motion.

$$
\begin{aligned}
&i\partial_t P_0 = (\Omega_0 - i\Gamma_0)P_0 - V_{01}P_1 + d(t)n_0 + V_{01}P_1^L\left(n_0 - 2N_{01}^*\right) \\
&-V_{01}P_0^L\left(n_1 - 2N_{01}\right) - P_0^L\sum_{\mathbf{q}} \upsilon_{01}^{01}(\mathbf{q})\left[\bar{n}_{\mathbf{q}} + \frac{1}{\sqrt{N}}\left(M_{1\mathbf{q}}^* - M_{0\mathbf{q}}\right)\right] \\
&-P_1^L\sum_{\mathbf{q}} \upsilon_{01}^{01}(\mathbf{q})\left[\bar{n}_{\mathbf{q}} - \frac{1}{\sqrt{N}}\left(M_{1\mathbf{q}} - M_{0\mathbf{q}}^*\right)\right] \\
&-\frac{1}{\sqrt{N}}\sum_{\mathbf{q}} \upsilon_{01}^{01}(\mathbf{q})P_0^L P_1^L \bar{P}_{\mathbf{q}}^{L*} - \frac{1}{\sqrt{N}}\sum_{\mathbf{q}} \upsilon_{01}^{01}(\mathbf{q})\bar{P}_{\mathbf{q}}
\end{aligned}
$$

$$
\begin{aligned}
&i\partial_t P_1 = (\Omega_1 - i\Gamma_1)P_1 - V_{01}P_0 + d(t)n_1 - V_{01}P_1^L\left(n_0 - 2N_{01}^*\right)\\
&+V_{01}P_0^L\left(n_1 - 2N_{01}\right) + P_0^L\sum_{\mathbf{q}}\upsilon_{01}^{01}(\mathbf{q})\left[\bar{n}_{\mathbf{q}} + \frac{1}{\sqrt{N}}\left(M_{1\mathbf{q}}^* - M_{0\mathbf{q}}\right)\right]\\
&+P_1^L\sum_{\mathbf{q}}\upsilon_{01}^{01}(\mathbf{q})\left[\bar{n}_{\mathbf{q}} - \frac{1}{\sqrt{N}}\left(M_{1\mathbf{q}} - M_{0\mathbf{q}}^*\right)\right]\\
&+\frac{1}{\sqrt{N}}\sum_{\mathbf{q}}\upsilon_{01}^{01}(\mathbf{q})P_0^L P_1^L\bar{P}_{\mathbf{q}}^{L*} + \frac{1}{\sqrt{N}}\sum_{\mathbf{q}}\upsilon_{01}^{01}(\mathbf{q})\bar{P}_{\mathbf{q}}
\end{aligned}
$$

$$
\begin{aligned}
&i\partial_t \bar{P}_{\mathbf{q}} = (\bar{\Omega}_{\mathbf{q}} - i\gamma)\bar{P}_{\mathbf{q}} + \frac{\upsilon_{01}^{01}(\mathbf{q})}{\sqrt{N}}\left(P_1 - P_0\right) + \frac{1}{N}\sum_{\mathbf{q}'}W_{\mathbf{q}\mathbf{q}'}\bar{P}_{\mathbf{q}'}\\
&+d(t)\left(P_1^{L*} + P_0^{L*}\right)\bar{P}_{\mathbf{q}}^L\\
&+\frac{\upsilon_{01}^{01}(\mathbf{q})}{\sqrt{N}}\left[P_1^L(N_{11} - P_0^{L*}P_0^L - N_{00}) - P_0^L(N_{00} - P_1^{L*}P_1^L - N_{11})\right]\\
&+\left[\upsilon_{01}^{01}(\mathbf{q}) - V_{01}\right]\left(P_1^L - P_0^L\right)\left(P_1^{L*}\bar{P}_{\mathbf{q}}^L + M_{1\mathbf{q}} - P_0^{L*}\bar{P}_{\mathbf{q}}^L - M_{0\mathbf{q}}\right)\\
&+\sum_{\mathbf{q}'}\frac{\upsilon_{01}^{01}(\mathbf{q}')}{\sqrt{N}}\bar{P}_{\mathbf{q}'}^L\left(M_{1\mathbf{q}} - M_{0\mathbf{q}}\right)\\
&+\frac{\upsilon_{01}^{01}(\mathbf{q})}{\sqrt{N}}\left(P_1^L - P_0^L\right)\left[2N\bar{n}_{\mathbf{q}} - 3\sum_{\mathbf{q}'}\bar{n}_{\mathbf{q}'}\right]\\
&+\left(P_1^L - P_0^L\right)\sum_{\mathbf{q}'}\frac{\upsilon_{01}^{01}(\mathbf{q}')}{\sqrt{N}}\bar{P}_{\mathbf{q}'}^{L*}\bar{P}_{\mathbf{q}}^L,
\end{aligned}
$$

, where P_0^L, P_1^L are the Linear polarizations for LL0 and LL1, and $\bar{P}_{\mathbf{q}}^L$ describes the coherences between the ground state and the Y_q states. Also N_{nn} and N_{nm} describes the X_n population and the $X_n \leftrightarrow X_m$ coherence and M_{qn} the $X_n \leftrightarrow Y_q$ coherence.

A.3 Results

The 2DFTS is very sensitive to excitation conditions. These conditions include the spectrum of the incident laser pulses.The relative strengths of the different features vary with tuning, a relatively straightforward effect caused by the changing excitation density due to spectral overlap. Below we present the main results for the real part of the 2DCS Signal $S(\omega_\tau, \omega_t, \Delta t_{12} = 0)$.

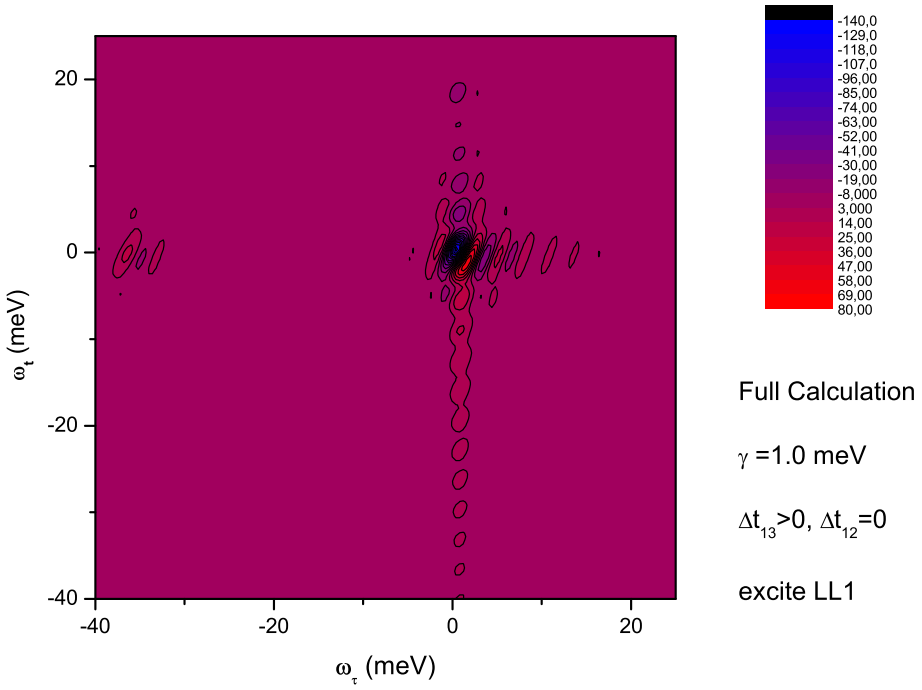

Figure A.2: Full Calculation

By exciting the LL1 ($\omega_p = 0meV$) we take Figure A.3 and Figure A.3. The first Figure shows the signal corresponding to the full calculation of our model and the other shows the PSF contribution ($d(t)n_n$) with $\bar{P}_q = 0$. If only the PSF terms are included no cross-

peaks occur, and the continuum states appear on the diagonal.

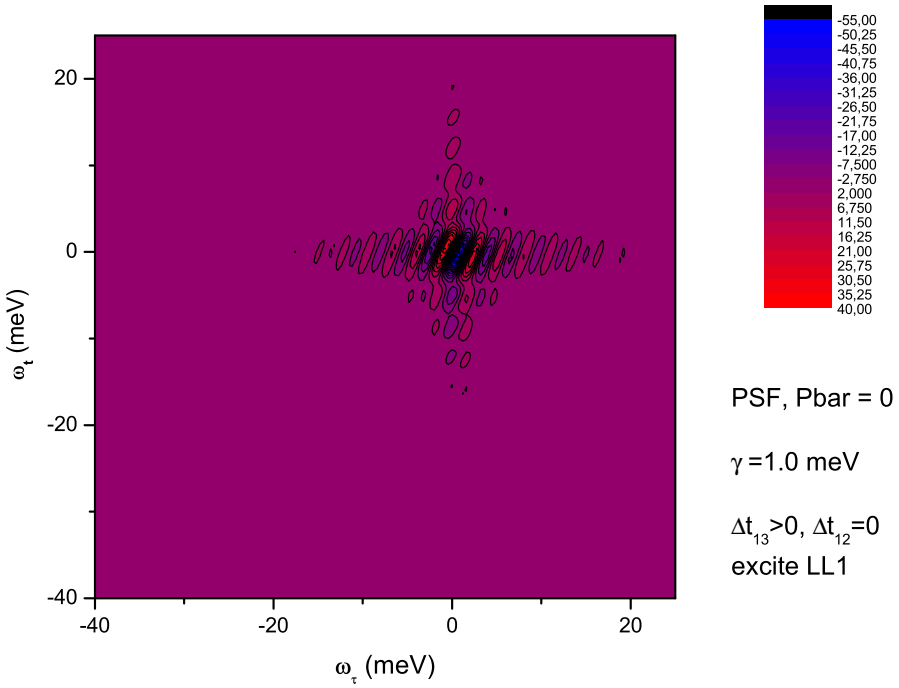

Figure A.3: The PSF contribution with $\bar{P}_q = 0$

If we excite both LL0 and LL1 ,by moving the pulse between the two LL, (centered at ω_p = - 10 meV) we get Figure A.3. The two resonances alling the diagonal correspond to the LLO ($\sim$ -20 meV)and LL1 ($\sim$ 0 meV) energy.The peaks above and below the diagonal indicate the exciton couplings .

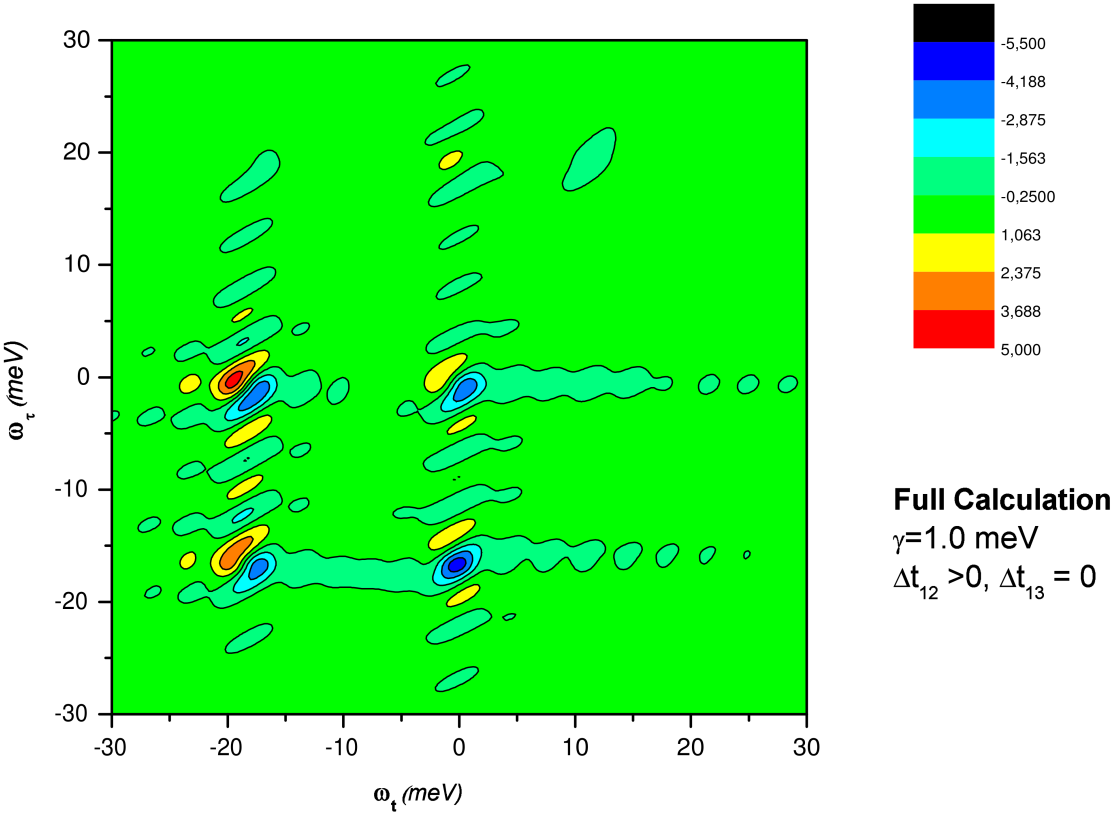

Figure A.4: Full Calculation for both excitation

Appendix B

Appendices

B.1 Appendix A

In the Landau gauge, the interaction matrix elements $v^{ij}_{\alpha_1\alpha_2,\alpha_3\alpha_4}$ (with $i,j = e,h$) are given by

$$v^{ij}_{\alpha_1\alpha_2,\alpha_3\alpha_4} = \int \frac{d\mathbf{q}}{(2\pi)^2}\, v_q\, F^i_{\alpha_1\alpha_2}(\mathbf{q}) F^j_{\alpha_3\alpha_4}(-\mathbf{q}), \tag{B.1}$$

where v_q is the Coulomb potential,

$$F^e_{\alpha_1\alpha_2}(\mathbf{q}) = \phi_{n_1 n_2}(\mathbf{q}) e^{iq_x(k_1+k_2)\ell^2/2}\delta_{k_1,k_2+q_y}\delta_{\sigma_1,\sigma_2}, \tag{B.2}$$

and

$$F^h_{\alpha_1\alpha_2}(\mathbf{q}) = F^e_{-\alpha_2,-\alpha_1}(\mathbf{q})\ ,\ -\alpha = (-k,n,\sigma). \tag{B.3}$$

In the above equations,

$$\phi_{mn}(\mathbf{q}) = \frac{n!}{m!}\left[\frac{(-q_y+iq_x)l}{\sqrt{2}}\right]^{m-n} L_n^{m-n}\left(\frac{q^2\ell^2}{2}\right) e^{-q^2\ell^2/4} \tag{B.4}$$

for $m \geq n$ and $\phi_{mn}(\mathbf{q}) = \phi^*_{nm}(-\mathbf{q})$ for $m < n$, where L_n^{m-n} is the generalized Laguerre polynomial.

B.2 Appendix B

The density matrix equation of motion for a general operator $\hat{O}$ is given by

$$i\partial_t\langle\hat{O}\rangle = \langle[\hat{O},H]\rangle - d(t)\sqrt{N}\sum_m\langle[\hat{O},\hat{X}_m^\dagger]\rangle$$
$$-d^*(t)\sqrt{N}\sum_m\langle[\hat{O},\hat{X}_m]\rangle. \tag{B.5}$$

The deviation from bosonic behavior of a LLn electron–LLm hole excitation is determined by the commutator

$$\left[\hat{X}_{\mathbf{q}nm},\hat{X}^\dagger_{\mathbf{q}'n'm'}\right] = \delta_{\mathbf{q}\mathbf{q}'}\delta_{nn'}\delta_{mm'}$$
$$-\frac{\hat{\rho}^h_{\mathbf{q}'-\mathbf{q},m'm\downarrow}}{\sqrt{N}}\delta_{nn'}e^{i(\mathbf{q}'\times\mathbf{q})_z l^2/2}$$
$$-\frac{\hat{\rho}^e_{\mathbf{q}'-\mathbf{q},n'n\downarrow}}{\sqrt{N}}\delta_{mm'}e^{-i(\mathbf{q}'\times\mathbf{q})_z l^2/2}. \tag{B.6}$$

The Pauli exchange effects between Xs and 2DEG collective excitations, as well as between photoexcited carriers, are described by the commutators

$$\left[\hat{\rho}^e_{\mathbf{q}nm\sigma},\hat{X}^\dagger_{\mathbf{q}'n'm'}\right] = \frac{1}{\sqrt{N}}\delta_{\sigma\downarrow}\delta_{mn'}e^{i(\mathbf{q}\times\mathbf{q}')_z\ell^2/2}\hat{X}^\dagger_{\mathbf{q}+\mathbf{q}'nm'} \tag{B.7}$$

and

$$\left[\hat{\rho}^h_{\mathbf{q}nm\sigma},\hat{X}^\dagger_{\mathbf{q}'n'm'}\right] = \frac{1}{\sqrt{N}}\delta_{\sigma\downarrow}\delta_{mm'}e^{-i(\mathbf{q}\times\mathbf{q}')_z\ell^2/2}\hat{X}^\dagger_{\mathbf{q}+\mathbf{q}'n'n}. \tag{B.8}$$

Finally, the Pauli exchange effects between the 2DEG excitations, which distinguish the QHS from the undoped system, are described by the commutators

$$\left[\hat{\rho}^e_{\mathbf{q}nn'\sigma},\hat{\rho}^e_{\mathbf{q}'mm'\sigma'}\right] = \frac{\delta_{\sigma\sigma'}\delta_{n'm}}{\sqrt{N}}e^{i(\mathbf{q}\times\mathbf{q}')_z\ell^2/2}\hat{\rho}^e_{\mathbf{q}+\mathbf{q}'nm'\sigma}$$
$$-\frac{\delta_{\sigma\sigma'}\delta_{nm'}}{\sqrt{N}}e^{-i(\mathbf{q}\times\mathbf{q}')_z\ell^2/2}\hat{\rho}^e_{\mathbf{q}+\mathbf{q}'mn'\sigma}. \tag{B.9}$$

B.3 Appendix C

In this Appendix we present the commutators with the many–body Hamiltonian given by Eqs. (3.1) and (3.2), which describe the interaction contribution to the equation of motion Eq. (B.5). For a general interband e–h excitation, we obtain after some straightforward algebra

$$\begin{aligned}
[\hat{X}_{\mathbf{q}nm}, H] &= \left[E_g + (n+1/2)\omega_c^e + (m+1/2)\omega_c^h\right]\hat{X}_{\mathbf{q}nm} \\
&- \sum_{n'm'} \bar{V}_{m'm,n'n}(\mathbf{q})\hat{X}_{\mathbf{q}n'm'} \\
&+ \frac{1}{2\pi l^2\sqrt{N}}\sum_{\mathbf{q}'n'} v_{q'}\,\hat{\rho}_{-\mathbf{q}'}\Bigg[\phi_{nn'}(\mathbf{q}')e^{-i(\mathbf{q}\times\mathbf{q}')_z l^2/2}\hat{X}_{\mathbf{q}-\mathbf{q}'n'm} \\
&\quad -\phi_{n'm}(\mathbf{q}')e^{i(\mathbf{q}\times\mathbf{q}')_z l^2/2}\hat{X}_{\mathbf{q}-\mathbf{q}'nn'}\Bigg]. \qquad \text{(B.10)}
\end{aligned}$$

In the QHS we must also consider the dynamics and interactions of the 2DEG collective excitation operators $\hat{\rho}^e_{\mathbf{q}mm'\sigma}$:

$$\begin{aligned}
\left[\hat{\rho}^e_{\mathbf{q}nm\sigma}, H\right] &= \left[\omega_c^e(m-n) + \sum_{n'} V_{n'n}\right]\hat{\rho}^e_{\mathbf{q}nm\sigma} - \sum_{n'm'}\bar{V}_{mm',nn'}(\mathbf{q})\,\hat{\rho}^e_{\mathbf{q}n'm'\sigma} \\
&+\frac{1}{2\pi\ell^2\sqrt{N}}\sum_{\mathbf{q}'n'} v_{q'}\hat{\rho}_{-\mathbf{q}'}\Big[\phi_{mn'}(\mathbf{q}')\,\hat{\rho}^e_{\mathbf{q}+\mathbf{q}'nn'\sigma}e^{i(\mathbf{q}\times\mathbf{q}')_z\ell^2/2} \\
&-\phi_{n'n}(\mathbf{q}')\,\hat{\rho}^e_{\mathbf{q}+\mathbf{q}'n'm\sigma}e^{-i(\mathbf{q}\times\mathbf{q}')_z\ell^2/2}\Big]. \qquad \text{(B.11)}
\end{aligned}$$

In the above equations we used the interaction matrix elements Eq. (5.4) and defined

$$\bar{V}_{nn',mm'}(\mathbf{q}) = \int \frac{d\mathbf{q}'}{(2\pi)^2}\, v_{q'}e^{i(\mathbf{q}\times\mathbf{q}')_z l^2}\;\phi_{nn'}(\mathbf{q}')\phi^*_{mm'}(\mathbf{q}'). \qquad \text{(B.12)}$$

Using the above equations and the ν=1 ground state, we obtain the dispersion of the X_{01} excitation,

$$\Omega_{\mathbf{q}01} = E_g + \frac{\Omega_c^c}{2} + \frac{3\Omega_c^v}{2} - \bar{V}_{11,00}(\mathbf{q}), \qquad \text{(B.13)}$$

and the energy of the MP excitations,

$$\omega_{\mathbf{q}} = \Omega_c^c + V_{00} - V_{10} + \upsilon_{01}^{01}(\mathbf{q}) - \bar{V}_{11,00}(\mathbf{q}). \tag{B.14}$$

B.4 Appendix D

In this Appendix we express the intraband density matrices in Eq. (3.36) in terms of Hubbard operators at ν=1 after restricting to the photoexcited (first two) LLs. First we consider the X–X density matrices $\langle \hat{X}^\dagger_{mn\mathbf{q}} \hat{X}_{m'n'\mathbf{q}} \rangle$. Using the commutator Eq. (B.6), we obtain

$$\langle X_l | \hat{X}^\dagger_{mn\mathbf{q}} \hat{X}_{m'n'\mathbf{q}} | X_{l'} \rangle = \delta_{\mathbf{q}0}\delta_{m'n'}\delta_{mn}\delta_{ml}\delta_{m'l'}, \tag{B.15}$$

$$\langle Y_{\mathbf{Q}} | \hat{X}^\dagger_{mn\mathbf{q}} \hat{X}_{m'n'\mathbf{q}} | Y_{\mathbf{Q}'} \rangle = \delta_{\mathbf{Q}'\mathbf{q}}\delta_{\mathbf{Q}\mathbf{q}}\delta_{m0}\delta_{n1}\delta_{m'0}\delta_{n'1}, \tag{B.16}$$

while $\langle X_l | \hat{X}^\dagger_{mn\mathbf{q}} \hat{X}_{m'n'\mathbf{q}} | Y_{\mathbf{Q}} \rangle = 0$. We thus obtain for the X populations and X$\leftrightarrow$X coherences

$$\begin{aligned} \langle \hat{X}^\dagger_{mn\mathbf{q}} \hat{X}_{m'n'\mathbf{q}} \rangle = {} & \delta_{\mathbf{q}0}\delta_{m'n'}\delta_{mn} \langle |X_m\rangle\langle X_{m'}| \rangle \\ & + \delta_{m0}\delta_{m'0}\delta_{n1}\delta_{n'1} \langle |Y_{\mathbf{q}}\rangle\langle Y_{\mathbf{q}}| \rangle, \end{aligned} \tag{B.17}$$

which differ from the undoped system due to the contribution of the Y–states. Next we consider the density matrices of the form $\langle \hat{\rho}_\sigma \hat{\rho}_\downarrow \rangle$. Using the commutators Eqs. (B.6), (B.7) and (B.8) and Eq. (3.33) we obtain the matrix elements

$$\langle X_{l'} | \hat{\rho}_{-\mathbf{q}} \hat{\rho}^e_{\mathbf{q}nm\downarrow} | X_l \rangle = \frac{\delta_{ml}}{N} \left[\phi^*_{nl}(\mathbf{q})\delta_{ll'} - \phi^*_{l'l}(\mathbf{q})\delta_{nl'} \right] \tag{B.18}$$

$$\langle X_{l'} | \hat{\rho}_{-\mathbf{q}} \hat{\rho}^h_{\mathbf{q}nm\downarrow} | X_l \rangle = \frac{\delta_{ml}}{N} \left[\phi^*_{ll'}(\mathbf{q})\delta_{nl'} - \phi^*_{ln}(\mathbf{q})\delta_{ll'} \right]. \tag{B.19}$$

The coupling between the X and Y states is described by the matrix elements

$$\langle Y_{\mathbf{Q}}|\hat{\rho}_{-\mathbf{q}}\hat{\rho}^{e}_{\mathbf{q}01\downarrow}|X_l\rangle = \frac{\phi^*_{01}(\mathbf{q})}{\sqrt{N}}\delta_{\mathbf{qQ}}\delta_{l1} \tag{B.20}$$

$$\langle X_l|\hat{\rho}_{-\mathbf{q}}\hat{\rho}^{e}_{\mathbf{q}10\downarrow}|Y_{\mathbf{Q}}\rangle = \frac{\phi^*_{10}(\mathbf{q})}{\sqrt{N}}\delta_{\mathbf{q},-\mathbf{Q}}\delta_{l1}, \tag{B.21}$$

$$\langle Y_{\mathbf{Q}}|\hat{\rho}_{-\mathbf{q}}\hat{\rho}^{h}_{\mathbf{q}10\downarrow}|X_l\rangle = \frac{\phi^*_{01}(\mathbf{q})}{\sqrt{N}}\delta_{\mathbf{qQ}}\delta_{l0}, \tag{B.22}$$

$$\langle X_l|\hat{\rho}_{-\mathbf{q}}\hat{\rho}^{h}_{\mathbf{q}01\downarrow}|Y_{\mathbf{Q}}\rangle = \frac{\phi^*_{10}(\mathbf{q})}{\sqrt{N}}\delta_{\mathbf{q},-\mathbf{Q}}\delta_{l0}, \tag{B.23}$$

while $\langle Y|\hat{\rho}\hat{\rho}^{e}_{\mathbf{q}10\downarrow}|X\rangle$=$\langle Y|\hat{\rho}\hat{\rho}^{h}_{\mathbf{q}01\downarrow}|X\rangle$=$\langle X|\hat{\rho}\hat{\rho}^{e}_{\mathbf{q}01\downarrow}|Y\rangle$= $\langle X|\hat{\rho}\hat{\rho}^{h}_{\mathbf{q}10\downarrow}|Y\rangle$=0. Finally, for $\mathbf{q}\neq 0$, we obtain that

$$\langle Y_{\mathbf{Q}'}|\hat{\rho}_{-\mathbf{q}}\hat{\rho}^{e}_{\mathbf{q}10\downarrow}|Y_{\mathbf{Q}}\rangle = \frac{\phi^*_{10}(\mathbf{q})\delta_{\mathbf{Q}'\mathbf{Q}}}{N} \tag{B.24}$$

$$\langle Y_{\mathbf{Q}'}|\hat{\rho}_{-\mathbf{q}}\hat{\rho}^{h}_{\mathbf{q}01\downarrow}|Y_{\mathbf{Q}}\rangle = -\frac{\delta_{\mathbf{QQ}'}}{N}\phi^*_{10}(\mathbf{q}), \tag{B.25}$$

while $\langle Y|\hat{\rho}\hat{\rho}^{h}_{10\downarrow}|Y\rangle$=$\langle Y|\hat{\rho}\hat{\rho}^{e}_{01\downarrow}|Y\rangle$=0. Using the above matrix elements and Eq. (5.16), we obtain

$$\begin{aligned}\langle\hat{\rho}_{-\mathbf{q}}\hat{\rho}^{e}_{\mathbf{q}10\downarrow}\rangle_c &= \phi^*_{10}(\mathbf{q})\big(N_{00}-N_{10}\\ &+ \sqrt{N}M_{1,-\mathbf{q}}+\sum_{\mathbf{q}'}\bar{n}_{\mathbf{q}'}\big),\end{aligned} \tag{B.26}$$

$$\begin{aligned}\langle\hat{\rho}_{-\mathbf{q}}\hat{\rho}^{e}_{\mathbf{q}01\downarrow}\rangle_c &= \phi^*_{01}(\mathbf{q})\big(N_{11}-N^*_{10}\\ &+ \sqrt{N}M^*_{1\mathbf{q}}\big),\end{aligned} \tag{B.27}$$

$$\begin{aligned}\langle\hat{\rho}_{-\mathbf{q}}\hat{\rho}^{h}_{\mathbf{q}10\downarrow}\rangle_c &= -\phi^*_{01}(\mathbf{q})\big(N_{00}-N_{10}\\ &- \sqrt{N}M^*_{0\mathbf{q}}\big),\end{aligned} \tag{B.28}$$

$$\begin{aligned}\langle\hat{\rho}_{-\mathbf{q}}\hat{\rho}^{h}_{\mathbf{q}01\downarrow}\rangle_c &= -\phi^*_{10}(\mathbf{q})\big(N_{11}-N^*_{10}\\ &- \sqrt{N}M_{0,-\mathbf{q}}+\sum_{\mathbf{q}'}\bar{n}_{\mathbf{q}'}\big)\end{aligned} \tag{B.29}$$

The photoexcited electron and hole incoherent populations are obtained after expanding the operators Eq. (3.15) in terms of Hubbard operators:

$$\bar{\nu}_0^e = N_{00} + \sum_q \bar{n}_{\mathbf{q}} \ , \ \bar{\nu}_0^h = N_{00} \tag{B.30}$$

gives the LL0 electron and hole populations, while

$$\bar{\nu}_1^e = N_{11} \ , \ \bar{\nu}_1^h = N_{11} + \sum_{\mathbf{q}} \bar{n}_{\mathbf{q}} \tag{B.31}$$

gives the LL1 carrier populations. The incoherent total carrier populations, $\bar{\nu}_n = \bar{\nu}_n^e + \bar{\nu}_n^h$, are then given by Eq. (4.21), while $\bar{\nu}_{10}^e = N_{10} = \bar{\nu}_{10}^h$. Substituting the above results into Eq. (3.36) we obtain the intraband interaction–induced density matrix contribution to Eqs. (A.3) and (A.3).

B.5 Appendix E

In this Appendix we derive the equation of motion for the correlated contribution $\bar{P}_{\mathbf{q}}$ to the nonlinear polarization equation of motion. At ν=1, we note that

$$\hat{X}_n|Y_{\mathbf{q}}\rangle = 0, \tag{B.32}$$

while $\langle Y_{\mathbf{q}}|\hat{\rho}_{01}|Y_{\mathbf{q}'}\rangle$=0 since we restrict to states with up to one MP. Using the property $[\hat{Y}_{\mathbf{q}}, \hat{X}_n]$= $[\hat{Y}_{\mathbf{q}}, \hat{Y}_{\mathbf{q}'}]$=0,

$$\begin{aligned}
\bar{P}_{\mathbf{q}} &= \frac{1}{\sqrt{N}}\langle\psi_0||G\rangle\langle Y_{\mathbf{q}}||\psi_1\rangle + \frac{1}{\sqrt{N}}\langle\bar{\psi}_0||G\rangle\langle Y_{\mathbf{q}}||\bar{\psi}_1\rangle \\
&+ \sum_m P_m^{L*}\langle Y_{\mathbf{q}}\hat{X}_m|\psi_2\rangle \\
&+ \frac{1}{\sqrt{N}}\sum_m \langle\bar{\psi}_1||X_m\rangle\langle Y_{\mathbf{q}}\hat{X}_m||\bar{\psi}_2\rangle \\
&+ \frac{1}{\sqrt{N}}\sum_{\mathbf{q}'}\langle\bar{\psi}_1||Y_{\mathbf{q}'}\rangle\langle Y_{\mathbf{q}}Y_{\mathbf{q}'}||\bar{\psi}_2\rangle,
\end{aligned} \tag{B.33}$$

where we introduced the Y–Y states $|Y_{\mathbf{q}}Y_{\mathbf{q}'}\rangle = \hat{Y}^\dagger_{\mathbf{q}}\hat{Y}^\dagger_{\mathbf{q}'}|G\rangle$. An analogous expression can be obtained for the nonlinear polarization P_n by substituting $\hat{Z}=\hat{X}_n$ in Eq. (3.62). Noting from Eqs. (3.14) and (3.64) that

$$\sum_m P^L_m \langle \bar{\psi}_{1L}|[\hat{X}_n, \hat{X}^\dagger_m]|\bar{\psi}_{1L}\rangle = -P^L_n \bar{\nu}_n + P^L_n \langle \bar{\psi}_{1L}|\bar{\psi}_{1L}\rangle \tag{B.34}$$

and using Eq. (B.32),

$$\begin{aligned} P_n &= \frac{1}{\sqrt{N}}\langle\psi_0|G\rangle\langle X_n|\psi_1\rangle + \frac{1}{\sqrt{N}}\langle\bar{\psi}_0||G\rangle\langle X_n||\bar{\psi}_1\rangle \\ &+ \sum_m P^{L*}_m \langle X_m X_n|\psi_2\rangle \\ &+ \frac{1}{\sqrt{N}}\sum_m \langle\bar{\psi}_1||X_m\rangle\langle X_n X_m||\bar{\psi}_2\rangle \\ &+ \frac{1}{\sqrt{N}}\sum_{\mathbf{q}'} \langle\bar{\psi}_1||Y_{\mathbf{q}'}\rangle\langle Y_{\mathbf{q}'}X_n||\bar{\psi}_2\rangle \\ &+ P^L_n\langle\bar{\psi}_{1L}|\bar{\psi}_{1L}\rangle - P^L_n\bar{\nu}_n. \end{aligned} \tag{B.35}$$

We obtain the equation of motion of $\bar{P}_{\mathbf{q}}$ from Eq. (B.33) after noting that the time evolution of the correlated 2–h state, obtained from Eq. (3.58), is given by Eq. (3.59). [**?**, 89] Similarly, [**?**, 89]

$$\begin{aligned} i\partial_t|\bar{\psi}_0\rangle &= H|\bar{\psi}_0\rangle - \sum_n \langle\hat{Y}_n\rangle^{L*}\hat{X}_n|\bar{\psi}_{1L}\rangle \\ &+ \sum_n \langle\hat{X}_n\rangle^{L*}\left[\hat{Y}_n|\bar{\psi}_{1L}\rangle - \langle\hat{Y}_n\rangle^L|G\rangle\right], \end{aligned} \tag{B.36}$$

where we used Eq. (B.32), and [**?**, 89]

$$i\partial_t|\bar{\psi}_{1L}\rangle = H|\bar{\psi}_{1L}\rangle + \sum_n \langle\hat{X}_n\rangle^L|Y_n\rangle - \sum_{n\mathbf{q}} W_{n\mathbf{q}}\bar{P}^L_{\mathbf{q}}|X_n\rangle. \tag{B.37}$$

Using Eqs. (B.5), (3.27) and (3.44), Eq. (3.14), the properties $H|G\rangle=0$ and

$$\hat{\nu}_n|Y_{\mathbf{q}}\rangle = \frac{1}{N}|Y_{\mathbf{q}}\rangle, \tag{B.38}$$

Eqs. (3.48), (3.49) and (3.50), Eq. (3.58), the orthogonality

$$\begin{aligned}&\langle Y_{\mathbf{q}}Y_{\mathbf{q}'}|X_nX_m\rangle = \langle Y_{\mathbf{q}}Y_{\mathbf{q}'}|X_nY_{q''}\rangle \\ &= \langle X_nY_q|X_{n'}X_{m'}\rangle = 0,\end{aligned} \tag{B.39}$$

and Eq. (3.45), we obtain after some algebra the equation of motion (exact at ν=1 within our subspace)

$$\begin{aligned}&i\partial_t\bar{P}_{\mathbf{q}} = (\bar{\Omega}_{\mathbf{q}} - i\gamma)\bar{P}_{\mathbf{q}} + \frac{1}{N}\sum_{\mathbf{q}'} W_{\mathbf{q}\mathbf{q}'}\bar{P}_{\mathbf{q}'} + \frac{1}{\sqrt{N}}\sum_n W_{\mathbf{q}n}P_n \\ &+d(t)\sum_n P_n^{L*}\bar{P}_{\mathbf{q}}^L + \frac{1}{\sqrt{N}}\sum_n W_{\mathbf{q}n}P_n^L\ \bar{\nu}_n + \frac{1}{\sqrt{N}}\sum_{n\mathbf{q}'} W_{\mathbf{q}'n}P_n^L\bar{P}_{\mathbf{q}'}^{L*}\bar{P}_{\mathbf{q}}^L \\ &+\sum_{nmm'} P_n^L\Big[P_m^{L*}P_{m'}^L\ \frac{N}{2}\langle G|[\hat{Y}_{\mathbf{q}},\hat{Y}_m]|X_nX_{m'}\rangle \\ &+N_{mm'}\ N\langle X_m|\Delta[\hat{Y}_{\mathbf{q}}\hat{Y}_n^\dagger]]X_{m'}\rangle\Big] + \sum_{nn'\mathbf{q}'} P_n^L\Big[P_{n'}^{L*}\bar{P}_{\mathbf{q}'}^L\ N\langle G|[\hat{Y}_{\mathbf{q}},\hat{Y}_{n'}]|X_nY_{\mathbf{q}'}\rangle \\ &+M_{n'\mathbf{q}'}\ N\langle X_{n'}\hat{Y}_{\mathbf{q}}|[\hat{Y}_n^\dagger,\hat{Y}_{\mathbf{q}'}^\dagger]|G\rangle\Big] \\ &+\sum_{n\mathbf{q}'\mathbf{q}''} P_n^L\bar{n}_{\mathbf{q}'\mathbf{q}''}N\left[\langle Y_{\mathbf{q}'}|\Delta[\hat{Y}_{\mathbf{q}}\hat{Y}_n^\dagger]|Y_{\mathbf{q}''}\rangle\ -\delta_{\mathbf{q}''\mathbf{q}}\langle Y_{\mathbf{q}'}|Y_n\rangle\right] \\ &+\frac{1}{\sqrt{N}}\sum_{nn'\mathbf{q}'} W_{n\mathbf{q}'}\bar{P}_{\mathbf{q}'}^L M_{n'\mathbf{q}}\ N\left[\delta_{nn'} - \langle X_{n'}Y_{\mathbf{q}}|X_nY_{\mathbf{q}}\rangle\right] \\ &+\sum_n P_n^{L*}\langle G|[\hat{Y}_{\mathbf{q}},\hat{Y}_n]|\bar{\psi}_2\rangle + \sum_{\mathbf{q}'}\bar{P}_{\mathbf{q}'}^{L*}\langle G|[\hat{Y}_{\mathbf{q}'},[\hat{Y}_{\mathbf{q}},H]]|\bar{\psi}_2\rangle.\end{aligned} \tag{B.40}$$

The following interaction matrix elements are obtained after straightforward algebra at ν=1 by using the commutators Eqs. (B.7), (B.8) and (B.9) and the definition of the Y operators, Eqs. (4.3) and (5.1):

$$\begin{aligned}&N\langle G|[\hat{Y}_{\mathbf{q}},\hat{Y}]|X_nX_m\rangle = \frac{\upsilon_{01}^{01}(q)}{\sqrt{N}}\times \\ &(\delta_{n1}\delta_{m0} + \delta_{n0}\delta_{m1}),\end{aligned} \tag{B.41}$$

$$N\langle X_m|\Delta[\hat{Y}_{\mathbf{q}}\hat{Y}^\dagger]|X_{m'}\rangle = -\frac{\upsilon_{01}^{01}(q)}{\sqrt{N}}\delta_{mm'} \tag{B.42}$$

describe X–X interactions mediated by the emission and reabsorption of a MP,

$$N\langle G|[\hat{Y}_{\mathbf{q}},\hat{Y}]|X_nY_{\mathbf{q}'}\rangle = \delta_{\mathbf{q}\mathbf{q}'}\left(\delta_{n1}-\delta_{n0}\right)\left[\upsilon_{01}^{01}(q)-V_{01}\right], \tag{B.43}$$

$$N\langle X_nY_{\mathbf{q}}|X_{n'}Y_{\mathbf{q}'}\rangle = \delta_{nn'}\delta_{\mathbf{q}\mathbf{q}'}(N-1) \tag{B.44}$$

describe X–Y interactions, while

$$\langle Y_{\mathbf{q}}Y_{\mathbf{q}'}|Y_{\mathbf{q}''}Y_{\mathbf{q}'''}\rangle = \Bigg[\delta_{\mathbf{q}\mathbf{q}'''}\delta_{\mathbf{q}'\mathbf{q}''}+\delta_{\mathbf{q}\mathbf{q}''}\delta_{\mathbf{q}'\mathbf{q}'''}$$

$$-\frac{2}{N}\delta_{\mathbf{q}+\mathbf{q}',\mathbf{q}''+\mathbf{q}'''}\cos\left[\frac{l^2}{2}(\mathbf{q}\times\mathbf{q}'+\mathbf{q}'\times\mathbf{q}''-\mathbf{q}\times\mathbf{q}'')_z\right]\Bigg]^2 \tag{B.45}$$

describes Y–Y interactions. Using the above results and Eq. (4.5), we obtain from Eq. (B.40) the equation of motion Eq.A.3. after neglecting the correlated 2–h contributions described by the amplitudes of $|\bar{\psi}_2\rangle$

Bibliography

[1] N.W. Ashcroft and Mermin,*Solid State Physics*,Saunders College Publishing (1975).

[2] D.S. Chemla and J. Shah, *Many-Body corellation effects in semiconductors*, Nature **411**(2837),549(2001)

[3] D.S. Chemla, *Ultrafast transient nonlinear processes in semiconductors*, in *Non-Linear Optics in Semiconductors*, edited by R.K. Willardson and A.C. Beers, Academic Press, New York (1999).

[4] S. Mukamel, *Principles of Nonlinear Optical Spectroscopy*,Oxford University Press (1995).

[5] J. Shah, *Ultrafast Spectroscopy of Semiconductors and Semiconductor Nanostructures*, vol. **115** of *Springer Series in Solid–State Sciences*,Springer-Verlag, Berlin Heidelberg New York, 2nd ed. (1999).

[6] H. Haug and S. W. Koch, *Quantum Theory of the Optical and Electronic Properties of Semiconductors*, World Scientific (1993).

[7] R.W.Boyd, *Nonlinear Optics*, Academic Press, San Diego, CA,2nd ed. (2003)

[8] V.M. Axt and A.Stahl*A dynamics-controlled truncation scheme for the hierarchy of density matrices in semiconductor optics*, Z.Phys.B Condens. Matter **93**(2),195(1994).

[9] V.M. Axt, K.Victor and A.Stahl, *Influence of a phonon bath one the hierarchy of electronic densities in an optically excited semiconductor*, Phys. Rev.B **53**(11),7244(1996)

[10] V.M. Axt and S. Mukamel, *Nonlinear optics of semiconductors and molecular nanostructures;a common perspective*,Rev. Mod. Phys. **70**(1),145(1998)

[11] F. Rossi and T. Kuhn, *Theory of ultrafast phenomena in photoexcited semiconductors*,Rev. Mod. Phys. **74**, 895 (2002).

[12] W. Schäfer and M. Wegener, *Semiconductor Optics and Transport Phenomena*, Springer (2002).

[13] S.T. Kundiff, M.Koch, W.H.Knox,J.Shah and W. Stolz, *Optical Coherence in Semiconductors: Strong Emmision Mediated by nondegenerate Interactions*, Phys.Rev. Lett. **77**(6),1107(1996)

[14] S. Wu ,X.-c. Zhang, and R.L. Fork, *Direct experimental observation of interactive third and fifht order nonlinearities in a time - and space-resolved four-wave mixing experiment*,Applied Physics Letters **61**(8), 919 (1992).

[15] D. Abramavicius, B. Palmieri, D. V. Voronine, F. Sanda, and S. Mukamel Chem. Rev. **109**, 2350 (2009); S. Mukamel and D. Abramavicius, Chem. Rev. **104**, 2073 (2004).

[16] D.B. Turner and K.A. Nelson, Nature **466**, 1089 (2010).

[17] F. Rossi and T. Kuhn, Rev. Mod. Phys. **74**, 895 (2002).

[18] I. E. Perakis and D. S. Chemla, Phys. Rev. Lett. **72**, 3202 (1994); T. V. Shahbazyan, N. Primozich, I. E. Perakis, and D. S.

Chemla, Phys. Rev. Lett. **84**, 2006 (2000); N. Primozich, T. V. Shahbazyan, I. E. Perakis, and D. S. Chemla, Phys. Rev. B **61**, 2041 (2000).

[19] I. Brener, W. H. Knox, and W. Schäefer, Phys. Rev. B **51**, 2005 (1995); I. E. Perakis, I. Brener, W. H. Knox, and D. S. Chemla, J. Opt. Soc. Am. B **13**, 1313 (1996).

[20] A. T. Karathanos, I. E. Perakis, N. A. Fromer, and D. S. Chemla, Phys. Rev. B **67**, 035316 (2003).

[21] M. E. Karadimitriou, E. G. Kavousanaki, I. E. Perakis, and K. M. Dani, Phys. Rev. B **82**, 165313 (2010).

[22] K. Nasu, Photoinduced Phase Transitions (World Scientific, Singapore, 2004).

[23] See e.g. D. Polli *et al*, Nature Materials **6**, 643 (2007); M. Rini *et al*, Nature **449**, 72 (2007); M. Fiebig *et al*, Science **280**, 1925 (1998).

[24] T. Chakraborty and P. Pietilainen, *The Quantum Hall Effects, Fractional and Integral*, Springer, 2nd ed. (1995).

[25] D. Yoshioka, *The Quantum Hall Effect*, vol. 133 of *Springer Series in Solid–State Sciences*, Springer–Verlag, Berlin Heidelberg New York (2002).

[26] A. Pinczuk, *Perspectives in Quantum Hall Effects:Novel Quantum Liquids in Low-Dimensional Semiconductor Structures*, chap. 8, Wiley, New York (1996).

[27] R. B. Laughlin, Phys. Rev. Lett. **50**, 1395 (1983).

[28] J.P.Eisenstein, L.N. Pfeiffer, and K.W.West,*Coulomb barrier to tunelling between paralle two-dimensional electron systems*,Phys.Rev.Lett.**69**(26),3804(1992).

[29] M.Linbberg and S.W.Koch,*Effective Bloch Equations for Semiconductors*, Phys.Rev.B**38**(5),3342(1988)

[30] A. Pinczuk, J. P. Valladares, D. Heiman, A. C. Gossard, J. H. English, C. W. Tu, L.Pfeiffer, and K.West, Phys. Rev. Lett. **61**, 2701 (1988); A. Pinczuk, B. S. Dennis, L. N. Pfeiffer, and K. West, Phys. Rev. Lett. **70**, 3983 (1993); M. A. Eriksson, A. Pinczuk, B. S. Dennis, S. H. Simon, L. N. Pfeiffer, and K. W. West, Phys. Rev. Lett. **82**, 2163 (1999).

[31] C. Kallin and B. I. Halperin, Phys. Rev. B **30** (10), 5655 (1984).

[32] S. M. Girvin, A. H. MacDonald, and P. M. Platzman, Phys. Rev. Lett. **54**, 581 (1985).

[33] A. H. MacDonald, H. C. A. Oji, and S. M. Girvin, Phys. Rev. Lett. **55**, 2208 (1985); H. C. A. Oji and A. H. MacDonald, Phys. Rev. B **33** (6), 3810 (1986); A. H. MacDonald, J. Phys. C: Solid State Phys. 18 1003 **18** (5), 1003 (1985).

[34] A.H.MacDonald and D.S.Ritchie, *Hydrogenic energy levels in two dimensions at arbitary magnetic fields* Phys. Rev. B **33**(12),8336(1986)

[35] O. Akimoto and H. Hasegawa, *Interband Optical Transitions in extremely Anisotropic Semiconductors.II.Coexistence of Exciton and the Landau levels*, Journal of the Physical Sociaty of Japan **22**(1),181(1967).

[36] M.Shinada and K. Tanaka, *Interband Optical Transitions in extremely Anisotropic Semiconductors.III.Numerical studies of Magneto-Optical Absorption*, Journal of the Physical Sociaty of Japan **29**(5),1258(1970).

[37] M.Shinada and S.Sugano, *Interband Optical Transitions in extremely Anisotropic Semiconductors.I. Bound and Unbound Ex-*

citon Absorption, Journal of the Physical Sociaty of Japan **21**(10),1936(1966)

[38] M.Altarelli, U.Ekenberg, and A.Fasolino, *Calculations of hall subbands in Semiconductor quantum wells and superlattices*, Phys.Rev.B **32**(8),5138 (1985)

[39] G.E.W.Bauer and T.Ando, *Theory of magnetoexcitons in quantum wells*, Phys.Rev.B**37**(6),3130(1988)

[40] D.A.Broido and L.J.Sham, *Effective masses of holes at GaAs-AlGaAs heterojunctions*, Phys.Rev.B **31**(2),888 (1985)

[41] U.Ekenberg and M.Altarelli, *Subbands and landau levels in the two dimensional hole gas at* $GaAs - Al_xGa_{1-x}As$ *interface*, Phys.Rev.B **32**(6),3712(1985)

[42] S.-R.E.Yang,D.A.Broido, and L.J.Sham, *Holes in the two dimensional hole gas at the* $GaAs - Al_xGa_{1-x}As$ *heterojunctions in magnetic fields*, Phys.Rev.B **32** (10), 6630 (1985)

[43] S.-R.E.Yang and L.J.Sham, *Theory of magnetoexcitons in quantum wells*, Phys.Rev.Lett.**58**(24),2598(1987)

[44] J.M.Luttinger, *Quantum Theory of Cyclotron Resonance in Semiconductors:General Theory*, Phys.Rev.**102**(4),1030(1956)

[45] W.Kohn,*Cyclotron Resonance and Haas-van Alphen Oscillations of a Interacting Electron Gas*, Phys.Rev.**123**(4),1242(1961)

[46] S.Schmitt-Rink and D.S. Chemla, *Collective Excitations and the Dynamical Stark Effect in a Coherently Driven Exciton System*,Phys.Rev.Lett.**57**(21),2752(1986)

[47] S.Schmitt-Rink,D.S.Chemla and H.Haug,*Nonequilibrium theory of the optical Stark effect and spectral hole burning in semiconductors*,Phys.Rev.B**37**,941(1988)

[48] S.Weiss,M.-A.Mycek,J.-Y.Bigot,S.Schmitt-Rink,and D.S.Chemla,*Collective effects in excitonic free induction decay:Do semiconductors and atoms emit coherent light in different ways?*, Phys.Rev. Lett **69**(18),2685(1992)

[49] S.Glutsch, U.Siegner,and D.S.Chemla,*Spatiotemporal dynamics of photon echoes from continuum states in semiconductors*, Phys.Rev.B **52**(7),4941)(1995)

[50] M.Lindberg,R.Binder,and S.W.Koch, *Theory of the semiconductor photon echo*,Phys.Rev.A **45**(3),1865(1992)

[51] K.Leo,M.Wegener,J.Shah,D.S.Chemla, E.O.G*Ö*bel,T.C.Damen,S.Schmitt-Rink,and W.Schaäfer,*Effects of coherent polarization interactions on time-resolved degenerate four-wave mixing*,Phys.Rev.Lett.**65**(11),1340(1990).

[52] M.Wegener,D.S.Chemla,S.Schmitt-Rink, and W.Schaäfer,*Line shape of time-resolved four-wave mixing*,Phys.Rev.A.**42**(9),5675(1990).

[53] F.Jahnke,M.Koch,T.Meier,J.Feldmann, W.Scäfer, P.Thomas, S.Koch,E.Göbel, and H.Nickel,*Simultaneous ifluence of disorder and Coulomb interaction on phonon echoes in semiconductors*,Phys.Rev.B**50**(11),8114(1994.

[54] C.Stafford,S.Schmitt-Rink,and W.Schaefer,*Nonlinear optical responce of two-dimensional magnetoexcitons*,Phys.Rev.B **41**(14),1000(1990)

[55] S.Schmitt-Rink.J.B.Stark,W.H.Knox,D.S.Chemla,and W.Schäfer,*Optical properties of quasi-zero-dimensional magnetoexcitons*,Applied Physics A:Materials Science & Processing **53**(6),491(1991)

[56] M.L.Cohen and J.R. Chelikowsky,*Electronic Structure and Optical Properties of semiconductors*,vol.75 of *Solid State Physics*, Springer, Berlin, Heidelberg, 2nd ed.(1989).

[57] S.Bar and I.Bar-Joseph,*Exciton spin dynamics in GaAs heterostructures*,Phys.Rev.Lett.**68**(3),349(1992).

[58] D.J.Lovering,R.T.Phillips,G.J.Dentin,and G.W.Smith,*Resonant generation of biexcitons in a GaAs quantum well*,Phys.Rev.Lett.**68**(12),1880(1992).

[59] P.Kner,S.Bar-Ad,M.V.Marquezini,D.S.Chempla,and W.Schäfer,*Magnetically enhanced exciton-exciton correlations in semiconductors*,Phys.Rev.Lett.**78**(7),1319(1997).

[60] K.Victor,V.M.Axt,and A,Stahl,*Hierarchy of density matrices in coherent semoconductor optics*,Phys.Rev.B **51**(20),14164(1995)

[61] W.Shäfer,D.S.Kim, J.Shah, T.C.Damen, J.E.Cunningham, K.W.Goossen, L.N.Pfeiffer,and K.Köhler,*Femptosecond coherent fields induced by many-particle correlations in transient four-wave mixing*Phys.Rev.B**53**(24),16429(1996)

[62] G.Bartels,A.Stahl,V.M. Axt,B.Haase,U.Neuhirch,and J.Gutowski,*Identification of Higher order electronic coherences in semiconductors by their signature in four-wave-mixing signals*,Phys.Rev.Lett.**53**(24),16429 (1996).

[63] L.J.S.S.R.Bolton,U.Neukirch,D.S.Chemla,and V.M.Axt,*Demonstration of sixth order coulomb correlations in a semiconductor single quantum well*,Phys.Rev.Lett.**85**(9)2002(2000).

[64] R.L.P.Kner,W.Schäfer and D.S.Chemla,*Coherence of four-particle correlations in semiconductors*,Phys.Rev.Lett.**81**(24),5386(1998).

[65] N.A.Fromer, P.Kner, D.S.Chemla, R.Lövenich, and W.Schäfer, *Correlation effects beyond Hartree-Fock theory and polarization dependence of four-wave mixing in bulk GaAs at high magnetic field*,Phys.Rev.B**62**(4),2516(2000).

[66] U.Neukirch, S.R.Bolton, N.A.Fromer, L.J.Sham, and D.S.Chempla,*Polariton-Biexciton transitions in a semoconductor microcavity*, Phys.Rev.Lett.**84**(10),2215(2000).

[67] U.Neukirch, S.R.Bolton,L.J.Sham, and D.S.Chempla,*Electronic four particle correlations in semiconductors: Renormalization of coherent pump-probe oscillations*, Phys.Rev.B**61**(12), R7835(2000).

[68] I. E. Perakis and T. V. Shahbazyan, Surface Science Reports **40**, 1 (2000); I. E. Perakis and T. V. Shahbazyan, Int. J. Mod. Phys. B **13**, 869 (1999); I. E. Perakis, Chemical Physics **210**, 259 (1996).

[69] M.Z.Maialle and L.J.Sham, *Interacting Electron Theory of Coherent Nonlinear Response*, Phys.Rev.Lett.**73**(24),3310(1994)

[70] T. Östreich, K. Schönhammer, and L. J. Sham, Phys. Rev. Lett. **74**, 4698 (1995); T. Östreich, K. Schönhammer, and L. J. Sham, Phys. Rev. B **58**, 12920 (1998).

[71] W.Schäfer, R.Lövenich, N.A.Fromer, and D.S.Chemla,*From Coherently Excited highly correlated states to incoherent relaxation processes in semiconductors*, Phys.Rev.Lett.**86**(2),344(2001).

[72] R. K. Kamilla, X. G. Wu, and J. K. Jain, Phys. Rev. B **54**, 4873 (1996).

[73] J. K. Jain, Phys. Rev. Lett. **63**, 199 (1989); Phys. Today **53**(4), 39 (2000).

[74] H. L. Stormer, D. C. Tsui, and A. C. Gossard, Rev. Mod. Phys. **71**, S298 (1999).

[75] A. Wójs, A. Gladysiewicz,and J. J. Quinn, Phys. Rev. B **73**, 235338 (2006); M. Byszewski, B. Chwalisz, D. K. Maude, M. L. Sadowski, M. Potemski, T. Saku, Y. Hirayama, S. Studenikin, D. G. Austing, A. S. Sachrajda, and P. Hawrylak, Nature Physics **2**, 239 (2006).

[76] J. Sinova, A. H. MacDonald, and S. M. Girvin, Phys. Rev. B **62**, 13579 (2000).

[77] E. H. Rezayi, Phys. Rev. B **36**, 5454 (1987); **43**, 5944 (1991).

[78] S. L. Sondhi, A. Karlhede, S A. Kivelson, E. H. Rezayi, Phys. Rev. B **47**, 16419 (1993)

[79] A. H. MacDonald, H. A. Fertig, and L. Brey, Phys. Rev. Lett. **76**, 2153 (1996); H. A. Fertig, L. Brey, R. Côté, and A. H. MacDonald, Phys. Rev. B **50**, 11018 (1994); H. A. Fertig, L. Brey, R. Côté, A. H. MacDonald, A. Karlhede, and S. L. Sondhi, Phys. Rev. B **55**, 10671 (1997);

[80] S. E. Barrett, G. Dabbagh, L. N. Pfeiffer, K. W. West, R. Tycko, Phys. Rev. Lett. **74**, 5112 (1995); R. Tycko, S. E. Barrett, G. Dabbagh, L. N. Pfeiffer, K. W. West, Science **268**, 1460 (1995).

[81] S. Das Sarma, M. Freedman, and C. Nayak, Phys. Rev. Lett. **94**, 166802 (2005).

[82] N. A. Fromer, C. Schüller, D. S. Chemla, T. V. Shahbazyan, I. E. Perakis, K. Maranowski, and A. C. Gossard, Phys. Rev. Lett **83**, 4646 (1999).

[83] N. A. Fromer, C. E. Lai, D. S. Chemla, I. E. Perakis, D. Driscoll, and A. C. Gossard, Phys. Rev. Lett. **89**, 067401 (2002).

[84] K. M. Dani, J. Tignon, M. Breit, D. S. Chemla, E. G. Kavousanaki, and I. E. Perakis, Phys. Rev. Lett. **97**, 057401 (2006).

[85] N. A. Fromer, C. Schüller, C. W. Lai, D. S. Chemla, I. E. Perakis, D. Driscoll, and A. C. Gossard, Phys. Rev. B **66**, 205314 (2002).

[86] C. Schüller, I. E. Perakis, N. A. Fromer, and D. S. Chemla in *Nonequilibrium Physics at Short Time Scales: Formation of Correlations*, edited by K. Morawetz, pp. 209, Springer Verlag, Berlin, Heidelberg, New York (2004).

[87] K. M. Dani, J. Tignon, M. Breit, D. S. Chemla, E. G. Kavousanaki, and I. E. Perakis, Physica E **34**, 206 (2006).

[88] I. E. Perakis and D. S. Chemla, Phys. Stat. Sol. (b) **234**, 242 (2002); I. E. Perakis, Phys. Stat. Sol. (b) **238**, 502 (2003); I. E. Perakis and D. S. Chemla, Solid State Commun.**127**, 147 (2003).

[89] I. E. Perakis and E. G. Kavousanaki, Chemical Physics **318**, 118 (2005).

[90] K. M. Dani, E. G. Kavousanaki, J. Tignon, D. S. Chemla, and I. E. Perakis, Solid State Commun. **140**, 72 (2006).

[91] E. G. Kavousanaki, K. M. Dani, J. Tignon, D. S. Chemla, and I. E. Perakis, Phys. Stat. Sol. (b) **243**, 2397 (2006).

[92] J. Hubbard, Proc. Royal Soc. of London A, **285**, 542 (1965).

[93] A. E. Ruckenstein and S. Schmitt-Rink, Int. J. Mod. Phys. B **3**, 1809 (1989); J. Igarashi, J. Phys. Soc. Jpn. **52**, 2827 (1983); **54**, 260 (1985); J. Igarashi, M. Takahashi, and T. Nagao, *ibid.* **68**, 3682 (1999).

[94] M. D. Kapetanakis and I. E. Perakis, Phys. Rev. B **78**, 155110 (2008); M. D. Kapetanakis and I. E. Perakis, Phys. Rev. B **75**,

140401(R) (2007); M. D. Kapetanakis, A. Manousaki, and I. E. Perakis, Phys. Rev. B **73**, 174424 (2006); M. D. Kapetanakis and I. E. Perakis, Phys. Rev. Lett. **101**, 097201 (2008).

[95] K.-B. Broocks, B. Su, P. Schröter, Ch. Heyn, D. Heitmann, W. Wegscheider, V. M. Apalkov, T. Chakraborty, I. E. Perakis, and C. Schüller, Phys. Stat. Sol. (b) **245**, 321 (2008)

[96] J. G. Groshaus, V. Umansky, H. Shrtrikman, Y. Levinson, and I. Bar–Joseph, Phys. Rev. Lett. **93**, 096802 (2004); G. Yusa, H. Shtrikman, and I. Bar–Joseph, Phys. Rev. Lett. **87**, 216402 (2001).

[97] D. R. Yakovlev, V. P. Kochereshko, R. A. Suris, H. Schenk, W. Ossau, A. Waag, G. Landwehr, P. C. M. Christianen, and J. C. Maan, Phys. Rev. Lett. **79**, 3974 (1997).

[98] C. Schüller, K.–B. Broocks, Ch. Heyn, and D. Heitmann, Phys. Rev. B **65**, 081301(R) (2002).

[99] A. Wójs, J. J. Quinn, and P. Hawrylak, Phys. Rev. B **62**, 4630 (2000); A. Gladysiewicz, L. Bryja, A. Wójs. and M. Potemski, Phys. Rev. B **74**, 115332 (2006).

[100] P. Kner, S. Bar-Ad, M. V. Marquezini, D. S. Chemla, and W. Schäfer, Phys. Rev. Lett. **78**, 1319 (1997); R. L. P. Kner, W. Schäfer and D. S. Chemla, Phys. Rev. Lett. **81**, 5386 (1998).

[101] G. Kotliar, S. Y. Savrasov, K. Haule, V. S. Oudovenko, O. Parcollet, and C. A. Marianetti, Rev. Mod. Phys. **78**, 865 (2006).

[102] M. D. Kapetanakis, I. E. Perakis, K. J. Wickey, C. Piermarocchi, and J. Wang, Phys. Rev. Lett. **103**, 047404 (2009)

[103] T. V. Shahbazyan, N. Primozich, and I. E. Perakis, Phys. Rev. B **62**, 15925 (2000).

[104] T. J. Park and J. C. Light, J. Chem. Phys. **85**, 5870 (1986).

[105] A. B Dzyubenko and A. Yu. Sivachenko, Phys. Rev. Lett. **84**, 4429 (2000); A. B. Dzyubenko, Phys. Rev. B **69**, 115332 (2004).

[106] I. V. Lerner and Yu. E. Lozovik, Zh. Eksp. Teor. Fiz. **80**, 1488 (1981) [Sov. Phys. JETP **53**, 763 (1981)]; A. H. MacDonald and E. H. Rezayi, Phys. Rev. B **42**, R3224 (1990).

[107] V. M. Apalkov and E. I. Rashba, Phys. Rev. B **46** (3), 1628 (1992); V. M. Apalkov and E. I. Rashba, Phys. Rev. B **48**, 18312 (1993).

[108] N. R. Cooper and D. B. Chklovskii, Phys. Rev. B **55**, 2436 (1997).

[109] E. H. Aifer, B. B. Goldberg, and D. A. Broido, Phys. Rev. Lett. **76**, 680 (1996).

[110] K. M. Dani, I. A. Cotoros, J. Wang, J. Tignon, D. S. Chemla, E. G. Kavousanaki, and I. E. Perakis, Phys Rev B **78**, R041301 (2008).

[111] E.J.Mayer, G.O.Smith, V.Heuckeroth, J.Kuhl, K.Bott, A.Schulze, T.Meier, S.W.Koch, P.Thomas, R.Hey,and K.Ploog,*Polarization dependence of beating phenomena at th enenergetically lowest exciton transition in GaAs quantum wells*,Phys.Rev.B**51**(16),10909(1995).

[112] L.Schultheis,J.Kuhl,A.Honold,and C.W.Tu,*Picosecond Phase coherence and Orientational Relaxation in GaAs*,Phys.Rev.Lett.**57**(14),1797(1986).

[113] L. Yang and S. Mukamel, Phys. Rev. Lett. **100**, 057402 (2008); L. Yang, T. Zhang, A. D. Bristow, S. T. Cundiff, and S. Mukamel, J. Chem. Phys. **129**, 234711 (2008); L. Yang, I. V. Schweigert, S. T. Cundiff, and S. Mukamel, Phys. Rev. B **75**, 125302 (2007).

List of Figures